

The Chemical Compositions of Galactic Disk F and G Dwarfs

Bacham E. Reddy, Jocelyn Tomkin, David L. Lambert, Carlos Allende Prieto

Department of Astronomy, University of Texas, Austin, Texas 78712

2 October 2018

ABSTRACT

Photospheric abundances are presented for 27 elements from carbon to europium in 181 F-G dwarfs from a differential LTE analysis of high-resolution and high signal-to-noise spectra. Stellar effective temperatures (T_{eff}) were adopted from an infrared flux method calibration of Strömberg photometry. Stellar surface gravities (g) were calculated from *Hipparcos* parallaxes and stellar evolutionary tracks. Adopted T_{eff} and g values are in good agreement with spectroscopic estimates. Stellar ages were determined from evolutionary tracks. Stellar space motions (U, V, W) and a Galactic potential were used to estimate Galactic orbital parameters. These show that the vast majority of the stars belong to the Galactic thin disc.

Relative abundances expressed as $[X/Fe]$ generally confirm previously published results. We give results for C, N, O, Na, Mg, Al, Si, S, K, Ca, Sc, Ti, V, Cr, Mn, Co, Ni, Cu, Zn, Sr, Y, Zr, Ba, Ce, Nd, and Eu. The α -elements – O, Mg, Si, Ca, and Ti – show $[\alpha/Fe]$ to increase slightly with decreasing $[Fe/H]$. Heavy elements with dominant contributions at solar metallicity from the s -process show $[s/Fe]$ to decrease slightly with decreasing $[Fe/H]$. Scatter in $[X/Fe]$ at a fixed $[Fe/H]$ is entirely attributable to the small measurement errors, after excluding the few thick disc stars and the s -process enriched CH subgiants. Tight limits are set on ‘cosmic’ scatter. If a weak trend with $[Fe/H]$ is taken into account, the composition of a thin disc star expressed as $[X/Fe]$ is independent of the star’s age and birthplace for elements contributed in different proportions by massive stars (Type II SN), exploding white dwarfs (Type Ia SN), and asymptotic red giant branch stars.

By combining our sample with various published studies, comparisons between thin and thick disc stars are made. In this composite sample, thick disc stars are primarily identified by their V_{LSR} in the range -40 to -100 km s $^{-1}$. These are very old stars with origins in the inner Galaxy and metallicities $[Fe/H] \leq -0.4$. At the same $[Fe/H]$, the sampled thin disc stars have $V_{LSR} \sim 0$ km s $^{-1}$, and are generally younger with a birthplace at about the Sun’s Galactocentric distance. In the range $-0.35 \geq [Fe/H] \geq -0.70$, well represented by present thin and thick disc samples, $[X/Fe]$ of the thick disc stars is greater than that of thin disc stars for Mg, Al, Si, Ca, Ti, and Eu. $[X/Fe]$ is very similar for the thin and thick disc for – notably – Na, and iron-group elements. Barium ($[Ba/Fe]$) may be underabundant in thick relative to thin disc stars. These results extend previous ideas about composition differences between the thin and thick disc.

Key words: stars: atmospheric parameters – stars: abundances – stars: thick and thin disc – stars: kinematics – Galaxy: evolution – Galaxy: abundances

1 INTRODUCTION

Lower main sequence stars have lifetimes comparable to the age of the Galaxy and presumably atmospheric compositions that are essentially identical to those of their natal interstellar clouds. Spectroscopic and photometric analysis of these stars provides a sensitive probe of the major processes that

have shaped the chemical evolution of our Galaxy. This paper, which describes a survey of 181 F and G main sequence stars, was inspired by Edvardsson et al.’s (1993, hereafter EAGLNT) analysis of abundances for 13 elements for 189 F and G disc dwarfs with metallicities in the range $-1.1 \leq [Fe/H] \leq +0.25$. We sought to examine more closely several conclusions advanced by EAGLNT.

One conclusion concerned the variation of chemical composition with the distance of a star's birthplace from the Galactic centre. EAGLNT gave estimates of this distance (R_m) derived from a star's kinematics and a model of the Galactic potential. A striking dependence on R_m was found for the relative abundances of α -elements (Si and Ca) and iron. As was already known (cf. Lambert 1989; Wheeler, Sneden, & Truran 1989; McWilliam 1997), $[\alpha/\text{Fe}]$ increases with decreasing $[\text{Fe}/\text{H}]$, rising from $[\alpha/\text{Fe}] = 0$ at $[\text{Fe}/\text{H}] = 0$ to about 0.3 at $[\text{Fe}/\text{H}] = -1$. EAGLNT found that the trend of $[\alpha/\text{Fe}]$ with $[\text{Fe}/\text{H}]$ depends on R_m , being more marked for small R_m than large R_m . They interpreted this dependence of $[\alpha/\text{Fe}]$ on R_m at a given $[\text{Fe}/\text{H}]$ as due to an early rapid rate of star formation in the inner parts of the Galactic disk resulting in Type II supernovae dominating the enrichment of the interstellar gas to a greater extent than they did locally where the more slowly evolving Type Ia supernovae have been important contributors. Models of the Galactic chemical evolution have predicted abundance gradients of the kind inferred by Edvardsson et al. (e.g., Chiappani, Matteucci, & Gratton 1997).

Others have examined this and other of EAGLNT's conclusions. Fuhrmann (1998) finds that $[\text{Mg}/\text{Fe}]$ gets successively smaller in halo, thick disc, and thin disc stars, and there is a segregation of $[\text{Mg}/\text{Fe}]$ between two disc populations such that even at the same $[\text{Fe}/\text{H}]$ their $[\text{Mg}/\text{Fe}]$ are distinct. Chen et al. (2000), who analysed a sample of 90 F and G disc dwarfs for 13 elements, found a group of stars in the metallicity range $-1.0 \leq [\text{Fe}/\text{H}] \leq -0.6$ having small R_m (≤ 7 kpc) that are older than other disc stars and probably belong to the thick disc.

Our present survey covers 181 nearby F and G dwarfs observed with the McDonald Observatory's 2.7-m telescope and 2dcoudé spectrometer at a resolving power of about 60,000 with broad spectral coverage, and at S/N ratios of 300 to 400 for most stars. The wavelength coverage and S/N ratios are a significant improvement over EAGLNT's observations, which covered four or five spectral regions of 100 Å each at a S/N ratio of about 200. Also, EAGLNT's northern stars were observed at a resolving power of about 30,000, and only the southern stars were observed at the resolving power of 60,000. Our new spectra lead to more accurate abundances for more elements. Our analysis benefits also from the use of improved fundamental parameters for the stars. In particular, the effective temperatures are determined from the $b-y$ colour and a recent calibration based on the infrared flux method, while surface gravities come from a comparison of the stars' positions in the colour-magnitude diagram, which are precisely fixed by the *Hipparcos* parallaxes, with theoretical isochrones.

2 OBSERVATIONS

2.1 Stellar Spectra

Programme stars were selected from the *wby β* catalogue of Olsen (1983, 1988). Among the selection criteria were an effective temperature in the range 5600 K to 7000 K, and a surface gravity indicative of little or moderate evolution off the zero age mainsequence (ZAMS) (see Fig 1.).

All the observations were made at the Harlan J.

Smith 2.7-m telescope at McDonald Observatory, using the 2dcoudé echelle spectrometer (Tull et al. 1995) with a 2048×2048 pixel Tektronix CCD as detector. A resolving power of $\approx 60,000$ was attained. Spectral coverage was complete from 4000 to 5600 Å and substantial but incomplete from 5600 Å to about 9000 Å. In order to minimize the influence of cosmic rays, two observations in succession, rather than one longer observation, were generally made of each star. From about 5500 Å to about 9000 Å the extracted stellar spectra have a typical S/N ratio of about 400, while at wavelengths shorter than about 5500 Å the S/N ratio decreases with decreasing wavelength. We also observed the asteroid Iris in order to have a solar spectrum recorded under similar circumstances as the stellar spectra. The data were processed and wavelength calibrated in a conventional manner with the IRAF* reduction package. Double-lined spectroscopic binaries and broad-lined stars ($v \sin i \geq 20 \text{ km s}^{-1}$) were dropped from the programme. The remaining 181 stars were subjected to an abundance analysis, and are listed in Table 1.

Absorption lines suitable for measurement were chosen for having clean line profiles, as judged by inspection of the solar flux spectrum at extremely high resolving power and S/N ratio (Kurucz et al. 1984), that could be reliably measured in all, or most of, the programme stars. Moore, Minnaert, & Houtgast (1966) was our primary source for line identification. The equivalent width of each line was measured with the IRAF *splot* measurement option most suited to the situation of the line. This was usually the fitting of a single (or multiple) Gaussian profiles to the stellar line, but for stronger lines with significant damping wings a Voigt profile was used; for a few lines direct integration provided the best method of measurement and was preferred. Table 2 gives basic information for the selected lines; the list includes 170 lines of 27 elements. The spectrum of Iris, which was reduced and measured in the same manner as the programme stars, provided solar equivalent widths.

2.2 Stellar Kinematics

The space motions of the programme stars can be used to calculate their Galactic orbits. In order to determine the space motions we need the stellar distances, proper motions, and radial velocities.

Parallaxes and proper motions for nearly all the programme stars are available from the *Hipparcos* Catalogue (ESA 1997). All the stars in our sample are within 150 pc from the Sun, so their *Hipparcos* parallaxes are accurate; the average percentage error is 6.1 ± 3.2 . The proper motion errors are much less. For the few (7) programme stars not in the *Hipparcos* catalogue *wby β* photometry was used to calculate photometric distances following the prescriptions of EAGLNT. A comparison of photometric and *Hipparcos* distances showed that the average ratio $d(\text{phot})/d(\text{Hip})$ is 1.10 ± 0.15 (20 stars, standard deviation).

Accurate CORAVEL radial velocities have been taken from the survey of kinematical data for F-G dwarfs in the

* IRAF is distributed by the National Optical Astronomical Observatories, which is operated by the Association for Universities for Research in Astronomy, Inc., under contract to the National Science Foundation.

solar neighborhood by Pont et al. (1999). These data were kindly provided by J. Andersen prior to publication. The CORAVEL data show that 19 of the programme stars[†] have variable radial velocities, presumably a result of their membership in low-amplitude spectroscopic binary systems. Small corrections ($< 1 \text{ km s}^{-1}$) to the observed velocities due to gravitational or convective shifts were neglected.

The space velocities with respect to the Sun were then calculated. A solar motion $(-10.0, +5.2, +7.2) \text{ km s}^{-1}$ in (U, V, W) [‡], derived from *Hipparcos* data by Dehnen & Binney (1998), was adopted in adjusting the space velocities to be with respect to the Local Standard of Rest. Table 1 gives $(U_{\text{LSR}}, V_{\text{LSR}}, W_{\text{LSR}})$. Our space velocities may be compared with those of Chen et al. (2000) who use the same solar motion. For the 19 stars in common to our investigation and theirs, which are also in the *Hipparcos* catalogue and also show no sign of radial-velocity variation so their space velocities are based on identical proper motions and distances and very similar radial velocities, the (U, V, W) velocities agree to about 1 km s^{-1} , or better.

The Galactic orbital parameters, R_p and R_a (peri- and apogalactic distances), Z_{max} (maximum distance from the Galactic plane), and the e (orbital eccentricity) were computed using a Galactic potential integrator developed by D. Lin (1999, provided by Jon P. Fulbright with the kind permission of D. Lin).

In computing orbital parameters we have adopted the above solar space motion, a solar galactocentric distance of 8.5 kpc, and a solar circular velocity of 220 km s^{-1} . Grenon (1987) argues that $R_m = (R_p + R_a)/2$ is a likely stable quantity and, hence, a measure of a star's birthplace. In Table 1, we give the orbital parameters R_m , Z_{max} , and e .

We have only 3 stars in this study which are common with EAGLNT's sample. The orbital parameters derived in this study are different from EAGLNT's by $\leq 5\%$, except Z_{max} which differs by $\sim 25\%$. The differences become smaller ($\leq 2\%$) if we adopt the same values for the Sun as that of EAGLNT [EAGLNT used $(U, V, W) = (-10, +6, +6 \text{ km s}^{-1})$, 8.0 kpc for galactocentric distance, and 226 km s^{-1} for the solar circular velocity].

3 ANALYSIS

3.1 Introduction

Elemental abundances are derived from an LTE analysis of equivalent widths using the code MOOG (Snedden 1973). ATLAS9 (Kurucz 1998) plane-parallel, line-blanketed, flux-constant LTE model atmospheres with convective overshooting are used. The models are linearly interpolated for the appropriate values of the fundamental atmospheric param-

eters (T_{eff} , $\log g$, $[M/H]$ [§], ξ_t), which are determined independently of the spectroscopy. The effective temperatures T_{eff} and metallicities $[M/H]$ are derived from *uvby* β -photometry. The surface gravities g are determined from the comparison of the position of the star in the $(B - V) - M_V$ plane with calculations of stellar evolution, using *Hipparcos* parallaxes to determine M_V . The microturbulence ξ_t is set by an empirical relation between ξ_t , T_{eff} , and $\log g$ derived from spectroscopic analysis of a subset of the programme stars. The large number of lines available for elements such as iron allows an independent spectroscopic determination of T_{eff} and $\log g$, and, hence, a comparison of the photometric estimates of these quantities.

3.2 Selection of The Model Atmosphere Grid

Over the last decade we have witnessed exciting developments in stellar atmosphere modeling well beyond classical LTE one-dimensional models. Full NLTE structures (e.g. Hauschildt et al. 1999), LTE 3D time-dependent hydrodynamical models (e.g. Asplund et al. 2000), and 1.5D and 3D NLTE radiative transfer calculations (e.g. Shchukina & Trujillo Bueno 2001) are examples of the recent advances. Application of these modeling techniques to a large sample of stars, and elements is still unpractical for several reasons: the new models are available only for a few values of the atmospheric parameters; NLTE calculations with realistic model atoms are generally time consuming and, for some species, unreliable, due to uncertainties in the atomic data. Recent studies (Nissen et al. 2002; Chen et al. 2002) provide comparisons for some elements of abundances derived from 1D and 3D models. For stars with $[\text{Fe}/\text{H}]$, T_{eff} , and $\log g$ corresponding to our dwarfs, these authors find $[\text{O}/\text{Fe}]$, $[\text{S}/\text{Fe}]$, and $[\text{Si}/\text{Fe}]$ from 3D are lower by less than 0.04 dex than results from an equivalent 1D model. The differential effect on such abundance ratios across our sample of similar stars should be very small. Effects of replacing 1D models by 3D models may vary from element to element. While we are confident that the the situation will change in the near future, we have considered only well-tested flux-constant 1D model atmospheres: the MARCS models originally developed by Gustafsson et al. (1975), and the ATLAS9 models incorporating improvements to the treatment of convection and convective overshoot (Kurucz 1998). We also tested recently developed atmospheric models known as NEXTGEN models by Hauschildt, Allard, & Baron (1999).

In comparisons against observations of the Sun, the ATLAS9 solar model fares better than the MARCS solar model. This is clearly the case for limb darkening in the continuum at optical and near-infrared wavelengths (Blackwell et al. 1995). A better fit to limb darkening data is achieved with the empirical model atmosphere known as the Holweger-Müller (1967,1974) model; a not surprising result given that the model was derived in large part from limb darkening measurements. Models may also be compared by their ability to fit those Fe I lines having an accurately determined

[†] These stars are: HD 3454, 6840, 22521, 85902, 89010, 101472, 112756, 124819, 156635, 192145, 200580, 201444, 201639, 204559, 210718, 210985, 219497, 220908, and 225239.

[‡] In this study U is defined to be positive in the direction of the Galactic anticentre.

[§] The usual bracket notation is used throughout the paper for the abundance of an element M with respect to hydrogen $[M/H] = \log \frac{(N_M/N_H)_\star}{(N_M/N_H)_\odot}$ where, N represents number density.

gf -value from laboratory experiments. Iron abundances derived from lines of different lower excitation potential are less dependent on the lower potential in the case of the ATLAS9 than for the MARCS model (Blackwell et al. 1995). The empirical Holweger-Müller model, as revised by Grevesse & Sauval (1999), and the MISS (Allende Prieto et al. 2001a) empirical model, also return iron abundances that are independent of the lower excitation potential. Ionization equilibrium, as measured by the iron abundance derived from Fe I and Fe II lines, is well satisfied by the ATLAS9, and the Grevesse-Sauval or the MISS empirical models, but less well by the MARCS and NEXTGEN models. ATLAS9 models come in two flavors - with and without convective overshooting considered as part of the treatment of convection. Castelli et al. (1997) suggest that the model with overshooting (OVER model) reproduces observed properties (limb darkening etc.) of the Sun better than the model without overshooting (NOVER model).

Our choice of OVER ATLAS9 over MARCS models for the abundance analysis is based on the solar comparison. It should be noted, however, that almost all of the programme stars are within ± 500 K of the Sun's temperature. If the difference between an ATLAS9 and a MARCS model is partly attributable to the different treatments of line blanketing, the differences in abundances derived from them should be smaller for the typical star in our sample than they are for the Sun. Similarly, the small differences between NOVER and OVER ATLAS9 solar models will become even smaller for the programme stars where we are concerned with differential abundances relative to Sun. We comment below on the effects of replacing the preferred OVER with the NOVER models.

3.3 Fundamental Atmospheric and other Parameters

Three of the four parameters listed above are used to select a model from the OVER ATLAS9 grid. These - T_{eff} , $\log g$, and $[M/H]$ - are first determined from photometry, and checked subsequently against the spectroscopic analysis. Microturbulence, the fourth parameter, is only determined spectroscopically. In addition, it is not used in the selection of a model from the grid; the grid was computed for single value of the microturbulence ($\xi_t = 2.0 \text{ km s}^{-1}$) which is fairly representative of values determined here spectroscopically.

3.3.1 The Effective Temperature

The $uvby\beta$ photometry, especially the $b - y$ colour, is used to determine the T_{eff} . First, we must consider and, if necessary, correct for the effects of interstellar reddening. The programme stars are all within 150 pc of the Sun, with the majority within 100 pc. Interstellar reddening is negligible within 100 pc (Schuster & Nissen 1989). In order to check for reddening at greater distances we considered the average value and distribution of $E(b - y)$ for stars closer than 100 pc and likewise for the stars further away than 100 pc. $E(b - y)$ came from the observed $b - y$ and the unreddened $(b - y)_0$ derived from the β index, which is unaffected by reddening, together with Olsen's (1988) calibration.

For stars within 100 pc, the average $E(b - y)$ is very

small: $E(b - y) = -0.005 \pm 0.010 \text{ mag}$ from 170 stars, and the distribution is essentially Gaussian with the dispersion explained by the errors in the photometry. For the more distant 21 stars, $E(b - y)$ is positive: $E(b - y) = +0.010 \pm 0.013 \text{ mag}$, and the distribution is asymmetric with a tail of positive $E(b - y)$ caused by a few stars with significant reddening. In the light of these results, we assume that all of our programme stars are unreddened and use the observed $b - y$ to determine T_{eff} , except for 5 stars beyond 100 pc with significant reddening ($E(b - y) \geq 0.025$) for which we use the corrected $b - y$.[¶]

We use the calibration of Strömgren indices given by Alonso et al. (1996). This calibration, which uses a large number of lower main sequence stars and subgiants whose temperatures were measured by the infrared flux method, spans ranges of $4000 \text{ K} \leq T_{\text{eff}} \leq 7000 \text{ K}$ and $-2.5 \leq [\text{Fe}/\text{H}] \leq 0$, and is well suited to the programme stars. The calibration relates T_{eff} with $b - y$, c_1 , and $[\text{Fe}/\text{H}]$, with $b - y$ making the major contribution to the calibration and c_1 , the gravity sensitive index, and $[\text{Fe}/\text{H}]$ making minor contributions. To apply the calibration $b - y$ and c_1 were taken from Hauck & Mermilliod (1998), while $[\text{Fe}/\text{H}]$ values were estimated from Strömgren photometry (see below). (The effect of reddening on c_1 is negligible.) The error in the derived T_{eff} may come from different sources: uncertainties in the Strömgren photometry, reddening, and the calibration of the absolute flux in the infrared. Alonso et al. (1996) estimated an uncertainty of 1.5% (90 K) by taking into account both the systematic and accidental errors in the calibration.

3.3.2 The Surface Gravity

The surface gravity of a programme star is estimated by comparing its position in the colour-magnitude diagram with theoretical isochrones. This comparison provided the stellar masses and radii and, thus, the surface gravities. Isochrones were taken from Bertelli et al. (1994); they span all required stellar masses and metallicities. Allende Prieto & Lambert (1999) have used these isochrones similarly to determine fundamental parameters for stars in the *Hipparcos* catalogue within 100 pc.

Application of the method began by selecting the subset of isochrones with a metallicity immediately below that of the star's photometric metallicity. With this subset, we searched for those that reproduced the observed $B - V$ and M_V within the observational errors; $B - V$, V , and the parallax (p) were adopted from the *Hipparcos* catalogue. Then, the different possible solutions, corresponding to different masses and ages, were averaged to obtain mean values for the stellar parameters and an estimate of the uncertainty from the standard deviation. This procedure was then repeated for a subset of isochrones with a metallicity immediately above the star's photometric metallicity. The observational error box for a given star is defined by the uncertainty in the observed $B - V$ (which is taken from the *Hipparcos* catalogue or put at 0.01 mag, whichever is larger), and the M_V , as determined from the 1- σ errors in the parallax and V ,

[¶] The stars are HD 15398, HD 157467, HD 159972, HD 163363, and HD 213802.

$$\sigma^2(M_V) \simeq \sigma^2(V) + 25 \frac{\sigma^2(p)}{p^2} \log^2 e \quad (1)$$

assuming $\sigma(V) = 0.07$ mag to force a minimum error in M_V . Given that our sample satisfies $\sigma(p)/p < 0.1$ we neglected the small bias in M_V and $\sigma(M_V)$ introduced by the non-linear dependence of M_V on the parallax (e.g. Brown et al. 1997). In the majority of the cases, the error in M_V is dominated by the uncertainty in the parallax (as quoted in the *Hipparcos* catalogue). The estimated final errors for $\log g$ range from 0.03 to 0.10 dex.

3.3.3 Photometric Metallicity

The metallicity $[M/H]$ ^{||} was determined from the $b-y$, m_1 , and c_1 indices using either Equation 2 (for F stars) or Equation 3 (for G stars) of Schuster & Nissen (1989) with photometric data from Hauck & Mermilliod (1998). Using the quoted uncertainties in $(b-y)$, m_1 , and c_1 from Hauck & Mermilliod, we estimate an uncertainty of $\simeq 0.2$ dex in our photometric metallicity. Hauck & Mermilliod estimate a standard deviation of 0.16 dex in the $[Fe/H]$ derived from their calibration.

3.3.4 Microturbulence

Earlier studies of the microturbulence in the atmospheres of F and G dwarfs have shown that similar stars have very similar levels of microturbulence which depends weakly on T_{eff} and g (Nissen 1981). The microturbulence is determined spectroscopically from the condition that the abundance derived from lines of the same species should be independent of a line's equivalent width. Often, Fe I lines are used for obvious reasons.

We determined ξ_t for 87 of the 181 stars using 33 well defined Fe I lines with accurate gf -values (see below) and equivalent widths of up to about 80 mÅ. Results are well described by the relation

$$\xi_t = 1.28 + 3.3 \times 10^{-4} (T_{\text{eff}} - 6000) - 0.64 (\log g - 4.5) \quad (2)$$

where ξ_t is in km s^{-1} , and T_{eff} and g in their usual units. This relation is derived for a sample of stars which have T_{eff} ranging from 5650 K to 6300 K, $\log g$ ranging from 3.6 to 4.5, and metallicity of $-0.8 \leq [Fe/H] \leq 0.1$. The entire sample of our stars falls in the above range of T_{eff} , $\log g$, and $[Fe/H]$. Thus, we can safely use the above derived relation for the rest of the stars in our sample expecting $\sigma \approx 0.15 \text{ km s}^{-1}$, which is the *rms* error in the least-squares fit.

A similar linear regression has been used by others. Use of published formulae results in slightly different results. For example, adoption of EAGLNT's recipe gives a mean ξ_t that is about 0.2 km s^{-1} greater. Nissen's (1981) original expression returns greater values but by only 0.1 km s^{-1} . Chen et al. (2000) remark that their ξ_t are 0.3 km s^{-1} greater than EAGLNT's. Quite possibly, the lower values of ξ_t found here are due to our use of rather weak lines which are inherently

less sensitive to microturbulence. The difference is unimportant as far as the abundance analysis is concerned; a change of ξ_t by $\pm 0.25 \text{ km s}^{-1}$ changes the abundance of lines with equivalent widths of 50 mÅ or less by less than 0.01 dex. Even at 100 mÅ the abundance changes by no more than 0.04 dex.

3.3.5 Comparison of Photometry and Spectroscopy

As a check on the photometrically derived fundamental parameters we used Fe I and Fe II lines to determine T_{eff} and $\log g$ by the classical conditions that the Fe abundance be independent of the lower excitation potential for Fe I lines, and Fe I and Fe II lines yield the same abundance. Lines with reliable gf -values (see below), and equivalent widths less than 60 mÅ were used, a restriction that effectively eliminates the sensitivity to the microturbulence. About 25 - 30 Fe I and 4 Fe II lines were used.

Photometric and spectroscopic T_{eff} 's and metallicities $[Fe/H]$ are compared in Figure 2. On average, spectroscopic temperatures are hotter than their photometric counterparts by $71 \pm 47 \text{ K}$ with a hint that the difference is T_{eff} -dependent. For $[Fe/H]$, the mean difference between spectroscopic and photometric estimates is merely 0.05 ± 0.09 dex with no detectable trend over the range -0.2 to -0.8 in $[Fe/H]$.

Surface gravity is checked using Fe I-Fe II, and Cr I-Cr II lines. The comparison is made in Figure 3. It is seen that the neutral lines give a slightly lower abundance: $\log \epsilon(\text{Fe I}) - \log \epsilon(\text{Fe II}) = -0.02 \pm 0.05$ with just a hint of a dependence on $[Fe/H]$. Chromium gives a very similar result: $\log \epsilon(\text{Cr I}) - \log \epsilon(\text{Cr II}) = -0.04 \pm 0.06$. We conclude that the surface gravities do not introduce appreciable systematic errors into the abundance analysis. Reducing the differences to exactly zero calls for adjustments to the adopted atmospheric parameters that are within their estimated uncertainties given above. Additionally, the negative differences may signal departures from LTE effects, principally the overionization (relative to LTE) of the neutral atoms (see, e.g., Trujillo Bueno & Shchukina 2001).

3.4 Stellar Ages

We have estimated ages for the sample by comparison with the isochrones published by Bertelli et al. (1994). As most of our stars have already evolved off the main sequence, we can constrain their age very precisely. For some of the stars which are too close to the main sequence we can, at most, obtain upper limits. Our method resembles that described by Lachaume et al. (1999). Some aspects, however, are different, and therefore we describe it below.

We chose to use as observed quantities effective temperature and surface gravity. The isochrones describe these parameters as functions of the initial stellar mass M_i , the mass fraction of metals Z , and the age t . A Gaussian distribution of relative errors was assumed for both parameters by adopting a probability density

^{||} The photometric metallicity $[M/H]$ represents the elements heavier than H and He, particularly iron peak elements whose lines are numerous in the spectra

Table 1. Atmospheric parameters: T_{eff} , $\log g$, and $[\text{Fe}/\text{H}]$, and kinematic properties: U_{LSR} , V_{LSR} , W_{LSR} , R_{m} , Z_{max} , e , and age for the programme stars. See the appendix

Table 2. Line data used in the analysis. Wavelength (\AA), ion, low-excitation potential (eV), gf -value, measured solar equivalent width, and the references for the gf -values are given for each line. Table 2 is available electronically.

$$P(\log T_{\text{eff}}, \log g) \propto \exp \left[- \left(\frac{\log g - \log g^*}{\sqrt{2} \sigma(\log g)} \right)^2 \right] \exp \left[- \left(\frac{\log T_{\text{eff}} - \log T_{\text{eff}}^*}{\sqrt{2} \sigma(\log T_{\text{eff}})} \right)^2 \right], \quad (3)$$

which was used to determine the probability distribution for the age

$$P(\log t) = \iint P(\log T_{\text{eff}}, \log g) dM_i dZ. \quad (4)$$

In practice, to find the best age estimate for each star, we discretized the problem by sampling the isochrones of Bertelli et al. with constant steps of $0.006 M_{\odot}$ in the initial mass M_i , 0.05 in $\log t$ (t in years), and 0.125 in $\log Z$. We then converted the integral in Eq. 4 into a sum over the area confined by an ellipse centered at the adopted temperature and gravity (as listed in Table 1), with semi-major axes three times the estimated $1\text{-}\sigma$ uncertainties in $\log T_{\text{eff}}$ and $\log g$. We imposed an additional constrain to the possible solutions by requiring a metallicity within 0.25 dex from that spectroscopically determined.

Finally, the derived $P(\log t)$ was normalized and, whenever appropriate, fit with a Gaussian to derive the mean and a $1\text{-}\sigma$ uncertainty for the age of the star, which are included in Table 1. Figure 4 shows an example of the practical application to two well-known nearby stars, the Sun and Procyon A. The upper panels show the position of the star in the $\log T_{\text{eff}} - \log g$ plane. The dots are grid points within the $3\text{-}\sigma$ error bar ellipse, which therefore were included in the solution. In the lower panels, the probability density for the age is displayed, as well as a best estimate and $1\text{-}\sigma$ limits. Given the typical error bars for our sample, a star with the solar parameters is too close to the ZAMS to determine but an upper limit. For a star with the parameters of Procyon A (see, e.g. Allende Prieto et al. 2002a), it is possible to constrain the age very precisely – a case more representative of our sample regarding the evolutionary status. The ages derived in this study show a range consistent with those published by Chen et al. (2000) and EAGLNT for thin disc stars, but small differences are noticeable in Figure 8.

4 ATOMIC DATA

The critical atomic datum is the gf -value of a line. Our general procedure was to search the literature for accurate theoretical calculations or laboratory measurements of the

gf -values. Our search left gaps which were filled in various ways, including an inverted solar analysis.

References to the principal sources of data on gf -values for individual elements are given in Table 2. We comment here on the Fe I and Fe II gf -values because these lines play a special role in the abundance analysis, as already noted. Our search uncovered accurate gf -values for 33 of the 56 Fe I and 2 of the 8 Fe II lines in our lists of measured weak unblended stellar lines. In the case of the Fe I lines, these values come mainly from three sources (see references in Table 3). These and other sources were reviewed by Lambert et al. (1996) who remarked on their inter-agreement and suggested corrections to put all gf -values on a common scale. To obtain gf -values for the remaining Fe I and Fe II lines, we calculated astrophysical gf -values from the *solar* (Iris) spectrum using average abundances derived from Fe I and Fe II lines that have accurate theoretical or laboratory gf values.

We chose 9 Fe II lines that are unblended and measurable in most stars in the sample. For 3 of the Fe II lines (6369.46 \AA , 6432.68 \AA , and 7515.84 \AA) laboratory measured gf -values are available. For the Fe II line at 6369.46 \AA Heise & Kock (1990) measure $\log gf$ -value of -3.55 which is significantly higher than our derived solar value of -4.10 . Our derived value is in fair agreement with the predicted $\log gf$ -value of -4.25 (Kurucz 1998) and solar value of -4.36 (Blackwell, Shallis, & Simmons 1980). By adopting the laboratory gf -value, this line yields a lower abundance than the mean Fe abundance (7.42) derived from 6432 \AA and 7515 \AA . The 6369.46 \AA Fe II line appears to be blended with another Fe II line at 6369.375 \AA (Kurucz 1998), but, the blend’s contribution is negligible. For this line, we adopted the gf -value derived in this study (Table 3). A search for laboratory Fe II lines at $\lambda > 3000 \text{\AA}$ has been presented by Allende Prieto et al. (2002a). They noticed that Fe II 5234.6 \AA was measured by Kroll & Kock (1987) and Heise & Kock (1990). The re-scaled and averaged value (-2.23 ± 0.08) is in excellent agreement with our astrophysical determination (-2.22).

Astrophysical gf -values were also determined from the spectra of two of the programme stars: HD 145937 with $[\text{Fe}/\text{H}] = -0.55$, and HD 217877 with $[\text{Fe}/\text{H}] = -0.14$. The iron abundances and the model atmospheres were derived using the Fe I and Fe II lines with accurate experimental gf -values. For the Fe I and Fe II lines lacking measured or accurate theoretical gf -values, we have computed them by inverting the two stellar spectra, and using the mean Fe I and Fe II abundances, respectively. Finally, a mean of the solar and stellar gf -values were adopted. A similar procedure is adopted for the rest of the elements. Results are in Table 3.

In addition to the gf -values, hyperfine (hfs) and/or isotopic splitting must be considered for a few lines. Lines of Sc II, V I, and Co I are broadened by hfs but test calculations showed that the effect on the abundances is negligible for lines of the observed equivalent widths. This is not the case for the Mn I and Cu I lines. In these cases, equivalent widths were calculated from synthetic line profiles and abundance found by matching these widths to the observed values. For the Mn I lines, the data on the splitting and strengths of the hfs components were taken from Kurucz (1998). The lines show so much hfs that without this detailed treatment they would return erroneous abundances. In the case of the Cu I lines, the 5105 \AA line required thorough consideration of the

Table 3. Selection of gf -values for Fe I and Fe II lines. For lines lacking laboratory gf -values astrophysical gf -values are derived by inverting solar and stellar spectra. Last column gives the adopted gf -values.

Ion	W_λ (Å)	LEP (eV)	$\log gf$					Adopted
			Oxford ^a	Hannover ^b	Solar	Star1	Star2	
Fe I	5141.75	2.424			-2.194	-2.224	-2.256	-2.205
	5247.06	0.087	-4.946					-4.946
	5358.12	3.300			-3.170	-3.154		-3.162
	5412.79	4.440		-1.716				-1.716
	5661.348	4.280		-1.756				-1.756
	5778.458	2.590	-3.475	-3.430				-3.453
	5784.661	3.400		-2.532				-2.532
	5809.220	3.884	-1.609					-1.609
	5849.690	3.695	-2.935					-2.935
	5852.23	4.549			-1.181			-1.161
	5855.090	4.608		-1.478				-1.478
	5856.10	4.294			-1.561	-1.545		-1.548
	5858.79	4.220			-2.190			-2.180
	5859.60	4.550			-0.617	-0.581	-0.597	-0.588
	5862.37	4.550			-0.265	-0.302	-0.351	-0.293
	5956.700	0.859	-4.605					-4.605
	6027.06	4.070			-1.167		-1.104	-1.116
	6151.620	2.176	-3.299	-3.265	-3.286			-3.282
	6159.38	4.610			-1.837	-1.841	-1.783	-1.820
	6165.36	4.143			-1.461	-1.452	-1.473	-1.455
	6173.340	2.223	-2.880					-2.880
	6200.320	2.609	-2.437					-2.437
	6213.44	2.223			-2.542	-2.600	-2.592	-2.558
	6240.652	2.220		-3.233				-3.233
	6265.141	2.176	-2.550					-2.550
	6271.283	3.330		-2.703				-2.703
	6297.801	2.223	-2.740	-2.727				-2.734
	6322.694	2.588	-2.426					-2.426
	6358.69	0.859			-4.056	-4.120	-4.222	-4.113
	6436.41	4.186			-2.364	-2.319		-2.342
	6481.878	2.279	-2.972					-2.972
	6498.950	0.958	-4.699					-4.699
	6518.374	2.830		-2.450				-2.450
	6574.233	0.990	-5.004					-5.004
	6581.214	1.480		-4.680				-4.680
	6591.33	4.593			-1.949	-1.873		-1.911
	6608.04	2.279			-3.913	-3.929	-3.929	-3.924
	6625.027	1.010	-5.336					-5.336
	6699.142	4.590		-2.101				-2.101
	6713.75	4.795			-1.389	-1.367	-1.367	-1.374
	6725.36	4.103			-2.158	-2.149	-2.195	-2.167
	6739.524	1.560		-4.794				-4.794
	6750.160	2.424	-2.621					-2.615
	6752.711	4.640		-1.204				-1.204
	6837.009	4.590		-1.687				-1.687
	6733.15	4.638			-1.400			-1.390
	6857.25	4.076			-2.040	-2.025		-2.028
	6971.936	3.020		-3.340				-3.340
	7112.173	2.990		-2.990				-2.990
	7751.12	4.990			-0.727	-0.704	-0.666	-0.692
	7802.51	5.080			-1.332	-1.294	-1.274	-1.300
	7807.92	4.990			-0.492	-0.499	-0.525	-0.499
	8365.644	3.250		-2.037				-2.037
	8757.200	2.845	-2.118					-2.118

Table 3 – *continued*

Ion	W_λ (Å)	LEP (eV)	$\log gf$					
			Oxford ^a	Hannover ^b	Solar	Star1	Star2	Adopted
Fe II 5234.620	3.221			-2.22			-2.22	
	5425.26	3.200			-3.246	-3.187	-3.129	-3.177
	6149.25	3.889			-2.713	-2.737	-2.611	-2.680
	6247.56	3.892			-2.341	-2.329	-2.204	-2.281
	6369.46	2.891			-4.100	-4.083	-4.043	-4.072
	6432.680	2.891		-3.520				-3.520
	6456.39	3.903			-2.124	-2.146		-2.115
	7479.700	3.892			-3.602	-3.640	-3.517	-3.586
	7515.840	3.903		-3.407				-3.42 ^c

^a gf -values measured at Oxford (Blackwell et al. 1995 and references therein)

^b gf -values measured at Hannover (Bard et al. 1991; Bard & Kock 1994)

^c Mean of gf -values measured by Hannaford et al. (1992) and Hiese & Kock (1990)

hfs and isotopic splitting: the hfs data were taken from Kurucz (1998) and the isotopic ratio was assumed to be the solar system value for all stars ($^{63}\text{Cu}/^{65}\text{Cu} = 2.24$). The effect of the hfs on the final abundances can be as large as 0.6 dex for the stronger Mn lines where the spacing between hfs components is large. In the case of the 6021 Å Mn line and the 5218 Å Cu line, the separation between the components is very small.

5 THE SOLAR ABUNDANCES

The spectrum of Iris for the Sun was treated in the same way as the programme spectra, using an ATLAS9 model for the accepted solar parameters $T_{\text{eff}} = 5780$ K, $\log g = 4.44$, and a solar composition ($\log \epsilon(\text{Fe}) = 7.50$ was adopted). Equivalent widths were measured for the lines in Table 2. The microturbulence adopted was $\xi_t = 1.22$ km s⁻¹, which was derived using the Fe I lines having accurate gf -values. Analysis of the iron lines returned the parameters $T_{\text{eff}} = 5760 \pm 50$ K, $\log g = 4.44 \pm 0.10$ and $\log \epsilon(\text{Fe}) = 7.45 \pm 0.06$. The parameters, T_{eff} and $\log g$ are within their uncertainty, equal to the accepted values. The derived solar Fe abundance $\log \epsilon(\text{Fe}) = 7.45 \pm 0.05$ is close to the Grevesse & Sauval photospheric value of $\log \epsilon(\text{Fe}) = 7.50 \pm 0.05$. The difference of 0.05 dex is partly attributable to the use of different model atmospheres. Replacing ATLAS9 by Holweger-Müller, the abundance increases to $\log \epsilon(\text{Fe}) = 7.53$.

Elemental abundances derived for the Sun from lines with adopted gf -values, and equivalent widths measured from the *solar* Iris spectrum (Table 2) are summarized in Table 4. Agreement with the solar photospheric abundances given by Grevesse & Sauval (1998) was taken as evidence of reliable gf -values. Their analysis uses an empirical solar model atmosphere and this difference in models introduces small differences in the abundances derived from identical sets of atomic data. In general, our results from a few lines are in good agreement with standard results from usually more lines.

6 STELLAR ABUNDANCES

Elemental abundances for all the programme stars were determined using the OVER ATLAS9 model computed for the

Table 4. The adopted solar abundances derived by employing the Kurucz (1998) solar model in this study are compared with the photospheric solar abundances from the literature (Grevesse & Sauval 1998). The values in the brackets are the standard deviations for the species represented by 3 or more lines.

Species	no. of lines	$\log \epsilon(X)$		Diff.
		This study	Literature	
C I	5	8.51 (0.06)	8.39 ^a	0.12
N I	2	8.06	7.92	0.14
O(7774)	3	8.86 (0.05)	8.69 ^a	0.17
[O I]	1	8.73	8.69	0.04
Na I	2	6.27	6.33	-0.06
Mg I	3	7.54 (0.06)	7.58	-0.04
Al I	5	6.28 (0.05)	6.47	-0.19
Si I	7	7.62 (0.05)	7.55	-0.07
Si II	1	7.64	7.55	-0.09
S I	3	7.34(0.09)	7.33	0.01
K I	1	5.22	5.12	0.10
Ca I	5	6.33 (0.07)	6.36	-0.03
Sc II	3	3.24 (0.14)	3.17	-0.07
Ti I	7	4.90 (0.06)	5.02	-0.12
V I	6	3.93 (0.03)	4.00	-0.07
Cr I	4	5.68 (0.07)	5.67	0.01
Cr II	1	5.65	5.67	-0.02
Mn I	3	5.37 (0.05)	5.39	-0.02
Fe I	56	7.45 (0.04)	7.50	-0.05
Fe II	9	7.45 (0.07)	7.50	-0.05
Co I	3	4.93 (0.04)	4.92	0.01
Ni I	18	6.23 (0.04)	6.25	-0.02
Cu I	3	4.19 (0.05)	4.21	-0.02
Zn I	2	4.47	4.60	-0.13
Sr I	1	2.64	2.97	-0.35
Y II	4	2.12 (0.04)	2.24	-0.12
Zr II	1	2.45	2.60	-0.15
Ba II	3	2.20 (0.10)	2.13	0.07
Ce II	3	1.58 ^b	1.58	0.00
Nd II	2	1.50 ^b	1.50	0.00
Eu II	1	0.61	0.51	0.10

^a Carbon and oxygen abundances are taken from Allende Prieto et al. (2001b, 2002b)

^b The gf -values are derived by inverting the solar spectrum using the literature solar abundance

Table 5. Elemental abundance for elements from C to Ti relative to Fe for the programme stars. See the Table in appendix

Table 6. Elemental abundance for elements from V to Eu relative to Fe for the programme stars. See the Table in Appendix

T_{eff} and $\log g$ derived from the photometry and *Hipparcos* parallaxes, respectively. Adopted model parameters, and the gf -values are given in Table 2. The stellar abundance results are referenced to the solar abundances determined in the current study (Table 4) using the same lines, and a similar procedure as for the programme stars, i.e., we derive and discuss differential abundances $[X/H]$ and $[X/Fe]$. Abundances relative to iron for the entire sample are presented in Table 5 and Table 6. Before discussing astrophysical implications of our results, we assess their accuracy, and present a few comparisons with some recent analyses of F-G disc dwarfs.

6.1 Internal Assessment of the Errors

This assessment of the errors afflicting the derived abundances is made without questioning the assumptions in the approach (i.e., LTE is accepted as valid). In what is now a standard procedure, we calculate the effect on the abundances of the errors in the observed equivalent widths, the defining model atmosphere parameters, and the atomic data.

6.1.1 Equivalent Widths

On a typical spectrum, the accuracy of an equivalent width W_λ is about 2 mÅ. This estimate arrived at from independent attempts to measure a given line is roughly consistent with the prescription given by Cayrel (1988):

$$\Delta W_\lambda = \frac{1.6\sqrt{w\delta x}}{S/N} \quad (5)$$

where w is the FWHM of the line, δx is the pixel size in Å, and S/N is the signal-to-noise ratio per pixel in the continuum. For our spectra, w is in the range 0.15 Å to 0.25 Å, $\delta x = 0.041$ Å, and $S/N \simeq 200$ to 400. These parameters give $\Delta W_\lambda \simeq 0.4$ mÅ to 0.9 mÅ. Given that the recipe does not consider blends and the normalization to a local continuum, our adoption of a 2 mÅ limit is reasonable. For elements represented by more than one line, there is a reduction of the abundance error arising from the measurement error of the W_λ s. We suppose that the reduction scales as \sqrt{N} , where N is the number of lines, down to a minimum value.

An external check is possible using our measurements of the Iris (solar) spectrum with those from lunar/day sky spectra by EAGLNT and Chen et al. We have 47 lines in common with EAGLNT and 59 with Chen et al. Equivalent widths are compared in Figure 5 (upper panels). The solar abundance differences using a common model and atomic data are shown in the lower panels of Figure 5. EAGLNT's W_λ s are on average 1.4 mÅ smaller than ours. Chen et al.'s measurements are close to ours: the mean difference in W_λ is just 0.3 mÅ. Our stellar spectra are typically of the quality of the Iris spectrum.

6.1.2 Atmospheric Parameters

In Section 3.3, we derived the atmospheric parameters and discussed their uncertainties concluding that $\Delta T_{\text{eff}} \simeq \pm 100$ K, $\Delta \log g \simeq \pm 0.1$, $\Delta \xi_t \simeq \pm 0.25$ km s⁻¹, and $\Delta [M/H] \simeq \pm 0.2$. Assuming that the effects of these errors on the derived abundances are uncorrelated for the small range of the various Δ s, it is a simple matter to determine their effect on the abundances. We have done this for a sample of stars spanning the parameters range of the entire sample. Predicted values of the total abundance uncertainty are summarized in Table 7.

6.2 External Errors

Before making intercomparisons of our abundances with earlier studies, we compare the abundances derived from the adopted Kurucz OVER models with those derived from NOVER models. For 16 stars in our sample, spanning the full range of T_{eff} and $[Fe/H]$ of the sample, we recomputed abundance ratios $[X/Fe]$ using the same atmospheric parameters, but with NOVER models. The abundance differences from OVER and NOVER models are very small (see Figure 6 for representative elements). In the case of high excitation lines (see $[C/Fe]$ and $[O/Fe]$), there appears to be a trend of the abundance difference with $[Fe/H]$ which is possibly due to the fact that these excited lines are formed deep in the atmosphere where differences between OVER and NOVER models are larger. Differences may be overestimated, as we have used atmospheric parameters and gf -values derived from OVER models in computing abundances from NOVER models.

Chen et al.'s sample of 90 F-G dwarfs includes 23 from our collection. Intercomparison of their and our results offers a check on our results, but it must be deemed incomplete in that the methods of analysis are very similar. First, we note that there is close agreement over the adopted atmospheric parameters. In the sense Chen – ours, we find $\Delta T_{\text{eff}} = 7 \pm 42$ K, $\Delta \log g = 0.04 \pm 0.13$, $\Delta [Fe/H] = -0.02 \pm 0.06$, and $\Delta \xi_t = 0.39 \pm 0.22$ km s⁻¹. This broad agreement reflects the similarity in the approaches to the determination of atmospheric parameters. For example, both studies use ($b - y$) and Alonso et al.'s calibration to obtain T_{eff} .

Second, there is good agreement over the derived abundances for elements in common. Both studies adopt a differential approach using the solar spectrum. There is partial overlap in the lists of selected lines. Model grids differ: Chen et al. used new MARCS models, and we used the OVER ATLAS9 models. In this initial comparison, we consider the mean differences between the two studies. Later, we comment on a few specific elements. Mean abundance differences from the 23 stars are given in Table 8. These small zero-point differences likely arise from a combination of factors: differences in the adopted solar equivalent widths, use of different grids of model atmospheres for the Sun and the programme stars, and selection of different lines with differing sensitivity to the various atmospheric parameters. We apply the appropriate zero-point difference in cases where we combine Chen et al.'s results with ours as a way to increase the sample size.

A direct comparison was made with EAGLNT's results for 3 stars (HD 69897, HD 216385, and HD 218470) that are in common with the present study. EAGLNT's

Table 7. Abundance uncertainties due to estimated uncertainties in atmospheric parameters for five representative stars. The σ 's are quadratic sum of variations in abundance ratios, $[X/Fe]$, due to uncertainties in model parameters. The column σ_{mod} , is the mean of σ 's and the quoted error *std* is the standard deviation.

	HD 70	HD 94385	HD 9670	HD 6834	HD 112887	
T_{eff}	5649 K	5814 K	6032 K	6290 K	6422 K	
$[Fe/H]$	-0.5	0.01	-0.30	-0.70	-0.30	
	σ_1	σ_2	σ_3	σ_4	σ_5	$\sigma_{mod} \pm std$
$[Fe/H]$	0.09	0.08	0.08	0.06	0.06	0.07±0.01
$[C/Fe]$	0.18	0.17	0.14	0.09	0.14	0.14±0.04
$[N/Fe]$...	0.20	0.17	0.19
$[O/Fe]$	0.20	0.17	0.15	0.14	0.13	0.16±0.03
$[Na/Fe]$	0.04	0.03	0.04	...	0.02	0.03±0.01
$[Mg/Fe]$	0.01	0.06	0.02	0.04	0.02	0.03±0.02
$[Al/Fe]$	0.05	0.05	0.04	0.03	0.03	0.04±0.01
$[Si I/Fe]$	0.08	0.06	0.05	0.03	0.02	0.05±0.02
$[S/Fe]$...	0.08	0.08	...	0.11	0.09±0.02
$[K/Fe]$	0.07	0.09	0.08	0.08±0.01
$[Ca/Fe]$	0.02	0.04	0.02	0.01	0.04	0.03±0.01
$[Sc/Fe]$	0.14	0.13	0.11	0.09	0.08	0.11±0.03
$[Ti/Fe]$	0.04	0.04	0.03	0.02	0.02	0.03±0.01
$[V/Fe]$	0.05	0.04	0.03	...	0.03	0.04±0.01
$[Cr/Fe]$	0.02	0.03	0.01	...	0.00	0.02±0.01
$[Mn/Fe]$	0.03	0.06	0.02	0.01	0.01	0.03±0.02
$[Co/Fe]$	0.03	0.02	0.02	...	0.01	0.02±0.01
$[Ni/Fe]$	0.03	0.03	0.02	0.01	0.01	0.02±0.01
$[Cu/Fe]$	0.02	0.03	0.01	0.02	0.03	0.02±0.01
$[Zn/Fe]$	0.08	0.06	0.05	0.03	0.02	0.05±0.02
$[Sr/Fe]$	0.02	0.05	0.01	0.03±0.02
$[Y/Fe]$	0.09	0.12	0.10	0.08	0.08	0.09±0.02
$[Zr/Fe]$...	0.12	0.11	...	0.08	0.10±0.02
$[Ba/Fe]$	0.12	0.13	0.11	0.13	0.12	0.12±0.01
$[Ce/Fe]$	0.12	0.12	0.10	...	0.08	0.11±0.02
$[Nd/Fe]$...	0.12	0.10	...	0.07	0.10±0.03
$[Eu/Fe]$	0.12	0.13	0.10	...	0.08	0.11±0.02

T_{eff} and $\log g$ are found to be greater than our values by 96 ± 41 K and 0.13 ± 0.07 dex, respectively. The difference in T_{eff} and $\log g$ can possibly be attributed to differences in adopted methods: EAGLNT determined both the T_{eff} and $\log g$ using Strömgren indices. The differences in abundance ratios, $[X/Fe]$, are small (< 0.1 dex). For a more reliable transformation of EAGLNT's abundances to our scale, we take advantage of the fact that Chen et al.'s selection of stars included 26 from EAGLNT. The principal difference in the adopted atmospheric parameters is in the effective temperatures for which the difference in the sense Chen - EAGLNT is -88 ± 56 K. Other differences are quite minor: $\Delta \log g = -0.07 \pm 0.08$, and $\Delta [Fe/H] = -0.02 \pm 0.07$. Abundance differences Chen - EAGLNT (see Table 2 of Chen et al.) are small. The abundance differences Chen - ours and EAGLNT - ours are given in Table 8.

7 CHEMICAL EVOLUTION OF THE DISC

Several signatures of chemical evolution of the Galactic disc may be looked for using our data. Here, we comment briefly on the age-metallicity relation, aspects of the evolution of the relative abundances (i.e., $[X/Fe]$ versus $[Fe/H]$), the scatter in relative abundances at a fixed $[Fe/H]$, and the difference in compositions of thick and thin disc stars.

Table 8. Average differences of atmospheric parameters and abundances for 24 stars that are found to be common with Chen et al. (2000), and differences between EAGLNT and ours (see the text for details).

Quantity	Chen-Ours	σ	EAGLNT - Ours	σ
T_{eff} (K)	7	42	77	41
$\log g$ (cm s ⁻²)	0.04	0.13	0.13	0.07
ξ_t (km s ⁻¹)	0.39	0.22	0.19	—
$[Fe I/H]$	-0.02	0.06	-0.01	0.04
$[Fe II/H]$	0.01	0.09	0.01	0.03
$[Na I/Fe]$	-0.09	0.06	-0.01	0.03
$[Mg I/Fe]$	0.06	0.04	0.08	0.09
$[Al I/Fe]$	-0.11	0.07	-0.07	0.08
$[Si I/Fe]$	0.01	0.03	0.03	0.02
$[K I/Fe]$	-0.05	0.05
$[Ca I/Fe]$	0.06	0.03	0.01	0.02
$[Ti I/Fe]$	0.01	0.07	0.11	0.09
$[V I/Fe]$	0.03	0.07
$[Cr I/Fe]$	0.03	0.05
$[Ni I/Fe]$	0.04	0.02	0.04	0.03
$[Ba II/Fe]$	0.06	0.08	0.03	0.02

Our sample is nearly homogeneous being comprised of thin disc stars to the almost total exclusion of thick disc representatives (see below for our definition of the thick disc).

Furthermore, our sample was selected to cover only a part of the $[\text{Fe}/\text{H}]$ range spanned by thin disc stars. As appropriate, we combine our data with published results.

7.1 Age-Metallicity Relation

EAGLNT's age-metallicity relation which hinted at a slow drop in metallicity with increasing age of the star was marked by a large spread in metallicity at a fixed age. Our sample taken at face value offers a cleaner relation – see Figure 7 where the relation is shown for $[\text{Ca}/\text{H}]$, $[\text{Fe}/\text{H}]$, and $[\text{Ba}/\text{H}]$. Figure 8 shows this relation with earlier results from Chen et al. and EAGLNT with their marked scatter in $[\text{Fe}/\text{H}]$ at a fixed age. The appearance of a cleaner age-metallicity relation is attributable to two selection effects. First and more important, we chose stars in a restricted $[\text{Fe}/\text{H}]$ range and, in particular, $[\text{Fe}/\text{H}] > -0.2$ are poorly represented. Second, our sample is kinematically homogeneous to the almost complete exclusion of thick disc stars. In short, we support earlier conclusions that the age-metallicity relation offered directly by local thin and thick disc stars is characterized by a large scatter about a slow monotonic decrease of metallicity with increasing age.

7.2 Relative Abundances

In discussing the variation of $[\text{X}/\text{Fe}]$ versus $[\text{Fe}/\text{H}]$ (Figures 9, 10 & 11), we begin by making brief comparisons with published results, principally those from the recent extensive surveys of disc F and G dwarfs by EAGLNT, Feltzing & Gustafsson (1998), Fulbright (2000), and Chen et al. over the common interval in $[\text{Fe}/\text{H}]$. Note that our stars sample well the interval $[\text{Fe}/\text{H}] \simeq -0.1$ to -0.6 . EAGLNT's stars covered a slightly broader range ($[\text{Fe}/\text{H}] = -0.8$ to $+0.2$) with Feltzing & Gustafsson adding metal-rich stars ($[\text{Fe}/\text{H}] = 0.0$ to $+0.2$). EAGLNT considered O, Na, Mg, Al, Si, Ti, Fe, Ni, Y, Zr, Ba, and Nd. Chen et al. provided good coverage for $[\text{Fe}/\text{H}] = -1.0$ to $+0.1$ for O, Na, Mg, Al, Si, K, Ca, Ti, V, Cr, Ni, and Ba. Fulbright (2000) analysed a sample of disc and halo stars with a wide range in T_{eff} , $\log g$, and metallicity, and provided abundances for 13 elements (Na, Mg, Al, Si, Ca, Ti, V, Cr, Ni, Y, Zr, Ba, and Eu). From his study we have selected 77 disc dwarfs/subgiants that have $-1.0 \geq [\text{M}/\text{H}] \leq +0.2$, and $3.8 \leq \log g \leq 5.0$. For elements (C, N, S, Sc, Mn, Co, Cu, Zn, and Ce) not covered by these surveys, we compare with other studies.

For many elements, inspection of the plots of $[\text{X}/\text{Fe}]$ versus $[\text{Fe}/\text{H}]$ shows that published results differ from ours by only a small zero-point correction. Table 8 lists the zero-point corrections between Chen et al. and us, and EAGLNT and us. Since we have only 3 stars in common with EAGLNT, we infer the mean zero-point correction between our and EAGLNT's results by combining the corrections between Chen et al. and us, and Chen et al. and EAGLNT. Each of the three analyses is a differential analysis conducted relative to the Solar spectrum. Given that theories of Galactic chemical evolution should not pretend to challenge observations at the 0.1 dex level, we shall not attempt to pin down the origins of the zero-point corrections; possible sources of a zero-point difference were discussed above. For applications where the largest possible sample size may be useful,

we shall apply the zero-point correction to place published results on our system of abundances.

Our results are in good agreement for elements common with EAGLNT. The trends of $[\text{X}/\text{Fe}]$ versus $[\text{Fe}/\text{H}]$ are identical for O, Na, Mg, Al, Si, Ca, Ti, Ni, and Ba. Differences may be noticeable for Y, and Zr. In the case of Y and Zr, we find $[\text{X}/\text{Fe}]$ to decline slightly with decreasing $[\text{Fe}/\text{H}]$, but EAGLNT found either no (Y) or an opposite trend (Zr). The most striking differences with respect to EAGLNT are not in the trends but in the scatter about a mean trend. Most notably, the scatter found here is considerably smaller than reported by EAGLNT for Mg, Al, and Ti, especially at $[\text{Fe}/\text{H}] \leq -0.4$. The scatter in $[\text{X}/\text{Fe}]$ for these and other elements is discussed below.

There is also very good agreement with Chen et al.'s results. After allowing for a small zero-point difference, two differences are noted. First, there is a small but distinct difference between our (and EAGLNT's) and Chen et al.'s run of $[\text{Al}/\text{Fe}]$ versus $[\text{Fe}/\text{H}]$: we find $[\text{Al}/\text{Fe}]$ to increase slightly with decreasing $[\text{Fe}/\text{H}]$, but Chen et al. find an initial decrease from $[\text{Al}/\text{Fe}] \simeq +0.15$ at $[\text{Fe}/\text{H}] = 0$ to $[\text{Al}/\text{Fe}] \simeq -0.1$ at $[\text{Fe}/\text{H}] \simeq -0.4$ from which point $[\text{Al}/\text{Fe}]$ may increase slightly. Second, there are elements for which the analyses agree about the trends but give different results for the scatter in $[\text{X}/\text{Fe}]$ at a fixed $[\text{Fe}/\text{H}]$: notably, Cr for which Chen et al. report a flat trend but with stars spanning the range $[\text{Cr}/\text{Fe}] \simeq -0.1$ to $+0.2$ in contrast to our results (Figure 10).

Remarks on $[\text{X}/\text{Fe}]$ versus $[\text{Fe}/\text{H}]$ are offered for those elements not covered by either EAGLNT or Chen et al. Our reference is usually to the most recent work on an element. The elements in question are C, N, S, Sc, Mn, Co, Cu, Zn, Ce, and Eu. Oxygen is also discussed.

Carbon: Our results are in good agreement with abundances derived by Gustafsson et al. (1999) from the 8727 Å $[\text{C I}]$ line in 80 stars of EAGLNT's sample. We confirm the increase of $[\text{C}/\text{Fe}]$ with decreasing $[\text{Fe}/\text{H}]$. Scatter about the mean trend is larger from our C I lines than from the forbidden line, a difference attributed to the different sensitivities of the lines to the atmospheric parameters. The slight offset – our $[\text{C}/\text{Fe}]$ are larger by about 0.03 dex – is in line with the systematic difference in the adopted T_{eff} s.

Tomkin et al.'s (1995) analysis of C I lines in 105 of EAGLNT's stars gave a very similar slope for the $[\text{C}/\text{Fe}]$ – $[\text{Fe}/\text{H}]$ relation as found by us and by Gustafsson et al. but Tomkin et al.'s results are offset to lower $[\text{C}/\text{Fe}]$ by about 0.15 dex from ours. This offset arises because EAGLNT's T_{eff} scale is about 80 K hotter than ours.

Nitrogen: Atomic nitrogen is represented in spectra of F-G dwarfs by weak N I lines. Our $[\text{N}/\text{Fe}]$ values show considerable scatter at a fixed $[\text{Fe}/\text{H}]$, which is largely attributable to the weakness of the two N I lines, and the T_{eff} sensitivity of the derived abundances. At those metallicities ($[\text{Fe}/\text{H}] \simeq -0.2$) well represented in our sample, $[\text{N}/\text{Fe}]$ is about 0.2, which implies that, if $[\text{N}/\text{Fe}] = 0$ at $[\text{Fe}/\text{H}] = 0$, $[\text{N}/\text{Fe}]$ increases as $[\text{Fe}/\text{H}]$ falls below the solar value. The N I lines are not detectable in our stars with $[\text{Fe}/\text{H}] \leq -0.4$.

A selection of N I lines was used previously by Clegg, Lambert, & Tomkin (1981) to measure $[\text{N}/\text{Fe}]$ in 15 stars over the $[\text{Fe}/\text{H}]$ spanned by our stars to give $[\text{N}/\text{Fe}] \simeq 0.0$, a value smaller than ours by about 0.2 dex. Considering the similar sensitivities of the C I and N I lines to the adopted atmospheric parameters, $[\text{N}/\text{C}]$ is robustly model-

independent. Our result $[N/C] \simeq 0$ is consistent with that given by Clegg et al.

Oxygen: The forbidden $[O\text{I}]$ 6300 Å line in our spectra falls near the gap between the spectral orders and the line can be measured reliably only in stars where lines are blue-shifted. This and the weakness of the line limited us to measure the 6300 Å line in 60 stars ranging in metallicity from 0.0 to -0.5 dex. In analyzing the W_λ of 6300 Å we have considered the blend caused by a Ni I line at 6300.335 Å with the gf -value reported by Allende Prieto, Lambert & Asplund (2001b). The effect of the blend on the $[O\text{I}]$ abundance is significant, especially in stars of solar-metallicity. The abundance ratio $[O/Fe]$ is found to increase with decreasing $[Fe/H]$, in general agreement with other studies where the blend was recognized (Nissen et al. 2002).

Oxygen abundances also come from the relatively strong infrared triplet at 7775 Å. The strength of these lines allowed us to derive oxygen abundance for all the stars in our sample. Direct LTE analysis of these lines give $[O/Fe]$ values noticeably greater than from the $[O\text{I}]$ 6300 Å line, a discrepancy attributed to non-LTE effects on the permitted lines (Kiselman 1993). In order to extend the $[O/Fe]$ results to lower $[Fe/H]$ than possible with the $[O\text{I}]$ line, we derive the following empirical correlation from stars for which O I and $[O\text{I}]$ lines are analysed:

$$[O/Fe]_{6300} = [O/Fe]_{7775} + 0.1138 \times [Fe/H] - 0.5425 \times \log T_{\text{eff}} + 0.0925 \log g + 1.4891 \quad (6)$$

with an *rms* scatter of 0.11 dex. This equation is used to correct the $[O/Fe]$ from the 7775 Å to the scale of the forbidden line. Our final results for $[O/Fe]$ are shown in Figure 9.

Direct comparisons with the majority of the published analyses of the $[O\text{I}]$ lines are compromised by their neglect of the Ni I blending line. Our results are in fair agreement with Nissen et al. (2002).

Sulphur: Recently, Chen et al. (2002) reported S abundances for a sample of 26 disc stars. Our current results, based on 3 S I lines that are common with Chen et al (2002), in general, agree with their results. However, the scatter appears higher in our data. A difference between Chen et al. (2002) and our analysis is the $[S/Fe]$ offset from $[S/Fe] = 0$ even at $[Fe/H] \sim 0$. We discuss below the possible reasons for the small offsets.

Potassium: In spite of a large scatter, a weak trend of increasing K abundance with decreasing $[Fe/H]$ is noticeable (see Fig 9).

Scandium: Nissen et al. (2000) obtained Sc abundances for stars in the Chen et al. sample. These were revised by Prochaska & McWilliam (2000) using accurate hyperfine splittings for the Sc II lines. The revised results in the common $[Fe/H]$ interval are in good agreement with ours. Inspection of Figure 10 shows that Sc, as noted by Nissen et al. but disputed by Prochaska & McWilliam, behaves like the α -elements Ca and Ti. This similarity may not hold for stars with $[Fe/H] < -1$ (Prochaska & McWilliam 2000; Gratton & Sneden 1991).

Manganese: A decrease of the Mn abundance (relative to Fe) for decreasing $[Fe/H]$ was noted by Beynon (1978), explored with high quality spectra of a few stars by Gratton (1989), and defined for F-G disc dwarfs by Nissen et al.

(2000) and Prochaska & McWilliam (2000). For $[Fe/H] > -0.6$, the limit of our sample, the $[Mn/Fe]$ measured by us and by Prochaska & McWilliam are in good agreement as to slope and absolute value.

Cobalt: Data on cobalt in F-G disc dwarfs is especially sparse. Gratton & Sneden (1991) obtained $[Co/Fe] \simeq -0.1$ from a few stars in our $[Fe/H]$ range. This early result is consistent with ours.

Copper: Our results show little variation of $[Cu/Fe]$ with $[Fe/H]$. Earlier discussions have focussed on the run of $[Cu/Fe]$ with $[Fe/H]$ for halo stars for which $[Cu/Fe]$ declines steadily for decreasing $[Fe/H]$ (Sneden, Gratton, & Crocker 1991): $[Cu/Fe] = 0.38[Fe/H] + 0.15$. This slope is at odds with our results, but close inspection of the few results available to Sneden et al. for stars with $[Fe/H] > -1$ shows that a change of slope might have been anticipated.

Zinc: This element appears to behave similarly to the α -elements; $[Zn/Fe]$ increases slightly with decreasing $[Fe/H]$. This result is consistent with Sneden et al.'s (1991) analyses of Zn in disc and halo dwarfs and giants which gave $[Zn/Fe]$ constant ($= 0.04$) from $[Fe/H] = -0.1$ to -2.9 .

Cerium: In solar material, Ce is principally an *s*-process product. Thus, it is the expected result that $[Ce/Fe]$ and $[Ba/Fe]$ vary in very similar fashions. That the scatter at a given $[Fe/H]$ is larger for $[Ba/Fe]$ than $[Ce/Fe]$ is probably due (see below) to the fact that the Ba II but not the Ce II lines are strong, and so dependent on the adopted microturbulence and other factors.

Neodymium: Extending the argument just given for Ce, we note that the *s*-process contributions to solar abundances of Ba, Ce, Nd, and Eu are 81, 77, 56, and 6 per cent, respectively. Noting the opposite slopes of $[Ba/Fe]$ and $[Eu/Fe]$ versus $[Fe/H]$, it is not surprising that $[Nd/Fe]$ appears to be independent of $[Fe/H]$.

Europium: Recently, Eu abundances for samples of EAGLNT's stars using their atmospheres were published by Woolf, Tomkin, & Lambert (1995) and Koch & Edvardsson (2002). Their results for $[Eu/Fe]$ are consistent with ours.

7.3 Offsets in $[X/Fe]$

Given the differential analysis and the absence of cosmic scatter in our sample (see next section), one would expect stars of solar $[Fe/H]$ to have $[X/Fe] = 0$. However, Figures 9, 10, & 11 show $[X/Fe]$ of Mg, Al, Si, S offset by 0.03 to 0.05 dex at $[Fe/H] = 0.0$, and $[X/Fe]$ of elements Sc, V, Mn, Cu offset by ~ 0.05 at $[Fe/H] = 0.0$. A key to the origins of the small offsets may be the fact that the Sun is not fully representative of our sample. With $T_{\text{eff}} = 5780$ K, $\log g = 4.44$, and $[Fe/H] = 0$, the Sun is in a tail of the stellar distribution in all three parameters (Figure 1). This has several consequences. The equivalent widths of some lines in the stellar spectra may differ considerably from their strengths in the solar spectrum. Systematic errors such as those arising from the neglect of stellar granulation and departures from LTE which would cancel in a strictly differential analysis of quite similar stars may leave a small imprint here in the form of the offset in $[X/Fe]$ at $[Fe/H] = 0$. A leading NLTE effect may be overionization of the metals in the iron-group. One might suppose similar degrees of overionization such that $[Ni/Fe]$ may be reliably estimated from a combination of Ni I and Fe I lines. In the case of Mg, Si, and S, the offset disappears

Table 9. Heavy element abundances for *s*-process enhanced outliers.

[X/Fe]	HD 21922	HD 36667	HD 80218	HD 88446	HD 140324	HD 220842
[Fe/H]	-0.48	-0.45	-0.28	-0.52	-0.36	-0.31
[Sr/Fe]	0.25	0.33	0.33	0.57	...	0.27
[Y/Fe]	0.23	0.38	0.26	0.58	0.29	0.35
[Zr/Fe]	0.18	0.33	0.16	0.65	...	0.27
[Ba/Fe]	0.33	0.47	0.00	0.66	0.18	0.09
[Ce/Fe]	0.34	0.26	-0.07	0.58	0.29	0.05
[Nd/Fe]	0.17	0.40	0.04	0.69	...	0.12

when [X/Fe] is computed using iron abundance derived from Fe II lines.

7.4 Outliers

There are few stars in our sample whose abundances for one or more elements differ significantly from the mean abundances of the rest of the stars at the same [Fe/H] (see Figures 9, 10 & 11). Two stars, HD 110989 and HD 136925, are enhanced only in abundances of Mg, Al, Si, S, and Ti, and the rest of the abundances are normal. The kinematics of these stars suggest they belong to the thick disc population, for which such enhancements are characteristic (see below). Figures 9, 10 and 11 also reveal that half a dozen stars are enhanced in *s*-process elements, i.e., Sr, Y, Zr, Ba, Ce, and Nd. Abundances of these stars are summarized in Table 9. HD 88446 is known to be a *s*-process enriched CH sub-giant (Smith, Coleman & Lambert 1993). The current abundances are in very good agreement with the literature values. We assume that the other stars are also *s*-enriched dwarfs. The higher *s*-process abundances in unevolved stars are attributable to mass-transfer from a companion asymptotic giant branch (AGB) star that is now an unseen white dwarf.

7.5 Cosmic Scatter?

A first step towards an understanding of the scatter in the abundance ratios [X/Fe] is to quantify the scatter. To do this we fit a linear relation to the data and examine the residuals about the relation. A histogram of the residuals is fitted with a Gaussian. In very few cases is a Gaussian not a good fit. Figure 12 shows [X/Fe] versus [Fe/H] for X = Mg, and Si with the fitted linear relation, the residuals about this relation, and a histogram of these residuals with its fitted Gaussian. The σ_{gau} of the Gaussian varies from element to element. Table 10 summarizes the results. Note that in computing the measurement errors σ_{mod} for individual stars, we have not included the uncertainty in the EW measurements. Except for two elements K and Sr, abundances are computed using 2 or more lines and the net random error due to the EW measurement is very small.

An obvious question occurs - is there information about Galactic chemical evolution (GCE) in the σ_{gau} estimates, or do abundance measurement errors dominate? To address this, we compare the error σ_{mod} previously calculated (Table 10) with σ_{gau} .

Values of σ_{gau} are well matched to the estimates of σ_{mod} for almost every element (Figure 13). This is especially true

Table 10. The predicted uncertainty, σ_{mod} , is compared with σ_{gau} of the Gaussian fit to the residuals

[X/Fe]	σ_{mod}	σ_{gau}
[Fe/H]	0.07	...
[C/Fe]	0.14	0.07
[N/Fe]	0.19	0.10
[O/Fe]	0.16	0.07
[Na/Fe]	0.03	0.04
[Mg/Fe]	0.04	0.04
[Al/Fe]	0.04	0.05
[Si/Fe]	0.05	0.04
[S/Fe]	0.09	0.09
[K/Fe]	0.08	0.10
[Ca/Fe]	0.03	0.04
[Sc/Fe]	0.11	0.05
[Ti/Fe]	0.03	0.04
[V/Fe]	0.04	0.04
[Cr/Fe]	0.02	0.03
[Mn/Fe]	0.04	0.04
[Co/Fe]	0.02	0.04
[Ni/Fe]	0.02	0.03
[Cu/Fe]	0.02	0.06
[Zn/Fe]	0.05	0.06
[Sr/Fe]	0.04	0.08
[Y/Fe]	0.09	0.07
[Zr/Fe]	0.10	0.07
[Ba/Fe]	0.12	0.08
[Ce/Fe]	0.11	0.08
[Nd/Fe]	0.10	0.07
[Eu/Fe]	0.11	0.08

for Cr and Ni, two elements spectroscopically similar to Fe with similar nucleosynthetic origins (i.e., intrinsic star-to-star differences in [X/Fe] are minimized). For C and N, σ_{gau} is less than the estimated σ_{mod} which suggests the latter are overestimates. In these cases where the abundance is based on high excitation lines, we suspect the T_{eff} errors are significantly overestimated: the adopted error is likely an upper limit (see Alonso et al. 1996) to the combination of the random and systematic errors, but only the latter is a weak contributor to σ_{mod} . In the case of Cu, and Sr, σ_{gau} exceeds σ_{mod} . Abundance of Sr is dependent on a single line and it is, therefore difficult to argue that there is a real star-to-star scatter in [Sr/Fe].

The implication for GCE is clear: the intrinsic or cosmic scatter in [X/Fe] among these thin disc stars with birthplaces concentrated at galactocentric distances of 7 to 10 kpc is small, say $\sigma_{\text{cosmic}} < \sigma_{\text{gau}}$. Noting that the sampled ejecta come in differing proportions from the three principal sites

of stellar nucleosynthesis – SN II, SN Ia, and AGB stars – the lack of cosmic scatter implies that the ejecta from the different sites were well mixed into the gas from which the stars formed.

That there is cosmic scatter was suggested by EAGLNT’s study which showed a noticeably larger scatter in $[\text{Mg}/\text{Fe}]$, $[\text{Al}/\text{Fe}]$, and $[\text{Ti}/\text{Fe}]$ (relative to similar elements such as Si and Ca) for stars with $[\text{Fe}/\text{H}] \leq -0.4$. ** Reconciliation of this suggestion with the evident lack of comparable scatter in our sample is attempted below.

7.6 Chemical Evolution of the Thin Disc

Chemical evolution as portrayed by Figures 9, 10, and 11 is broadly interpreted as the consequence of mixing into the interstellar medium of ejecta from three principal sites of nucleosynthesis: Type II SN, Type Ia SN, and AGB stars. Qualitatively, the key features of Figures 9, 10, and 11 are widely accepted as understood. For example, the gradual decline in $[\text{X}/\text{Fe}]$ for α -elements (O, Mg, Si, Ca, and Ti) with increasing $[\text{Fe}/\text{H}]$ is taken to reflect the delayed contribution from Type Ia SN with a lower α/Fe ratio than the ejecta from Type II SN which dominated the chemical evolution at earlier times and, hence, low $[\text{Fe}/\text{H}]$. Detailed modeling has been attempted by many authors – see, for example, Timmes, Woosley, & Weaver (1995), Chiappin et al. (1997), Goswami & Prantzos (2000), and Alibés et al. (2001). Quantitative matching of predictions to observations of $[\text{X}/\text{Fe}]$ remains elusive.

Contributions from the AGB stars must be reflected in the abundances of C, N, and heavy elements synthesized predominantly by the s -process. Carbon and nitrogen are also synthesized by massive stars. These stars may also contribute Sr, Y, and Zr through the weak s -process and Eu through the r -process. While AGB stars also synthesize these ‘light’ elements, they dominate synthesis of ‘heavy’ s -process nuclides such that, as noted above, AGB stars control production of Ba, Ce, and Nd in thin disc stars. In contrast, europium is an r -process or Type II SN product.

Inspection of Figure 11 shows, as mentioned in Section 7.2, that Sr, Y, Zr, Ba, and Ce show very similar declines in $[\text{X}/\text{Fe}]$ with decreasing $[\text{Fe}/\text{H}]$. Europium shows an increase, as expected of this r -process product. Increasing Ba and Ce (relative to Fe) surely indicates the increasing prominence of AGB star ejecta relative to Type II and Type Ia ejecta which contribute Fe but very little Ba and Ce. The ratio of heavy to light s -process abundances is shown in Figure 14. The similarity of the slopes of $[\text{X}/\text{Fe}]$ versus $[\text{Fe}/\text{H}]$ for light (Sr, Y, Zr) and heavy (Ba, Ce) elements may reflect either unchanging relative contributions from AGB stars or a change in these contributions which is offset by a change in the weak s -process contribution from the massive stars. On the assumption that the AGB stars are the controlling influence, the unchanging abundance ratio of heavy to light elements indicates that the exposure to neutrons in the s -process site is essentially independent of the metallicity of the contributing AGB stars.

** EAGLNT’s suggestion that some metal-rich stars were enhanced in Na, Mg, and Al was not confirmed by Tomkin et al. (1997).

7.7 Thin and Thick Discs

The thick disc is considered by many to be the result of heating of the thin disc by accretion of, or merger with small stellar systems. Freeman & Bland-Hawthorn (2002) refer to the resulting thick disc as a “snap frozen” relic of the state of the (heated) early disc. The labels “thin” and “thick” were introduced by Gilmore & Reid (1983) and denote the different vertical scale heights of the populations: 300 pc for the thin disc and 1450 pc for the thick disc. The ratio of stellar density of thick to thin disc is a few per cent near the Sun. The thick disc is broadly described as slightly metal-poor and old relative to the thin disc.

In our sample, the lack of cosmic scatter in $[\text{X}/\text{Fe}]$ at a fixed $[\text{Fe}/\text{H}]$ is striking and in apparent conflict with results obtained by others. We noted above the contrast with EAGLNT’s results for Mg, Al, and Ti where a larger scatter – apparently, cosmic – was reported for stars with $[\text{Fe}/\text{H}]$ less than about -0.4 and more metal-rich than about -0.8 ; the lower bound is uncertain due to the paucity of very metal-poor stars in their sample. Fuhrmann (1998), in a notable contribution, attributed the scatter in $[\text{Mg}/\text{Fe}]$ to a mixing of thin with thick disc stars and a different chemical evolution of these two stellar populations (see also Gratton et al. 2000 for remarks on O, and Mg with respect to Fe). He suggested that at $[\text{Fe}/\text{H}] \approx -0.4$ the $[\text{Mg}/\text{Fe}]$ was either ‘high’ or ‘low’ with no stars having an intermediate value.

Prochaska et al. (2000) report results from the initial phases of a survey of thick disc main sequence stars in the solar neighborhood. Stars are selected to have V_{LSR} from -20 to -100 km s^{-1} , metallicities in the interval -0.4 to -1.1 , and a W_{LSR} that takes a star to at least 600 pc above the Galactic plane. The latter criterion in particular takes out thin disc stars. A color selection provides stars generally cooler than those comprising our and other surveys. Ten stars were analysed using model atmospheres and high resolution spectra, obtaining abundances for 20 elements. Presently, the sample lacks stars in common with other surveys, and, hence, there may be small offsets between the $[\text{X}/\text{Fe}]$ and those of the surveys considered here. Results^{††} are incorporated into Figures 15, 16 and 18.

Given the large stellar sample which may be assembled from various sources, we explore in greater detail the evidence for cosmic scatter in $[\text{Mg}/\text{Fe}]$ and other elements arising from the mixing at a fixed $[\text{Fe}/\text{H}]$ of thin and thick disc stars. Figure 15 shows $[\text{Mg}/\text{Fe}]$ and $[\text{Ti}/\text{Fe}]$ versus $[\text{Fe}/\text{H}]$ for stars drawn from the samples referenced in the caption. With the exception of the data from Prochaska et al. (2000) and Fulbright (2000), the published abundances have been adjusted to our scale using small corrections. Common stars among the samples were identified, and treated them only once: for common stars in our study and others, we have adopted our values, and for common stars in Chen et al. and EAGLNT, we have adopted Chen et al. values. The appearance of cosmic scatter at $[\text{Fe}/\text{H}] \simeq -0.4$ is intimately related to the mixing of stellar populations. For $[\text{Fe}/\text{H}] > -0.4$, the stars belong to the thin disc. At $[\text{Fe}/\text{H}] < -0.4$, thick disc stars comprise the majority. In simplest terms stars with

†† We adopt the values based on solar astrophysical g_f -values, denoted $[\text{X}/\text{Fe}]_n^S$ by Prochaska et al.

the higher [Mg/Fe] at a given [Fe/H] are old thick disc stars from the inner Galaxy. To justify this identification, we divide the stars into two groups according to whether [Mg/Fe] is greater than or less than +0.2 dex as shown in Figure 15.

In the four panels of Figure 16, we identify a star by its group membership in plots of V_{LSR} , W_{LSR} , R_m , and age. We have calculated these quantities when authors of the selected samples did not provide them. Low and high [Mg/Fe] stars occupy almost non-overlapping areas of the panels showing V_{LSR} , R_m , and age. Many stars of high [Mg/Fe] (large symbols in the plots) have a circular velocity less than that of the Sun, a range in W_{LSR} that shows they make excursions to about 1 kpc above the plane, an age that places them among the oldest stars in the Galaxy ($\log \tau_9 \approx 1.0$ to 1.3), and an origin in the inner Galaxy ($R_m \sim 5$ to 7 kpc). The high [Mg/Fe] stars are primarily representatives of the Galaxy’s thick disc. The low [Mg/Fe] stars of the same [Fe/H] as the thick disc stars are predominantly thin disc stars from galactocentric distances closer to the radius of the Sun’s orbit. This difference in populations is, as Fuhrmann recognized, responsible for appearance of cosmic scatter in [Mg/Fe] among slightly metal-poor stars. The difference between two disc populations is also clear from Figure 17, where the stars are binned in 0.5 kpc intervals of R_m . For this we have considered star samples of EAGLNT, Chen et al., Fulbright (2000), and ours, totalling around 500 disc stars. The entire sample is grouped into two classes: stars with [Mg/Fe] ≥ 0.2 as thick disc stars, and stars with [Mg/Fe] < 0.2 dex as thin disc stars. Thin disc stars fit a Gaussian centering at $R_m = 8.1$ kpc and thick disc stars peak at $R_m = 6.7$ kpc. The distribution suggests that thin disc stars are likely to have circular orbits and thick disc stars are relatively eccentric and formed closer to the Galactic centre.

The dispersion in W_{LSR} for thin disc stars increases progressively for lower [Fe/H] is in agreement with the correlation between σ_W and age determined by Gómez et al. (1997) who studied several thousand B- to F-type stars with *Hipparcos* data, and the [Fe/H] vs. age relationship depicted in Figure 8. Gómez et al. found the σ_W -age relationship to saturate at $\sim 4 - 5$ Gyr, which is also consistent with the scatter in W flattening for thin disc stars with [Fe/H] ≤ -0.3 in Figure 16.

To quantify the differences between the thin and thick disc samples, we choose a sample of thick disc stars as having [Fe/H] ≤ -0.35 and a V_{LSR} from -40 to -100 km s $^{-1}$, R_m of 5.5 to 7.0 kpc, and an age $\log \tau_9 \geq 1.0$. The upper bound chosen for [Fe/H] is seemingly the maximum [Fe/H] of thick disc stars seen in the solar neighbourhood; we are not aware of selection effects compromising the considered surveys which would have lead to the exclusion of stars of high [Mg/Fe] with [Fe/H] > -0.3 . The lower bound on [Fe/H] for thick disc stars is unknown and unimportant to our measurement of the difference in [X/Fe] between the two samples. Our comparison sample of thin disc stars has V_{LSR} between -40 and $+40$ km s $^{-1}$. Mean values for the thin disc stars are $R_m = 8.1$ kpc, and $\log \tau_9 = 0.6$ for those stars with [Fe/H] between -0.35 and -0.7 , the metallicity range for which present samples of thin and thick disc stars have an overlap.

Thin and thick disc stars with [Fe/H] between -0.35 and -0.7 differ in [X/Fe] (Figure 18). Table 11 gives the mean [X/Fe] for those elements well represented in both samples

Table 11. Mean abundance ratios, [X/Fe] and kinematic properties for thick and thin disc stars. Thin disc stars are taken from present study with [Fe/H] from -0.35 to -0.70 . Thick disc values are for stars whose metallicity is $-0.70 \geq [\text{Fe}/\text{H}] \geq -0.35$ and the kinematic values as defined in Figure 18 and in this table. Thick disc stars are from EAGLNT, Prochaska et al., and Woolf et al.

Quantity	Thin disc	Thick disc	$\Delta[\text{X}/\text{Fe}]$
V_{LSR} (Km s $^{-1}$)	+50 to -40	-40 to -100	
W_{LSR} (Km s $^{-1}$)	+40 to -40	+80 to -80	
R_m (kpc)	>7.0	5.5 to 7.0	
$\log \tau_9$ (yrs)	< 1.0	≥ 1.0	
[Na/Fe]	0.07 \pm 0.04	0.10 \pm 0.04	0.03
[Mg/Fe]	0.09 \pm 0.05	0.30 \pm 0.07	0.21
[Al/Fe]	0.11 \pm 0.06	0.27 \pm 0.08	0.16
[Si/Fe]	0.07 \pm 0.04	0.18 \pm 0.05	0.11
[Ca/Fe]	0.05 \pm 0.04	0.16 \pm 0.06	0.11
[Sc/Fe]	0.04 \pm 0.07	0.15 \pm 0.05	0.11
[Ti/Fe]	0.05 \pm 0.05	0.29 \pm 0.06	0.24
[V/Fe]	0.01 \pm 0.13	0.22 \pm 0.06	0.21
[Cr/Fe]	-0.02 \pm 0.03	0.02 \pm 0.01	-0.04
[Mn/Fe]	-0.16 \pm 0.05	-0.13 \pm 0.05	0.03
[Ni/Fe]	-0.02 \pm 0.02	0.03 \pm 0.02	0.05
[Ba/Fe]	-0.02 \pm 0.15	-0.10 \pm 0.06	-0.08
[Eu/Fe]	0.12 \pm 0.10	0.30 \pm 0.08	0.18

and the difference $\Delta[\text{X}/\text{Fe}] = [\text{X}/\text{Fe}]_{\text{thick}} - [\text{X}/\text{Fe}]_{\text{thin}}$ between the mean values. Our Δ -values are similar to those suggested by Prochaska et al. from a comparison between their [X/Fe] and those of published surveys of disc stars. $\Delta[\text{X}/\text{Fe}]$ is positive for several elements: Mg, Al, Si, Ca, Sc, Ti, V, and Eu. To within the uncertainty, $\Delta[\text{X}/\text{Fe}]$ is zero for Na, Cr, Mn, and Ni, and possibly negative for Ba. Particularly striking is the contrast between the odd- Z light elements Na and Al, a difference noted by EAGLNT. The Δ -values for Sc and V are largely dependent on Prochaska et al.’s results for thick disc stars and may be affected by a systematic offset arising from different abundance analysis techniques. We note in Figure 18 that our and Chen et al.’s results suggest a smaller Δ value for V.

Thick disc stars have a narrow spread in [Ba/Eu]. The spread in [Eu/Fe] evident from Figure 18 is much reduced when [Ba/Eu] is considered. Figure 19 shows this. A few thin disc stars share the [Ba/Eu] of the thick disc stars. For a pure r -process solar like mix, the [Ba/Eu] ≈ -0.7 . Evidently, the thick disc stars have a smaller fraction of s -process heavy elements than disc stars of the same [Fe/H]. This is an expected result given that the thick disc stars are older than the thin disc companion stars; the s -process elements are contributed by the more slowly evolving low mass AGB stars.

Our primary aim here was to establish that previous reports of cosmic scatter in [Mg/Fe] and similar ratios arise from the mixing of stellar populations. Cosmic scatter, as shown here, is undetectable in [X/Fe] at fixed [Fe/H] among local thin disc stars. It is apparently small for thick disc stars but a large sample subjected to a uniform analysis must be made available to test this suspicion.

Our selection of thick disc stars by negative V_{LSR} , high τ_9 , low [Fe/H], and small R_m excludes two interesting groups of stars. First, there are stars with [Mg/Fe] > 0.2 with positive V_{LSR} , and low [Fe/H] (Figure 16). Second, there are

a few stars with V_{LSR} characteristic of the thick disk but higher $[\text{Fe}/\text{H}]$.

The first group by virtue of their generally positive V_{LSR} appears to originate from outside the solar circle ($R_m \simeq 8.5$ to 10 kpc). They share the lower $[\text{Fe}/\text{H}]$ of the thick stars; none are present with $[\text{Fe}/\text{H}] \geq -0.3$. Although the sample size is small, there is a hint that, in contrast to the thick stars, these stars are not exclusively old. The amplitude in W_{LSR} across the sample appears to be smaller than that of the thick disk stars. However, it is interesting to note that abundance pattern of this group is very similar to that of thick disk stars as in Figure 18, and Table 11. This group appears to be related to the thick disk stars discussed above with R_m of 5 to 7 kpc.

The second group are apparently schizophrenic. Additional stars belonging to this group are to be found in Felzing & Gustafsson (1998). Their V_{LSR} ($\sim -50 \text{ km s}^{-1}$) would identify them as belonging to the thick disk. But by their W_{LSR} , R_m , spread in ages, and their $[\text{Fe}/\text{H}]$ they would be linked with the thin disc stars. These stars do not show the $[\text{X}/\text{Fe}]$ of the thick disc stars.

8 CONCLUDING REMARKS

Our stellar sample is comprised primarily of thin disc stars, but by drawing on samples which include thick disc stars, we may compare and contrast chemical compositions of thin and thick disc stars.

8.1 Thin Disc – Questions

Three aspects of the compositions of the thin disc stars attract our attention: (i) the lack of cosmic scatter in $[\text{X}/\text{Fe}]$, (ii) the dispersion in the age-metallicity relation, and (iii) the origin of the gas from which the most metal-poor thin disc stars were formed.

The thin disc, as sampled by stars which are passing through the solar neighbourhood, has a lower limit of $[\text{Fe}/\text{H}] \sim -0.7$, an upper bound to the age of about 10 Gyr, and origins from Galactocentric distances of between about 7 and 10 kpc. The restriction to $7 < R_m < 10$ likely emerges as a direct consequence of the small eccentricity of the orbits. Between these limits on the metallicity and age, variations in $[\text{X}/\text{Fe}]$ are small (Figures 9, 10, & 11). A more remarkable result concerning the thin disc is the confirmation of earlier work, showing that, although the thin disc stars sample a range in metallicity, age, and originate from different Galactocentric distances, these identifying characteristics vanish almost entirely when relative abundances of elements are considered. In particular, apart from weak trends with $[\text{Fe}/\text{H}]$, $[\text{X}/\text{Fe}]$ exhibits no scatter in excess of that attributable to measurement errors.^{‡‡} This fact stands as a challenge to models of Galactic chemical evolution.

Lack of scatter in $[\text{X}/\text{Fe}]$ suggests that the Galactic thin disc is chemically homogeneous at a given time, and mixing of the various ejecta into star-forming clouds in the disc is very efficient. This homogeneity refers to abundance ratios

^{‡‡} A few stars are evidently *s*-process enriched and presumably result from mass-transfer from a now deceased companion.

$[\text{X}/\text{Fe}]$ not to the abundances $[\text{Fe}/\text{H}]$ or $[\text{X}/\text{H}]$. As noted in the discussion of the age-metallicity relation, there is a spread in the latter quantities at a given age and a given galactocentric distance.

If the mild evolution of $[\text{X}/\text{Fe}]$ with $[\text{Fe}/\text{H}]$ is ignored, $[\text{X}/\text{Fe}]$ is independent of the birthplace (R_m) and birthdate of a thin disc star, always bearing in mind that we are sampling a small range in R_m . This independence extends to the present time. Massive stars being young and, therefore, observed at or very close to their birthplace may be used to trace the present composition of the Galaxy's thin disc. Observations show that $[\text{X}/\text{Fe}] \simeq 0.0$ irrespective of position in the Galaxy. This result is well shown by Andrievsky et al.'s (2002a,b) analyses of Cepheids with locations corresponding to Galactocentric distances of 4 to 10 kpc. (These authors assume the Sun to be at 7.9 kpc.) The mean $[\text{Fe}/\text{H}]$ of the Cepheids at the Sun's Galactocentric distance is not significantly different from zero. The authors suggest that the spread of about ± 0.15 dex in $[\text{Fe}/\text{H}]$ at this and other well sampled distances exceeds the measurement errors. A spread is reported from observations of young open clusters (Friel 1995; Edvardsson 2002). Iron abundance decreases slightly with increasing Galactocentric distance: Andrievsky et al. obtain a slope for $[\text{Fe}/\text{H}]$ of $-0.029 \pm 0.004 \text{ dex kpc}^{-1}$, a value of the same sign but slightly smaller than a majority of earlier measurements of this gradient. Other metals show rather similar gradients except that the heavy elements La, Ce, Nd, Eu, and Gd show a positive gradient (mean value of $+0.013 \text{ dex kpc}^{-1}$). Extension of the abundance analyses to Cepheids in the inner Galaxy shows that higher metallicity prevails inside about 6 kpc (Andrievsky et al. 2002b): $[\text{Fe}/\text{H}] \simeq +0.3$ from five stars at Galactocentric distances of 4.4 to 5.7 kpc, but $[\text{X}/\text{Fe}] \simeq 0.0$ with the exception of a few elements represented by very few lines. In short, the Cepheids, young stars sampling a wide range in Galactocentric distances, have a composition expressed as $[\text{X}/\text{Fe}]$ not distinctly different from that of thin disc stars. Examination of Andrievsky et al.'s results shows that the spread in $[\text{X}/\text{Fe}]$ is small and likely dominated by measurement errors.

Existence of a (weak) abundance gradient is pertinent to the question of scatter in the age-metallicity relation. Most determinations put the slope at a larger value than the above value from Cepheids, say $-0.1 \text{ dex kpc}^{-1}$ is typical. Grenon (1987, 1989) has adduced evidence that the gradient was of a similar magnitude in the past. EAGLNT's analysis offered supporting evidence. Presence of a shallow gradient is now widely linked to the presence of a stellar bar in the inner Galactic disc. Observationally, it is found that spiral galaxies with bars have flatter gradients than those without bars (Martin & Roy 1994). Theoretically, bars have been shown to homogenize the gas (Martinet & Friedli 1997). Recently, Cole & Weinberg (2002) have argued that the Galactic bar is younger than 6 Gyr, which, if the bar were the only mechanism for homogenizing the gas, would seem to imply the possibility of a different abundance gradient at very early times. However, there are other postulated ideas for maintaining a flat abundance gradient (see Andrievsky et al. 2002a).

Attention was drawn to the large spread in the age-metallicity relation by EAGLNT. At a fixed age, there is a spread of about 0.5 dex in $[\text{Fe}/\text{H}]$, or at a fixed $[\text{Fe}/\text{H}]$ there is a range in ages over about 8 Gyr. If stars migrate in Galacto-

centric distance and a Galactic abundance gradient existed over part of the time sampled by the age-metallicity relation, scatter in that relation would result. Feltzing, Holmberg, & Hurley (2001) from their analysis of nearly 6000 stars argue that stellar migration cannot account in full for the scatter, and interpret the scatter as ‘intrinsic to the formation processes of stars’. One might wonder if a contributing factor is an inability to predict accurately the Galactocentric distance R_m , especially for stars from the inner Galaxy which reach the Sun on ‘hot’ orbits thanks to the action of the inner bar of the Galaxy (Sparke & Sellwood 1987; Raboud et al. 1998).

Discovery of the earliest manifestation of the thin disc would provide an important datum about the disc’s history. According to our sample, the oldest stars (Figure 16) are slightly younger than the average thick disc star. These thin disc stars extend in $[\text{Fe}/\text{H}]$ to -0.7 with, on average, a birthplace outside the solar circle. The vertical velocities W_{LSR} are those of the thin disc and not the thick disc. The lower bound to $[\text{Fe}/\text{H}]$ was imposed as a selection criterion by EAGLNT, Chen et al., and ourselves. There are stars known at lower $[\text{Fe}/\text{H}]$ with thin disc kinematics (cf. Chiba & Beers 2000; Beers et al. 2002). Clearly, an important task is to measure compositions for a selection of these metal-poor stars, and, in particular, to determine accurately those $[\text{X}/\text{Fe}]$ which distinguish thin from thick disc stars. As important will be tracing the evolution of $[\text{X}/\text{Fe}]$ with $[\text{Fe}/\text{H}]$ and finding where (or if) $[\text{X}/\text{Fe}]$ merges with halo values.^{§§}

8.2 Thick Disc – Questions

Thick disc stars selected by V_{LSR} relative to thin disc stars of the same $[\text{Fe}/\text{H}]$ are older, exhibit a large dispersion in W_{LSR} , and originate from smaller Galactocentric distances (Figure 16). Given the larger eccentricity and velocity dispersion of the thick disc stars compared to the thin disc population, we would expect a larger range in R_m . If $\rho_{\text{thick}}(R)$ is nearly as flat as $\rho_{\text{thin}}(R)$, Figure 17 would reveal a wider Gaussian for the thick disc, but still centred at R_\odot . The fact that the distribution of thick disc stars is shifted to smaller mean galactocentric distances can be explained by assuming a steeper dependence of ρ_{thick} with galactocentric distance. Furthermore, the shift could be interpreted as the direct observation of the truncation radius of the thick disc, which, as pointed out by Freeman & Bland-Hawthorn, may be different from the thin disc’s, marking the size of the thin disc when the thick disc formed.

As we noted already, we confirm and extend an earlier

^{§§} There are halo stars ($V_{LSR} \simeq -200 \text{ km s}^{-1}$ with some $[\text{X}/\text{Fe}]$ similar to those of the thin disc at $[\text{Fe}/\text{H}] \sim -0.6$. These are the so-called α -poor stars found by Nissen & Schuster (1997). Disc and α -poor stars have similar $[\text{X}/\text{Fe}]$ for O, Mg, Si, Ca, Ti, Cr, Y, and Ba, but not for Na and Ni, which are underabundant (relative to Fe) in the α -poor stars. Thick disc (and other halo) stars analysed by Nissen & Schuster have $[\text{X}/\text{Fe}]$ like those of other thick disc stars, a similarity that excludes the possibility of systematic errors causing the Na and Ni abundance anomalies. It is difficult to see how to link the α -poor halo stars to a widespread property of thin disc stars. Nissen & Schuster supposed that these halo stars have been accreted from a dwarf galaxy with a history of nucleosynthesis different from ours.

result (Fuhrmann 1998; Gratton et al. 2000; Prochaska et al. 2000) that there are differences in $[\text{X}/\text{Fe}]$ between thick and thin disc stars of the same $[\text{Fe}/\text{H}]$. These differences are summarized in Table 11. Especially, notable is the different behaviour of Na, Mg, and Al (relative to Fe) between the thick and thin disc. In particular, as first stressed by EAGLNT, $[\text{Na}/\text{Mg}]$ at a fixed $[\text{Mg}/\text{H}]$ is lower by about 0.2 dex for the thick relative to thin disc stars but $[\text{Al}/\text{Mg}]$ is the same for both groups. These differences are clues to the origins of the populations, and to the nucleosynthesis of Na, Mg, Al, and other elements. The reader is referred to Prochaska et al. (2000) for discussion of these points.

Following Fuhrmann (1998), one may harbour the view that distribution functions for $[\text{X}/\text{Fe}]$ are non-overlapping for samples of thin and thick disc stars for elements such as Mg for which $\Delta[\text{X}/\text{Fe}]$ is large. Quantitative spectroscopy of a large sample of thick disc stars and a control sample of thin disc stars is now needed to establish the distribution functions. Thick disc stars at the low $[\text{Fe}/\text{H}]$ limit discussed here appear to merge with bulge/halo stars as far as $[\text{X}/\text{Fe}]$ is concerned. Feltzing & Gustafsson’s (1998) analysis of metal-rich F-G stars shows no change in $[\text{X}/\text{Fe}]$ with V_{LSR} , and so hints that the thick - thin disc differences disappear by $[\text{Fe}/\text{H}] \simeq 0.0$, but the low W_{LSR} of their stars imply that their stars do not travel far from the Galactic plane, and, hence, attribution to the thick disc may be questionable.

Prochaska et al. discuss at some length the implications for the evolution of the Galaxy of the different $[\text{X}/\text{Fe}]$ in thin and thick disc stars. As long noted, the extension of the halo $[\text{X}/\text{Fe}]$ for α -elements to higher $[\text{Fe}/\text{H}]$ in thick disc than thin disc stars is suggestive of a delay in the contribution made by SN Ia to the thick disc. Certainly, the thick-thin differences in $[\text{X}/\text{Fe}]$ raise interesting questions about the nucleosynthesis by SN II. A key point stressed by Prochaska et al. concerns the closely similar ages and $[\text{X}/\text{Fe}]$ for bulge, thick-disc, and (the majority of the) halo stars which suggests that these populations formed from the same gas at about the same time. Several speculations may be offered to account for the lack of thin disc stars with thick disc abundances: (i) the gas from which thick disc stars formed did not contribute to the thin disc; (ii) a delay in star formation in the thin disc enables SN Ia to enrich the gas in Fe-group elements and so reduce the Mg/Fe for the first generation of thin disc stars; (iii) perhaps, the thick disc gas was diluted with gas in the thin disc before the observed stars formed.

8.3 New Challenges

New challenges to the observer are presented by our survey of thin disc stars and the comparisons with published analyses of thick disc stars. A particular challenge is to find and survey the composition of thick disc stars over more of the space defined by R_m , τ_a , W_{LSR} , and $[\text{Fe}/\text{H}]$. Given the availability of high-resolution spectrographs and large telescopes and tools for standard abundance analysis, it should not be difficult to provide the compositions.

A different challenge should be noted: the need to step beyond a classical abundance analysis with its reliance on the classical model atmosphere and method of line analysis. One step is taken by replacing the assumption of LTE by non-LTE (i.e., statistical equilibrium) in analysing the absorption lines. A more challenging step involves using 3-

dimensional hydrodynamic model atmospheres in place of the classical atmosphere which adopts hydrostatic equilibrium among its defining assumptions. Ultimately, the combination of the hydrodynamical models with non-LTE is desired. Consummation of this marriage may be necessary in order to detect and quantify the cosmic scatter in the abundance ratios $[X/Fe]$, and to obtain finally definitive results for $[X/Fe]$.

9 ACKNOWLEDGMENTS

We thank Bengt Edvardsson for providing a list of stars with Strömgren photometry, from which the current sample is taken, and the code for calculating the U,V,W space motion components. Johannes Andersen and Stephane Udry for providing the CORAVEL radial velocities prior to publication. We thank Jon Fulbright for making available computer code, with the kind permission of D. Lin, to calculate orbital parameters. We thank David Yong, Gajendra Pandey, and Nils Ryde for many useful discussions. This research has been supported in part by National Science Foundation (grants AST 96-18414, AST 99-00846, AST 00-86321) and the Robert A. Welch Foundation of Houston, Texas. This research has made use of the SIMBAD data base, operated at CDS, Strasbourg, France, and the NASA ADS, USA.

REFERENCES

- Alibés, A., Labay, J., Canal, R. 2001, *A&A*, 370, 1103
Allende Prieto, C., Lambert, D.L. 1999, *A&A*, 352, 555
Allende Prieto, C., Barklem, P. S., Asplund, M., Ruiz Cobo, B. 2001a, *ApJ*, 558, 830
Allende Prieto, C., Lambert, D.L. Asplund, M. 2001b, *ApJL*, 556, 63
Allende Prieto, C., Asplund, M., García López, R. J., Lambert, D. L. 2002a, *ApJ*, 567, 544
Allende Prieto, C., Lambert, D.L. Asplund, M. 2002b, *ApJL*, 573, 137
Alonso, A., Arribas, S., Martinez-Roger, C. 1996, *A&A*, 313, 873
Andrievsky, S.M., Egorova, I.A., Korotin, S.A., Burnage, R. 2002a, *A&A*, 389, 519
Andrievsky, S.m., Bersier, D., Kovtyukh, V.V., Luck, R.E., Maciel, W.J., Lepine, J.R.D., Beletsky, Yu. V. 2002b, *A&A*, 384, 140
Asplund, M., Nordlund, Å., Trampedach, R., Allende Prieto, C., Stein, R.F. 2000, *A&A*, 359, 729
Bard, A., Kock, M. 1994, *A&A*, 282, 1014
Bard, A., Kock, A., Kock, M. 1991, *A&A*, 248, 315
Beers, T.C., Drilling, J.S., Rossi, S., Chiba, M., Rhee, J., Föhmeister, B., Norris, J.E., von Hippel, T. 2002, *AJ*, 124, 931
Bertelli, G., Bressan, A., Chiosi, C., Fagotto, F., Nasi, E. 1994, *A&AS*, 106, 275
Beynon, T.G.R. 1978, *A&A*, 64, 145
Biémont, E., Godfroid, M. 1980, *A&A*, 84, 361
Blackwell, D.E., Lynas-Gray, A.E., Smith, G. 1995, *A&A*, 296, 217
Blackwell, D.E., Shallis, M.J., Simmons, G.J. 1980, *A&A*, 81, 340
Brown, A. G. A., Arenou, F., van Leeuwen, F., Lindgren, L., & Luri, X. 1997, The First Results of Hipparcos and Tycho, 23rd meeting of the IAU, Joint Discussion 14, 25 August 1997, Kyoto, Japan., 14
Cardon, B.L., Smith, P.L., Scalo, J.M., Testerman, L. 1982, *ApJ*, 260, 395
Castelli, F., Gratton, R.G., Kurucz, R.L. 1997, *A&A*, 318, 841
Cayrel, R. 1988, in *The Impact of Very High S/N Spectroscopy on Stellar Physics*, ed. G. Cayrel de Strobel and M. Spite (Dordrecht: Kluwer), 345
Chen, Y.Q., Nissen, P.E., Zhao, G., Zhang, H.W., Benoni, T. 2000, *A&AS*, 141, 491
Chen, Y.Q., Nissen, P.E., Zhao, G., Asplund, M. 2002, *A&A*, 390, 225
Chiba, M., Beers, T.C. 2000, *AJ*, 119, 2843
Chiappini, C., Matteucci, F. & Gratton, R. 1997, *ApJ*, 477, 765
Clegg, R.E.S., Lambert, D.L., Tomkin, J. 1981, *ApJ*, 250, 262
Cole, A. A., Weinberg, M.D. 2002, *ApJL*, 574, 43
Davidson, M.D., Snoek, L.C., Volten, H., Doenszelmann, A. 1992, *A&A*, 255, 457
Dehnen, W., Binney, J.J. 1998, *MNRAS*, 298, 387
Edvardsson, B. 2002, *IAUS*, 187, 91
Edvardsson, B., Andersen, J., Gustafsson, B., Lambert, D.L., Nissen, P.E., Tomkin, J. 1993, *A&A*, 275, 101
ESA 1997, *The Hipparcos and Tycho Catalogues (ESA SP-1200)* (Noordwijk: ESA)
Feltzing, S., Gustafsson, B. 1998, *A&AS*, 129, 237
Feltzing, S., Homberg, J., Hurley, J.R. 2001, *A&A*, 377, 911
Freeman, K., Bland-Hawthorn, J. 2002, *ARA&A*, 40, 487
Friel, E.D. 1995, *ARA&A*, 33, 381
Fuhrmann, K. 1998, *A&A*, 338, 161
Fulbright, J.P. 2000, *AJ*, 120, 1841
Gilmore, G., Reid, N. 1983, *MNRAS*, 202, 1025
Gómez, A.E., Grenier, S., Udry, S., Haywood, M., Meillon, L., Sabas, V., Sellier, A., Morin, D. 1997, in " *Proceedings of the ESA Symposium: Hipparcos - Venice 97* ", Venice, Italy, ESA SP-402, p. 621
Goswami, A., Prantzos, N. 2000, *A&A*, 359, 191
Gratton, R.G. 1989, *A&A*, 208, 171
Gratton, R.G., Carretta, E., Matteucci, F., Sneden, C. 2000, *A&A*, 358, 671
Gratton, R.G., Sneden, C. 1991, *A&A*, 241, 501
Grenon, M. 1987, *JApA*, 8, 123
Grenon, M. 1989, *Ap&SS*, 156, 29
Grevesse, N., Sauval, A.J. 1998, *Space Sci. Rev.*, 85, 161
Grevesse, N., Sauval, A.J. 1999, *A&A*, 347, 348
Gustafsson, B., Bell., R.A., Eriksson, K., Nordlund, Å. 1975, *A&A*, 42, 407
Gustafsson, B., Karlsson, T., Olsson, E., Edvardsson, B, Ryde, N. 1999, *A&A*, 342
Hannaford, P., Lowe, R.M., Grevesse, N., Biémont, E., Whaling, W. 1982, *ApJ*, 261, 736
Hannaford, P., Lowe, R.M., Grevesse, N., Noels, A. 1992, *A&A*, 259, 301
Hauck, B., Mermilliod, M. 1998, *A&AS*, 129, 431
Hauschildt, P.H., Allard, F., Baron, E. 1999, *ApJ*, 512, 377
Heise, C., Kock, M. 1990, *A&A*, 230, 244
Holweger, H. 1967, *Zeitschrift für Astrophysik*, 65, 365
Holweger, H., Müller, E.A. 1974, *Solar Phy.*, 39, 19
Koch, A., Edvardsson, B. 2002, *A&A*, 381, 500
Kroll, S., Kock, M. 1987, *A&AS*, 67, 225
Kiselman, D. 1993, *A&A*, 275, 269
Kurucz, R.L., Furenlid, I., Brault, J., Testerman, L. 1984, *Solar Flux Atlas from 296 to 1300 nm* (Sunspot, N.M.: National Solar Observatory)
Kurucz, R.L. 1998, [HTTP://cfaku5.harvard.edu](http://cfaku5.harvard.edu)
Lachaume, R., Dominik, C., Lanz, T., Habing, H. J. 1999, *A&A*, 348, 897
Lambert, D.L. 1978, *MNRAS*, 182, 249
Lambert, D.L. 1989, in *Cosmic Abundances of Matter; Proceedings of AIP conference*, American Institute of Physics (New York), 183, p.168
Lambert, D.L., Heath, J.E., Lemke, M., Drake, J. 1996, *ApJS*, 103, 183

Lambert, D.L., Luck, R.E. 1978, MNRAS, 183, 79
Lambert, D.L., Warner, B. 1968, MNRAS, 138, 181
Lawler, J.E., Dakin, J.T. 1989, J.Opt.Soc.Am. B, 6, 1457
Lin, D. 1999, Private Communication
Martin, P., Roy, J-R. 1994, ApJ, 424, 599
Martinet, L., Friedli, D. 1997, A&A, 323, 363
McWilliam, A. 1997, ARA&A, 35, 503
Migdalek, J., Baylis, W.E. 1987, Can. J. Phys, 65, 162
Milford, P.N., O'Mara, B.J., Ross, J.E. 1994, A&A, 292, 276
Moore, C.E., Minnaert, M.G.J., Houtgast, J. 1966, The solar spectrum 2935Å to 8770Å, NBS, Washington
Nissen, P.E. 1981, A&A, 97, 145
Nissen, P.E., Chen, Y.Q., Schuster, W.J., Zhao, G. 2000, 353, 722
Nissen, P.E., Edvardsson, B. 1992, A&A, 261, 255
Nissen, P.E., Primas, F., Asplund, M., Lambert, D.L. 2002, A&A, 390, 235
Nissen, P.E., Schuster, W.J. 1997, A&A, 326, 751
Olsen, E.H. 1983, A&AS, 54, 55
Olsen, E.H. 1988, A&A, 189, 173
Pont, F., Fux, R., Mayor, M., Andersen, J., Nordström, B., Olsen, E.H. 1999, ASP, 182 (San Francisco: ASP) P. 305
Prochaska, J.X., McWilliam, A. 2000, ApJL, 537, 57
Prochaska, J.X., Naumov, S.O., Carney, B.W., McWilliam, A., Wolfe, A.M. 2000, AJ, 120, 2513
Raboud, D., Grenon, M., Martinet, L., Fux, R., Udry, S. 1998, A&A. Lett., 335, 61
Schuster, W.J., Nissen, P.E. 1989, A&A, 221, 65
Shchukina, N., Trujillo Bueno, J. 2001, ApJ, 550, 970
Smith, V.V., Coleman, H., Lambert, D.L. 1993, ApJ, 417, 287
Smith, G., Raggett, D. St.J. 1981, J. Phys. B - Atomic and Molecular Physics, 14, 4015
Snedden, C. 1973, PhD Thesis, Univ. of Texas at Austin (USA)
Snedden, C., Gratton, R.G., Crocker, D.A. 1991, A&A, 246, 354
Sparke, L.S., Sellwood, J.A. 1987, MNRAS, 225, 653
Timmes, F.X., Woosley, S.E., Weaver, T.A. 1995, ApJS, 98, 617
Tomkin, J., Edvardsson, B., Lambert, D.L., Gustafsson, B. 1997, A&A, 327, 587
Tomkin, J., Woolf, V.M., Lambert, D.L., Lemke, M. 1995, AJ, 109, 2204
Tull, R.G., MacQueen, P.J., Sneden, C., Lambert, D.L. 1995, PASP, 107, 251
Whaling, W., Hannaford, P., Lowe, R.M., Biémont, E., Grevesse, N. 1985, A&A, 153, 109
Wheeler, J.C., Sneden, C., Truran, J. W., Jr. 1989, ARA&A, 27, 279
Wickliffe, M.E., Lawler, J.E. 1997, ApJS, 110, 163
Wiese, W.L., Fuhr, J.R., Deters, T.M. 1996, in " Atomic transition probabilities of carbon, nitrogen, and oxygen: a critical data compilation" (NIST), QC 453
Woolf, V.M., Tomkin, J., Lambert, D.L. 1995, ApJ, 453, 660
Youssef, N.H., Amer, M.A. 1989, A&A, 220, 281

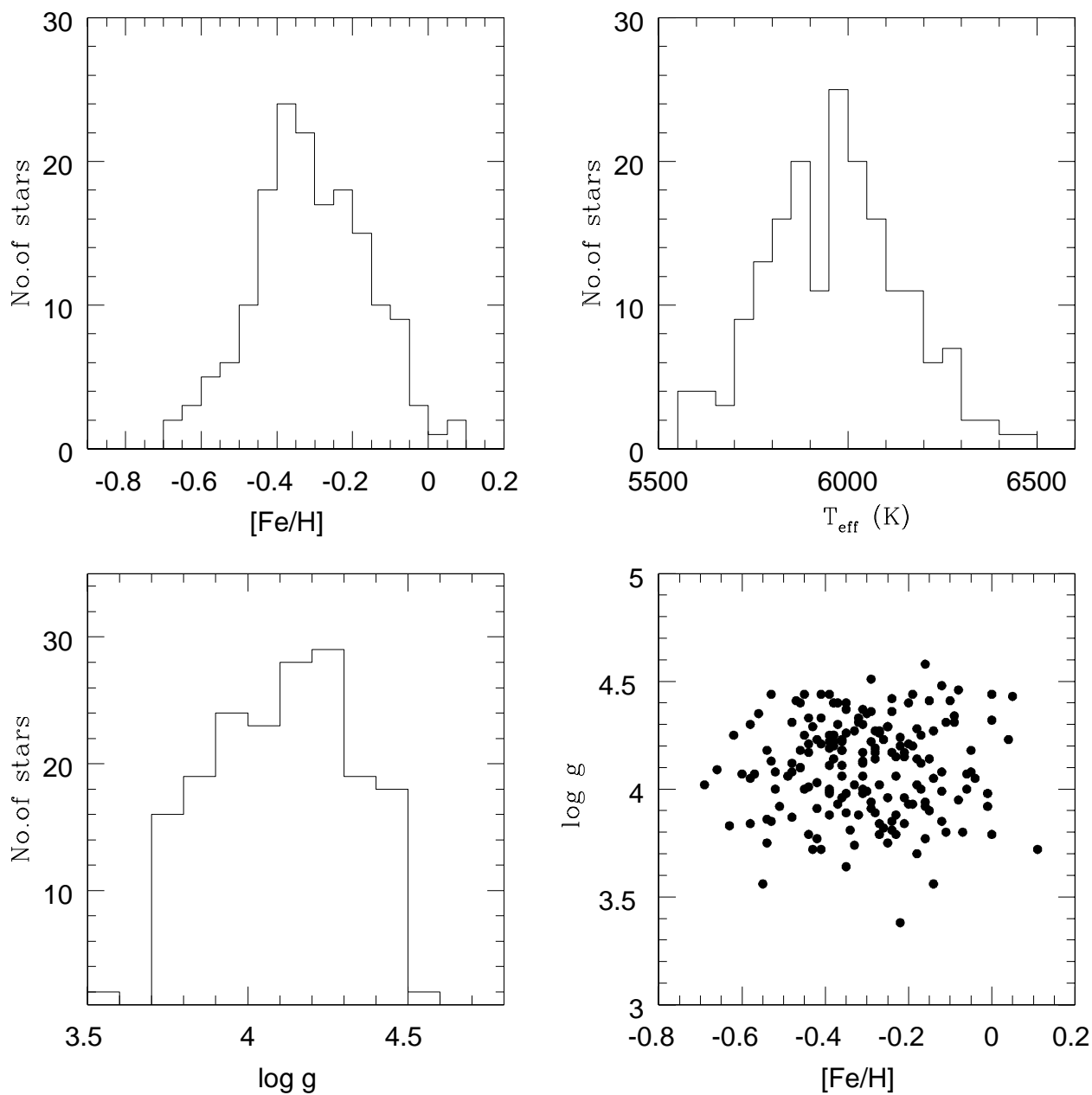


Figure 1. Distribution of our stellar sample in $[Fe/H]$, T_{eff} , and gravity. Also shown is the gravity versus metallicity.

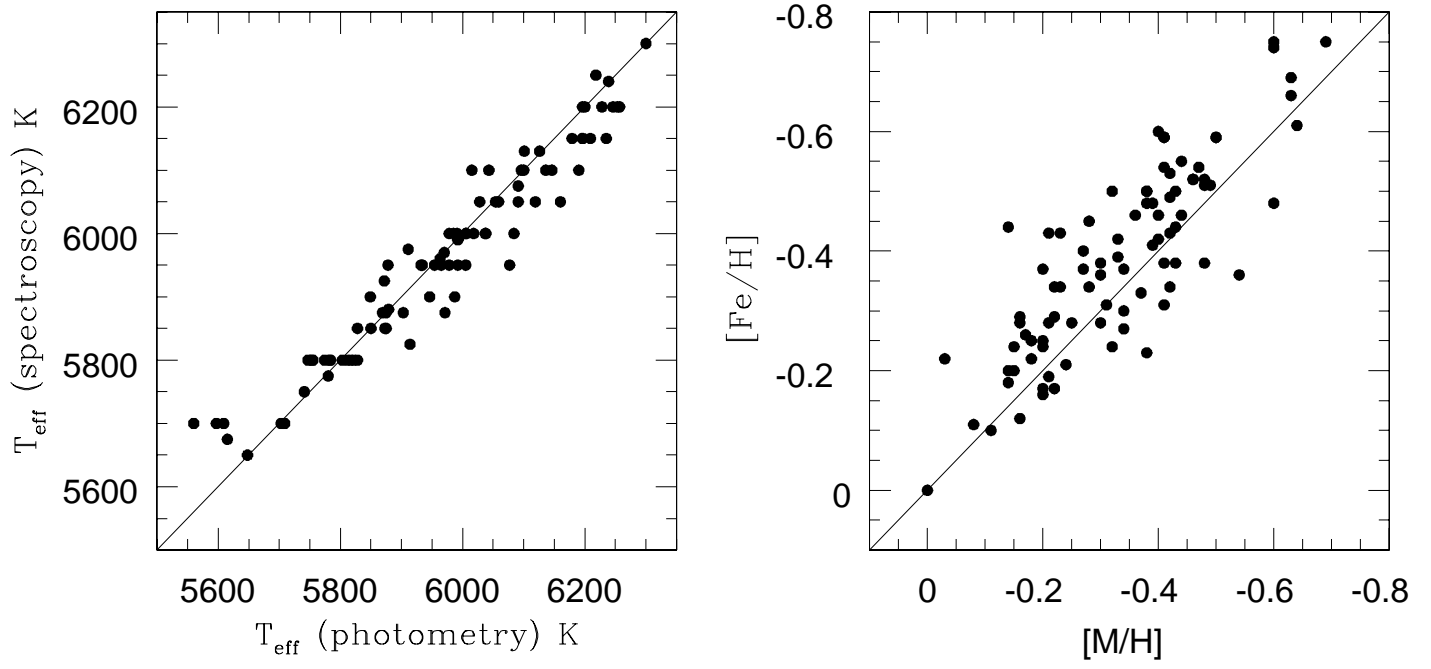


Figure 2. Photometric temperature, T_{eff} and metallicity, $[M/H]$ for a sample of 82 stars are compared with our spectroscopically derived T_{eff} and $[\text{Fe}/\text{H}]$ values (see the text for details).

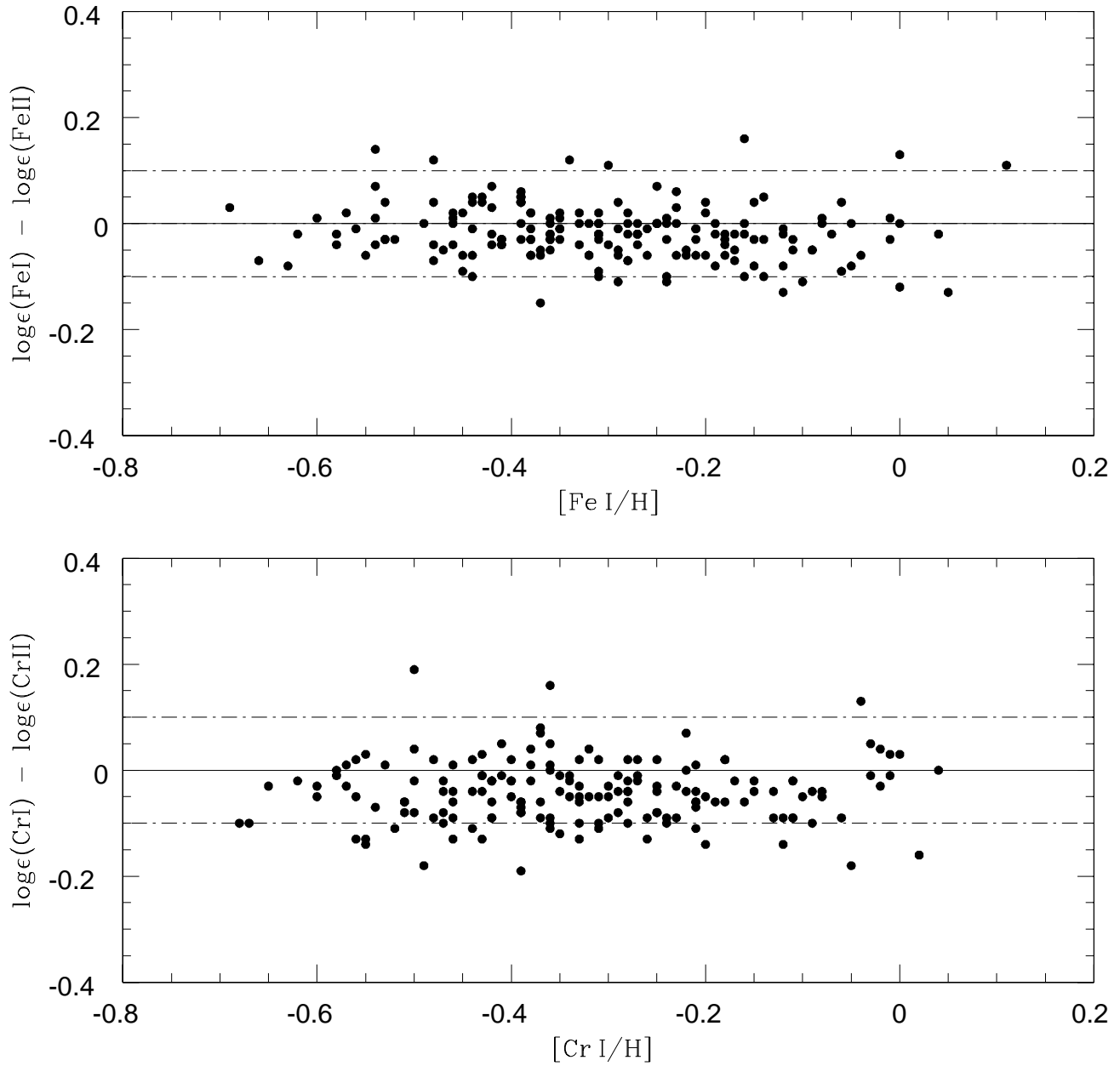


Figure 3. The abundance differences from neutral and singly ionized lines of Fe and Cr are plotted against the abundances from the neutral lines. The broken horizontal lines represent the differences of ± 0.1 dex.

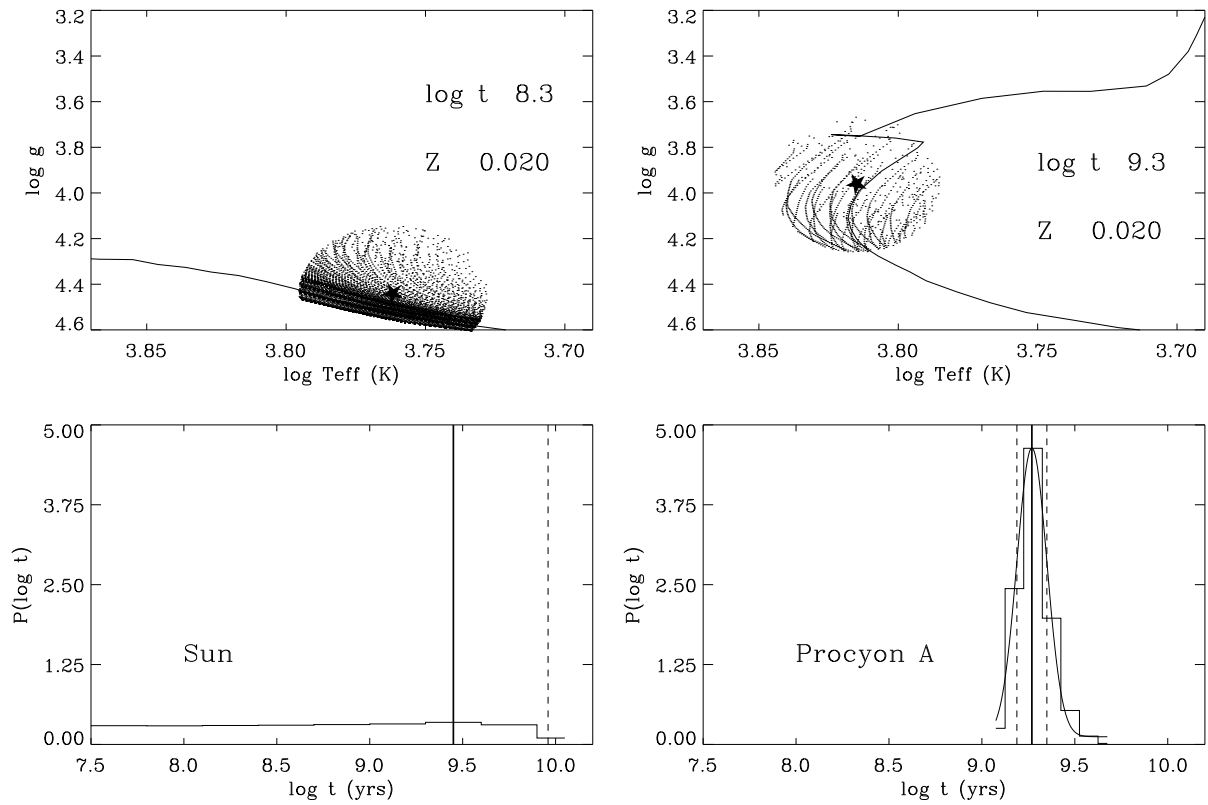


Figure 4. Upper panels: position of the star in the $\log T_{\text{eff}} - \log g$ plane. An isochrone with the indicated age and metallicity is shown as a reference. The dots are grid points within the 3σ error bar ellipse. Lower panels: the probability density for the age is displayed. The thick solid vertical line shows the best estimate for the age and the broken vertical lines mark the 1σ limits.

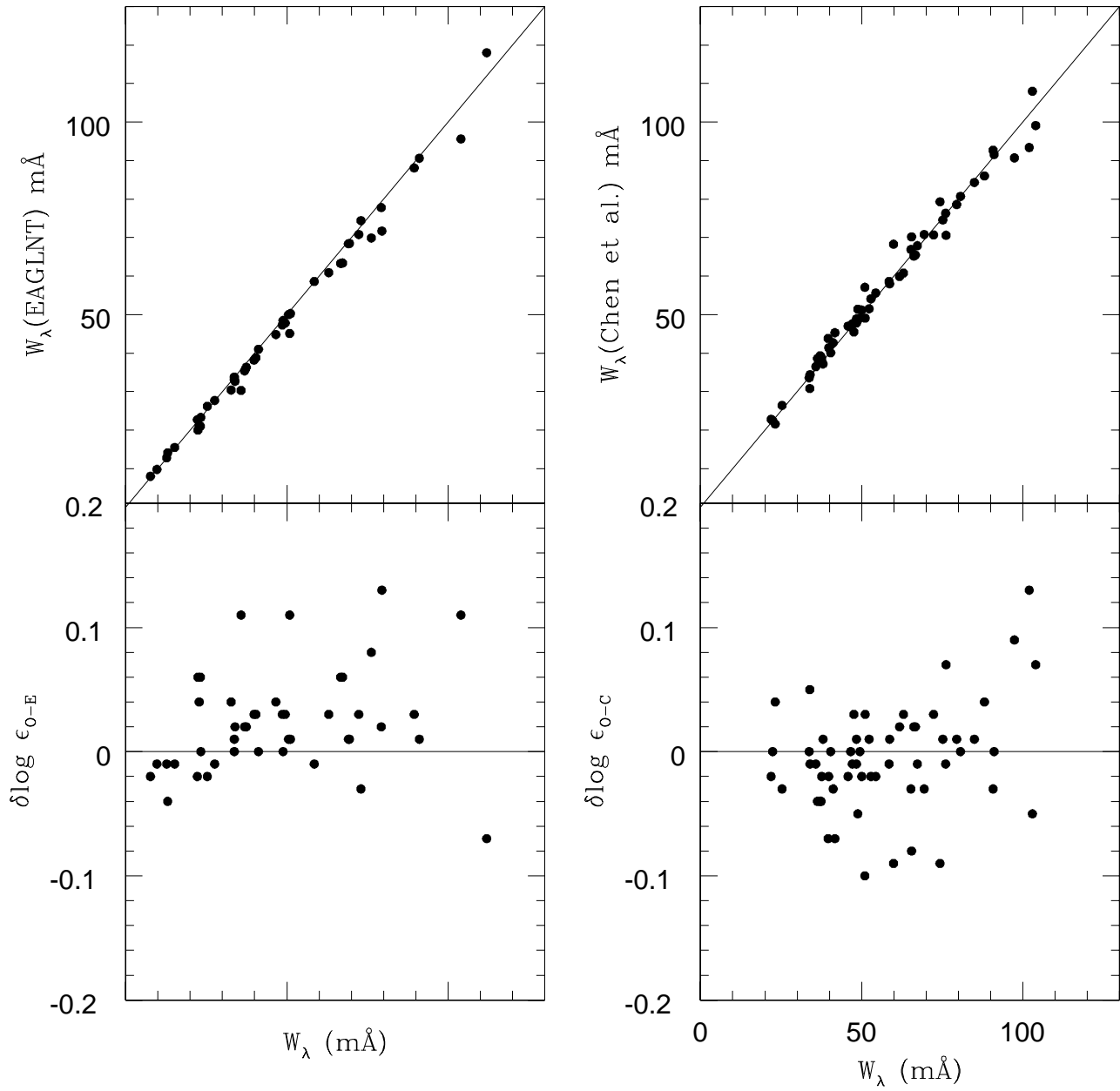


Figure 5. The measured equivalent widths and the derived abundances for the solar Iris spectrum are compared with the solar measurements of EAGLNT (left panels) and Chen et al. (right panels) studies.

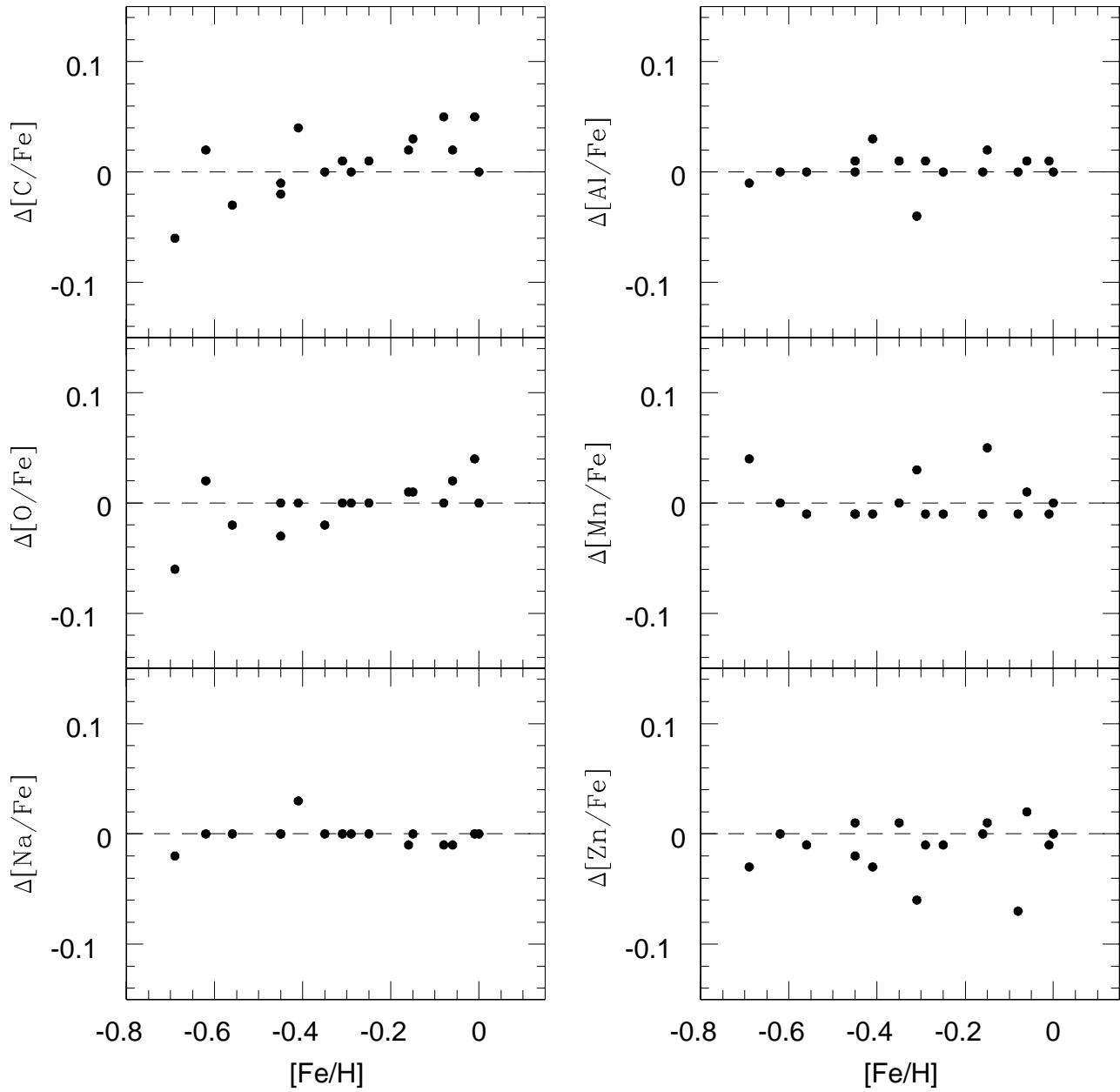


Figure 6. Differences in $[X/Fe]$ between OVER and NOVER models for 16 stars.

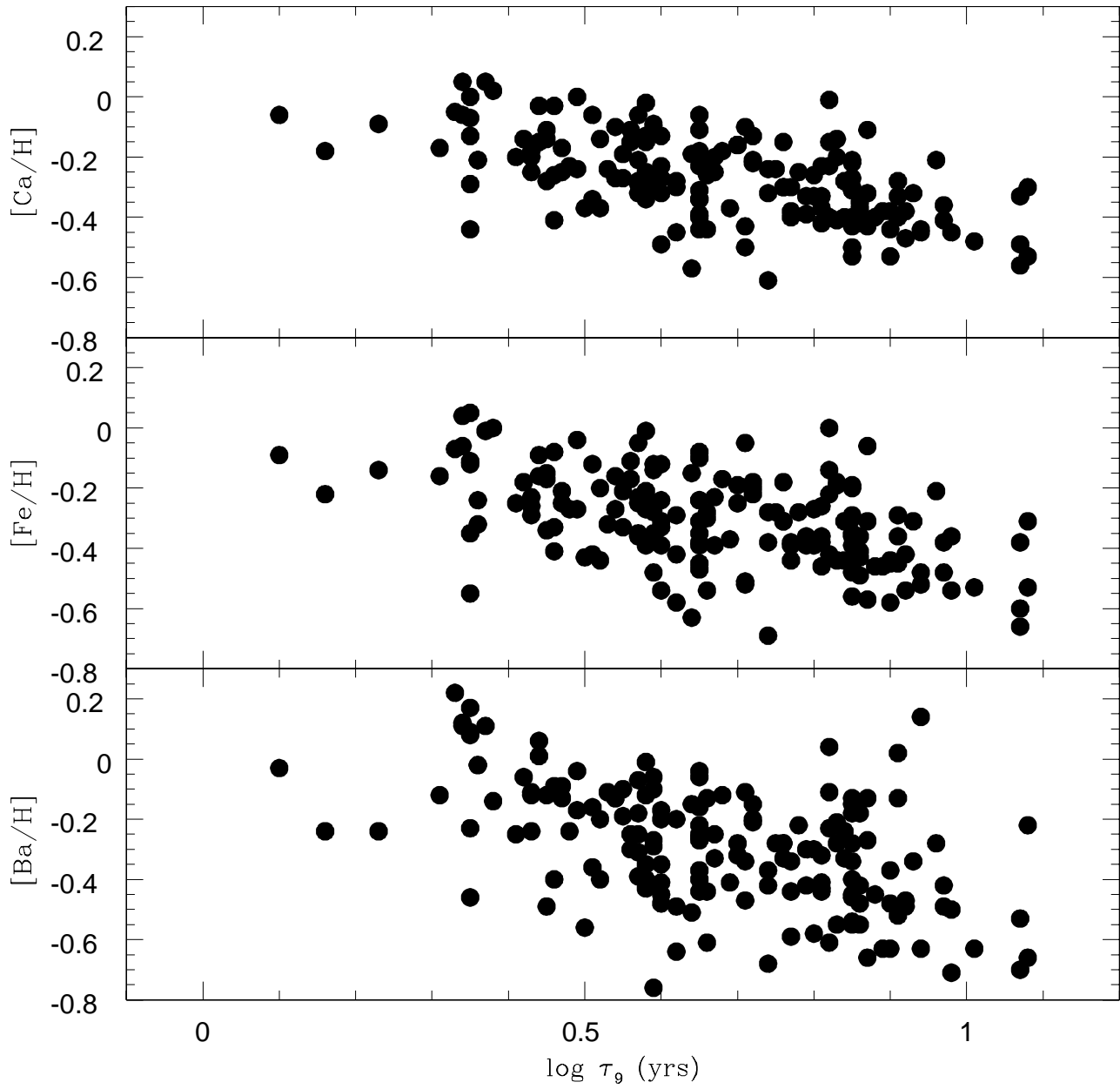


Figure 7. Relative abundances of Ca, Fe, and Ba are shown against the ages of the stars.

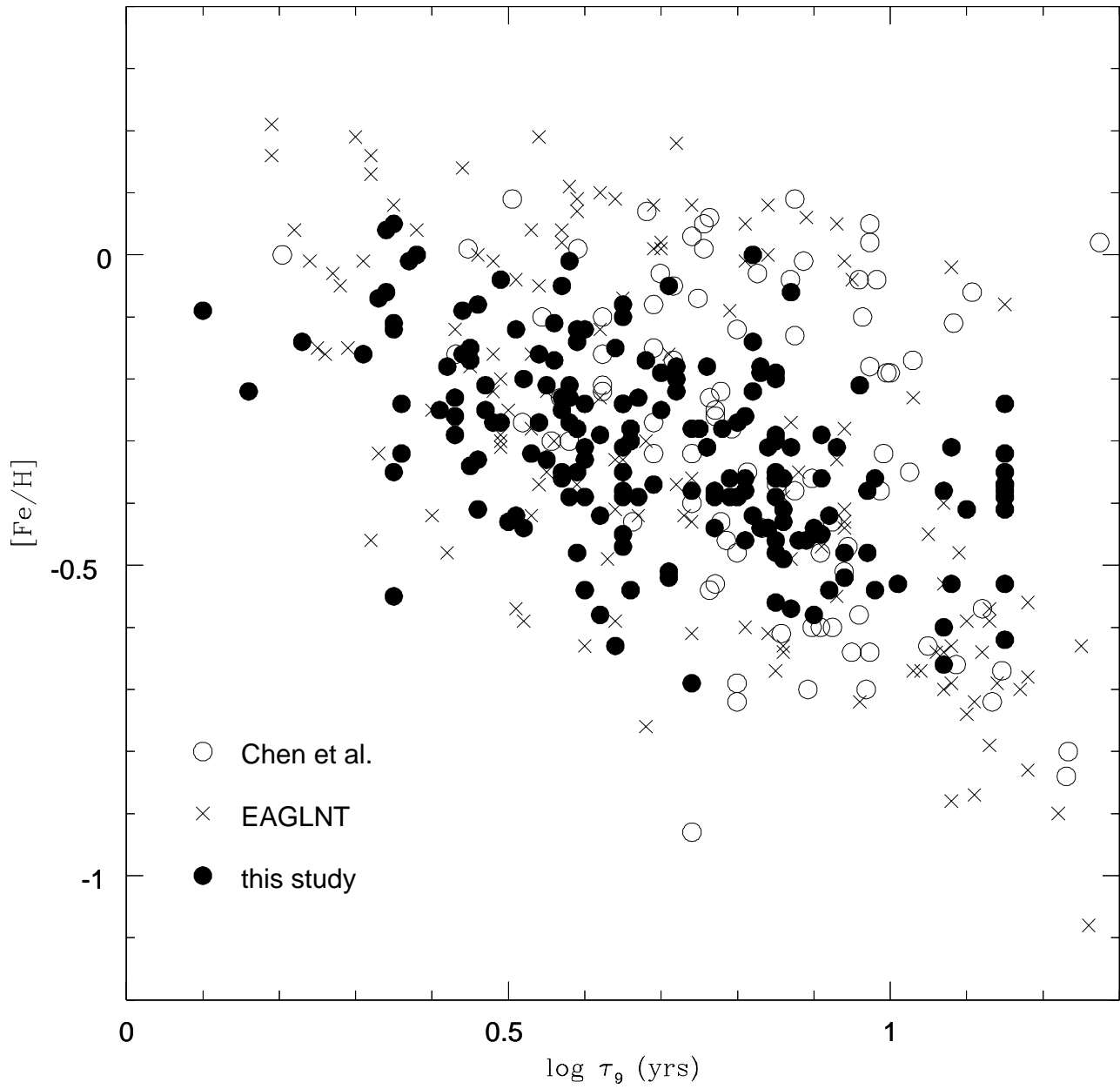


Figure 8. The Age-[Fe/H] relation derived in this study is compared with the two previous studies of Chen et al. and EAGLNT.

Figure 9. Abundance ratios $[X/Fe]$ from C to K, are plotted against the metallicity $[Fe/H]$. Note that oxygen abundances derived from permitted triplet lines at 7775 \AA are corrected using equation 3.

Figure 10. Abundance ratios $[X/Fe]$ from Ca to Zn, are plotted against the metallicity $[Fe/H]$.

Figure 11. Abundance ratios, $[X/Fe]$ from Sr to Eu, are plotted against the metallicity, $[Fe/H]$.

Figure 12. Abundances of Mg and Si relative to Fe (top panels) are plotted against $[Fe/H]$. The solid line is the least squares fit to the data. The residuals around the mean fit are shown in the middle panels. Bottom panels show histograms and the Gaussian fit to the residuals.

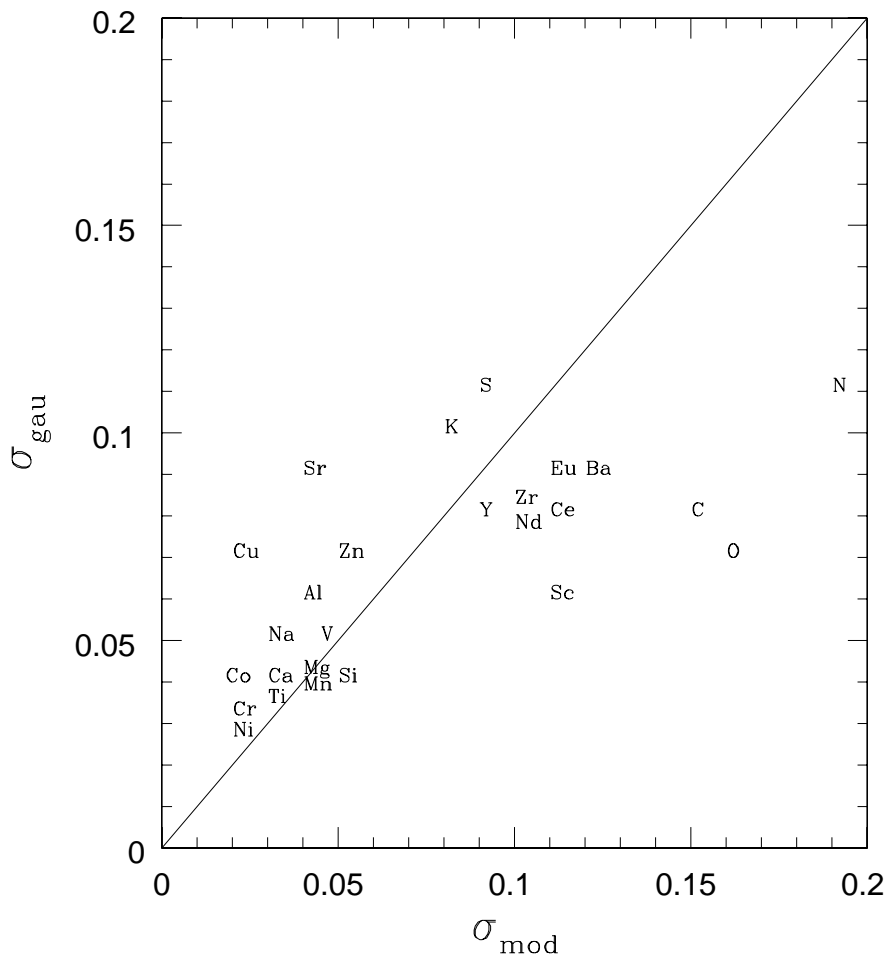


Figure 13. The errors in the abundance analysis as represented by σ_{mod} are compared with σ_{gau} , the dispersion of the Gaussian distribution of the abundance residuals.

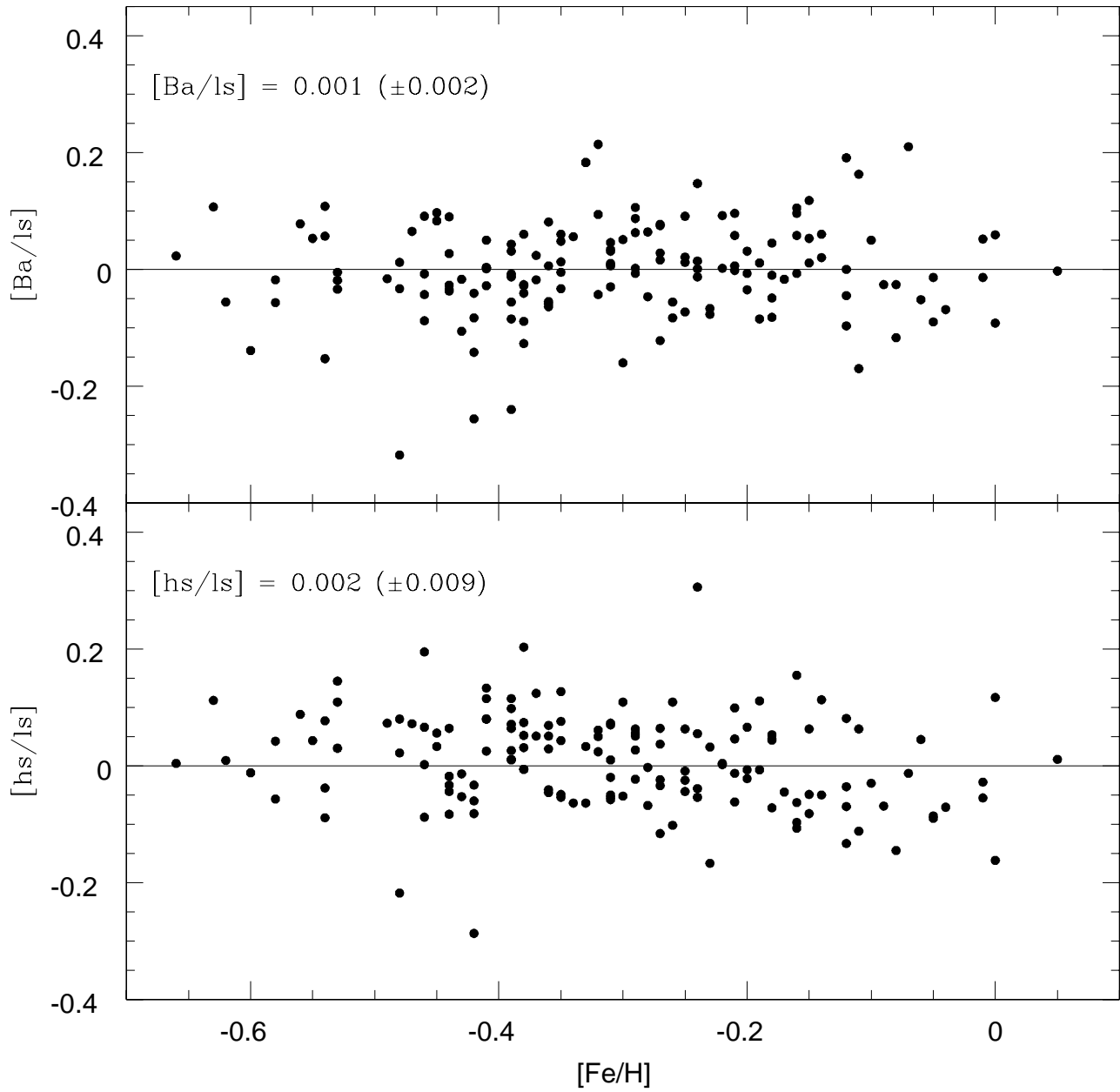


Figure 14. Abundance ratios of heavy (hs: Ba, Ce, and Nd) to light (ls: Sr and Y) *s*-process elements for our sample of stars are shown against metallicity.

Figure 15. Abundance ratios, $[\text{Mg}/\text{Fe}]$ and $[\text{Ti}/\text{Fe}]$ against $[\text{Fe}/\text{H}]$. Our data (filled circles) is compared with earlier studies of Chen et al. (2000: open circles), EAGLNT (open squares), Fuhrmann (1998: crosses), Fulbright (2000: stars), and Prochaska et al. (2000)(open triangles). The broken horizontal lines are drawn for the mean abundances of Fuhrmann and Prochaska et al. thick disc stars.

Figure 16. Plots of V_{LSR} , W_{LSR} , R_{m} , and age against $[\text{Fe}/\text{H}]$. Values determined in this study (filled circles) are compared with earlier studies: Chen et al. (open circles), EAGLNT (open squares), Fuhrmann (crosses), Fulbright (stars), and Prochaska et al. (open triangles). In all cases bigger symbols represent stars with $[\text{Mg}/\text{Fe}] \geq 0.2$.

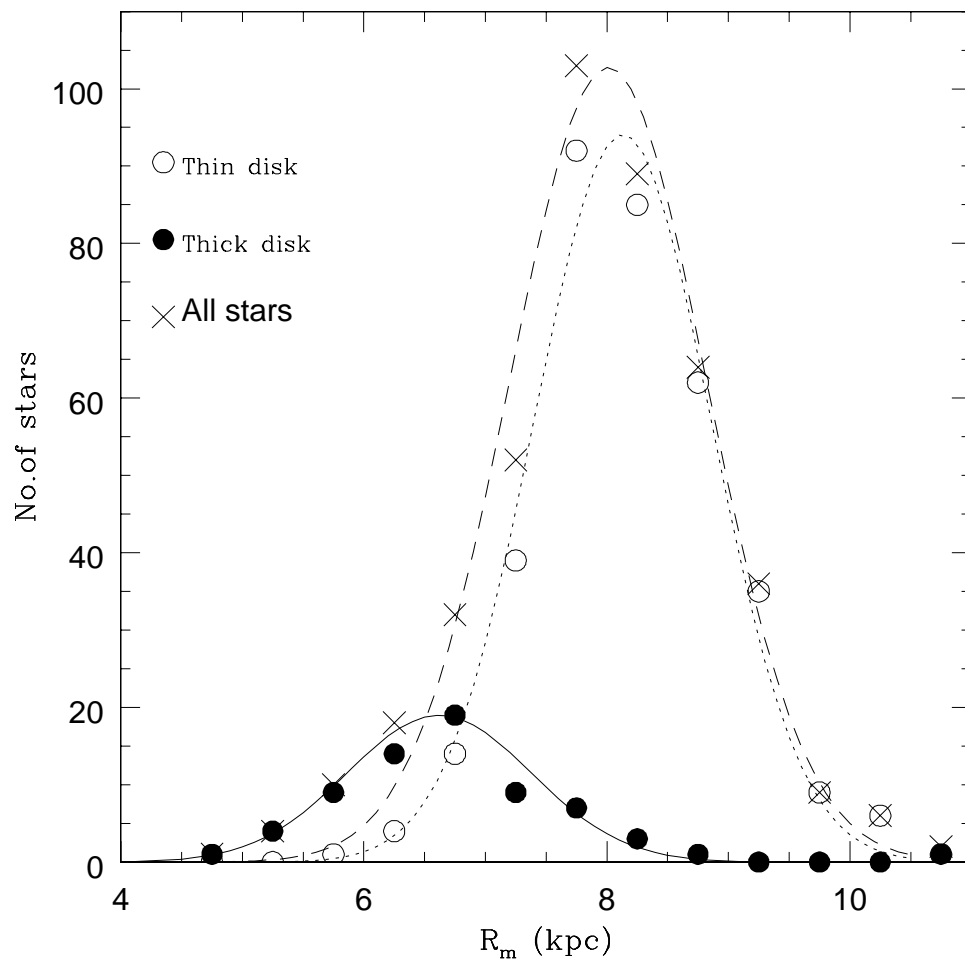


Figure 17. Distribution of around 500 disc stars in R_m . Sample is taken from three surveys: EAGLNT, Chen et al., Fulbright (2000), and ours. The Gaussian fit to the entire sample (crosses) is asymmetric (dashed line), however, fits are very symmetric for thin (dotted line), and thick (solid line) disc populations.

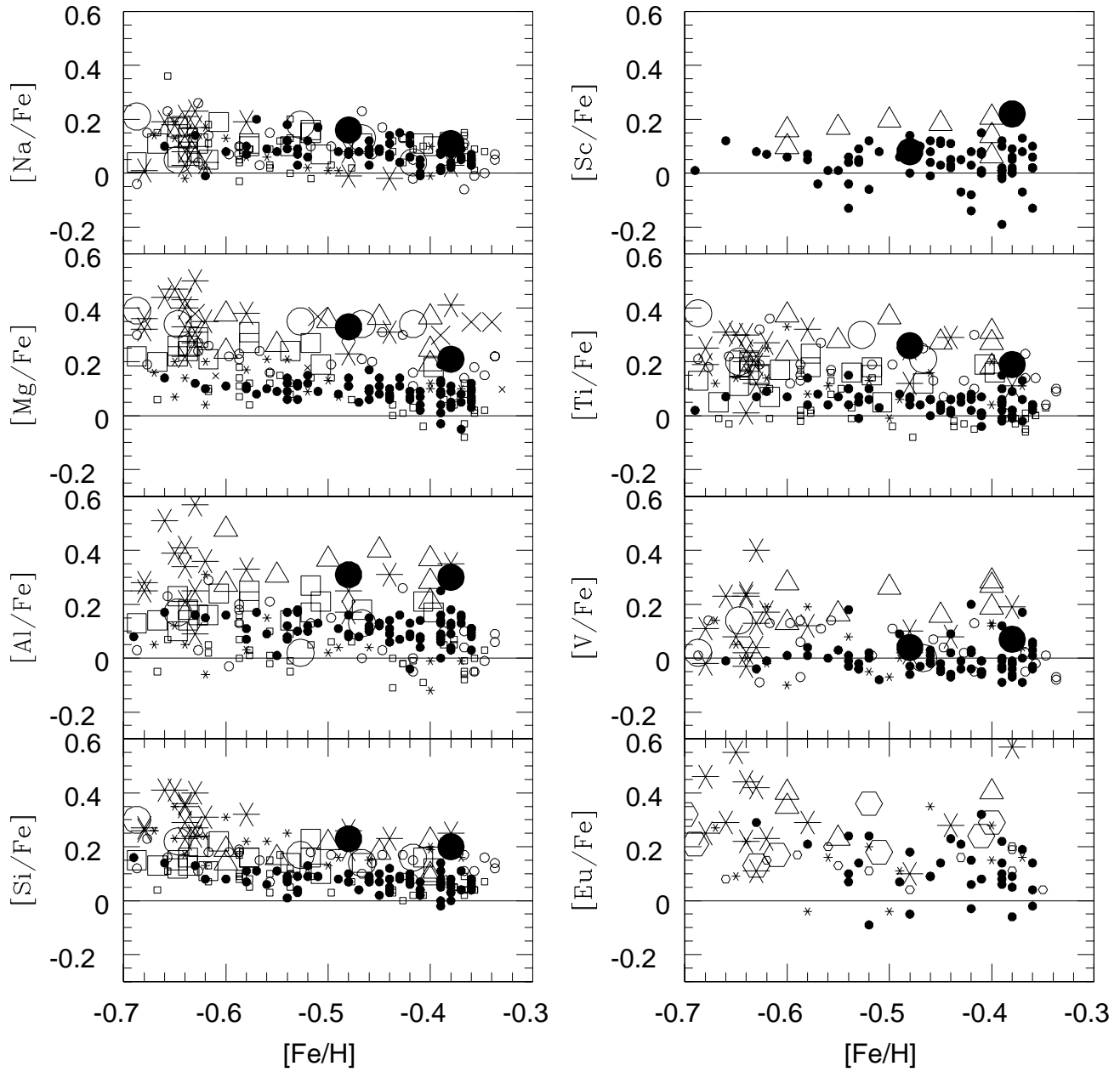


Figure 18. Abundance ratios $[X/Fe]$ of selected elements for stars in the current study (filled circles) in metallicity range from -0.35 to -0.70 , are compared with other studies: Chen et al. (2000: open circles), EAGLNT (open squares), Fuhrmann (1998: crosses), Fulbright (2000: stars), Prochaska et al. (2000)(open triangles), and Woolf et al. (1995: hexagons). In all the cases bigger symbols represent stars of thick disc.

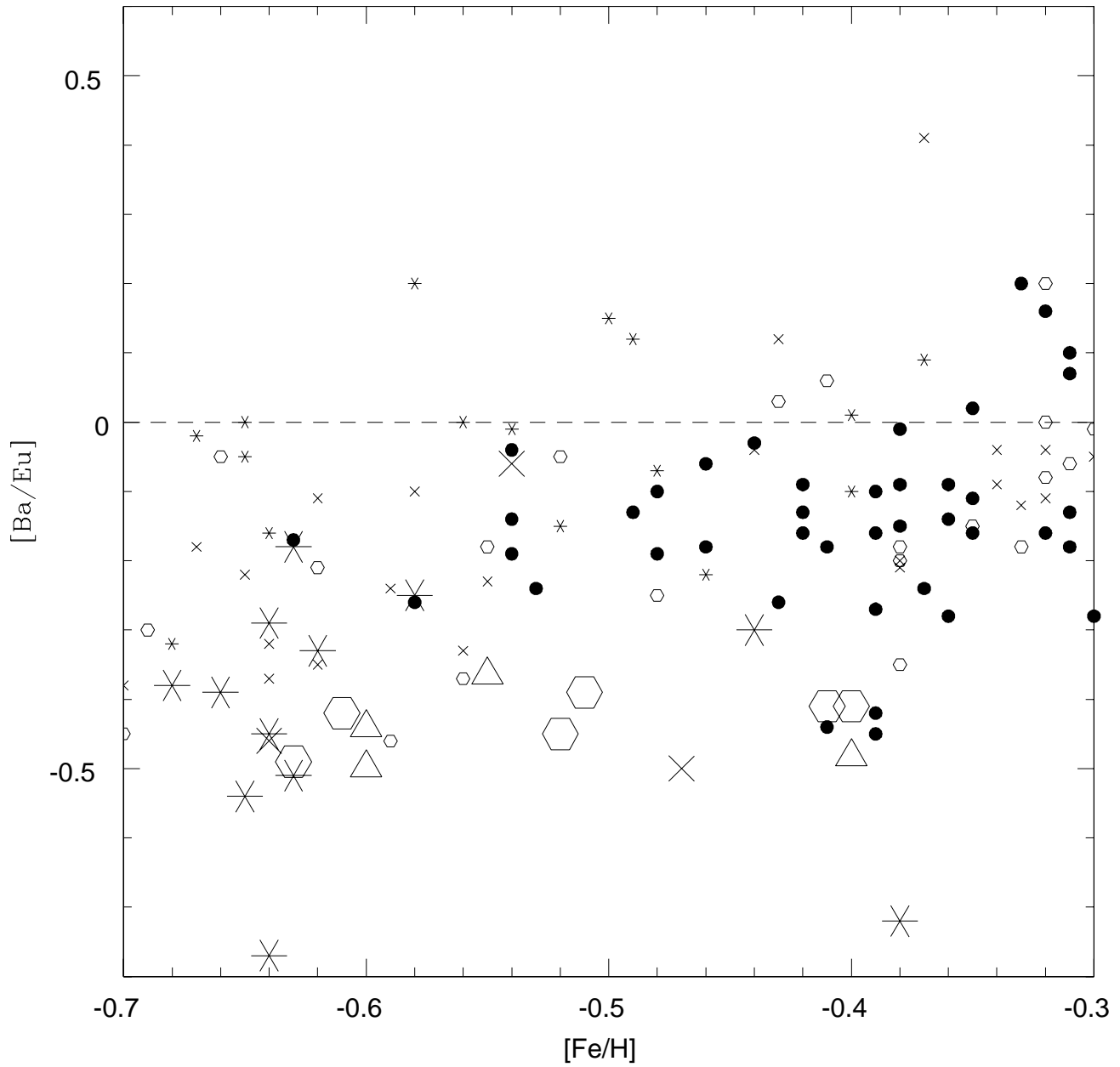


Figure 19. Abundance ratios $[Ba/Eu]$ against $[Fe/H]$ are shown. The symbols represent same as in Figure 18. For stars analysed by Woolf et al. (hexagons), and Kock & Edvardsson (2002: crosses) Ba abundances are taken from EAGLNT.

Table 1. Atmospheric parameters and kinematic data for the programme stars.

Star HD	T_{eff} (K)	$\log g$ (cm s^{-2})	[Fe/H]	U_{LSR} (km s^{-1})	V_{LSR} (km s^{-1})	W_{LSR} (km s^{-1})	R_{m} (kpc)	Z_{max} (kpc)	e	$\log \tau_9$ (yrs)
70	5649.	4.37	-0.35	-16.7	-25.9	-29.5	7.59	0.241	0.13	...
101	5826.	4.36	-0.29	-55.7	-28.8	23.9	7.67	0.199	0.22	0.85
153	5791.	3.80	-0.11	18.3	-43.0	9.9	7.11	0.075	0.21	0.56
330	5775.	3.84	-0.27	-4.1	-50.2	-21.8	6.91	0.171	0.23	0.58
912	6011.	3.82	-0.26	29.4	-5.5	6.8	8.26	0.053	0.10	0.43
2663	5982.	4.33	-0.41	47.0	-11.9	-10.1	8.13	0.080	0.16	0.86
3079	5892.	4.20	-0.19	62.6	-48.2	17.4	7.18	0.140	0.29	0.83
3440	5830.	4.11	-0.36	-43.9	-16.6	7.6	7.96	0.059	0.16	0.91
3454	6058.	4.30	-0.58	23.4	14.4	-20.9	8.98	0.175	0.09	0.90
3532	6146.	3.98	-0.35	4.5	-5.6	-5.8	8.20	0.043	0.04	0.59
3894	6103.	4.20	-0.38	3.2	-17.0	-4.9	7.83	0.036	0.09	0.74
5065	5811.	4.02	-0.18	-60.4	-38.6	45.1	7.45	0.424	0.25	0.76
5494	6083.	4.00	-0.17	-34.2	9.0	24.7	8.82	0.210	0.11	0.56
5750	6228	4.00	-0.39	62.3	-23.0	-8.8	7.89	0.070	0.22	0.60
6250	6127.	3.90	-0.15	-66.0	-6.4	-7.4	8.46	0.061	0.21	0.45
6312	5754.	4.33	-0.32	25.0	-52.7	-32.8	6.89	0.274	0.25	...
6834	6290.	4.02	-0.69	2.0	23.4	-21.9	9.31	0.187	0.09	0.74
6840	5851.	3.72	-0.43	39.6	-41.7	17.9	7.21	0.141	0.23	0.50
7228	6059.	4.08	-0.12	-51.6	-1.0	-4.6	8.54	0.037	0.16	0.59
8671	6196.	3.92	-0.16	24.6	11.4	-11.2	8.86	0.089	0.08	0.44
9091	5829.	4.26	-0.35	-49.2	-22.8	28.5	7.81	0.241	0.19	0.85
9670	6032.	4.27	-0.28	-13.3	-58.2	10.6	6.72	0.080	0.27	0.78
11007	5850.	4.00	-0.31	-35.1	23.4	46.6	9.45	0.477	0.14	0.76
11045	5703.	4.19	-0.39	17.0	2.8	-26.6	8.53	0.219	0.05	...
11592	6235.	4.22	-0.29	-68.4	-17.0	-23.0	8.14	0.197	0.22	0.62
14877	5971.	4.03	-0.42	52.1	-17.3	10.2	7.99	0.081	0.18	0.82
15029	6119.	3.98	-0.31	-73.2	-34.2	-55.3	7.70	0.573	0.27	0.60
15398	6190.	3.92	-0.01	14.2	-41.6	15.2	7.14	0.117	0.20	0.37
16067	5912.	3.85	-0.12	-19.0	-11.6	-18.2	8.03	0.142	0.08	0.51
20427	6091	4.00	-0.52	46.1	-20.4	0.2	7.86	0.016	0.17	0.71
20717	6257.	4.02	-0.33	51.5	-13.9	4.0	8.10	0.031	0.17	0.60
21922	5943.	4.31	-0.48	-9.6	-11.2	20.7	8.32	0.188	0.07	0.85
22255	6187.	4.14	-0.28	20.5	-3.3	-23.4	8.32	0.188	0.07	0.66
22521	5783.	3.96	-0.25	-59.2	-3.0	-29.7	8.54	0.264	0.18	0.70
22718	5729.	3.93	-0.19	-73.5	-1.3	22.1	8.73	0.195	0.23	0.70
23438	5785.	4.18	-0.36	-69.4	2.3	16.6	8.81	0.143	0.21	0.98
24421	5987.	4.14	-0.38	-53.9	14.4	9.2	9.14	0.077	0.17	0.81
26421	5737.	3.98	-0.39	-59.3	-18.2	74.0	8.14	0.870	0.20	0.80
27816	5965.	3.86	-0.54	2.2	15.5	-33.8	9.00	0.297	0.05	0.66
36066	5879.	3.98	-0.01	42.4	-27.5	10.7	7.62	0.083	0.18	0.58
36667	5776.	4.00	-0.45	-27.9	9.1	-5.8	8.78	0.046	0.09	0.91
36909	5900.	4.24	-0.22	-12.3	-6.5	-1.6	8.18	0.012	0.05	0.82
41640	6005.	4.35	-0.56	33.4	-25.8	10.8	7.63	0.083	0.16	0.85
42618	5653.	4.58	-0.16	-71.8	-6.9	18.2	8.50	0.156	0.22	...
45067	5946.	3.99	-0.12	7.5	-60.5	19.6	6.66	0.153	0.28	0.60
52711	5775.	4.40	-0.20	8.0	-72.3	-1.9	6.39	0.014	0.33	0.85
54182	5747.	3.81	-0.24	-0.1	-29.60	8.2	7.45	0.061	0.14	0.60
59360	5710.	4.15	-0.21	35.0	-39.5	25.6	7.26	0.208	0.21	0.96
63332	6261.	4.23	0.04	-8.7	14.0	3.6	8.92	0.028	0.05	0.34
63333	6054.	4.25	-0.38	-8.7	9.9	-20.2	8.77	0.163	0.04	0.77
69897	6247.	4.29	-0.25	14.2	-33.3	14.3	7.36	0.110	0.16	0.47
69965	5849.	4.49	9999	13.5	-12.7	19.4	7.98	0.151	0.08	...
71148	5703.	4.46	-0.08	-30.0	-33.0	-15.2	7.41	0.118	0.18	0.65
73400	6196.	4.17	-0.21	15.3	-5.8	-20.8	8.22	0.164	0.06	0.58
76272	5989.	4.23	-0.42	0.5	4.6	-11.7	8.56	0.089	0.01	0.92
76349	6004.	4.17	-0.44	15.1	-7.1	27.6	8.18	0.224	0.06	0.90
77134	5966.	4.51	-0.29	-36.7	-23.4	5.3	7.72	0.040	0.16	...
77408	6210.	4.15	-0.23	110.2	-4.2	-20.4	9.11	0.191	0.33	0.57
80218	6091.	4.19	-0.28	-9.4	-12.2	-26.5	8.00	0.213	0.07	0.75
85902	5721.	4.44	-0.53	37.4	-1.2	9.3	8.45	0.073	0.12	...
86560	5846.	4.21	-0.41	-87.3	-16.3	-20.4	8.35	0.178	0.28	1.10

Table 1 – *continued*

Star HD	T_{eff} (K)	$\log g$ (cm s^{-2})	[Fe/H]	U_{LSR} (km s^{-1})	V_{LSR} (km s^{-1})	W_{LSR} (km s^{-1})	R_{m} (kpc)	Z_{max} (kpc)	e	$\log \tau_9$ (yrs)
86884	5873.	3.89	-0.28	34.20	-52.0	-22.4	6.93	0.179	0.26	0.59
87838	6019.	4.29	-0.43	81.1	-9.1	-17.0	8.52	0.147	0.25	0.86
88446	5875.	4.08	-0.35	33.0	-95.8	8.9	5.95	0.067	0.45	0.94
89010	5611.	4.00	-0.06	-2.6	14.6	-36.9	8.97	0.329	0.05	0.87
90878	6285.	3.85	-0.24	4.0	-8.3	2.9	8.11	0.021	0.05	0.36
91638	6160.	4.29	-0.25	-24.6	-10.7	-9.7	8.07	0.074	0.09	0.57
94012	6064.	4.41	-0.47	-24.3	-40.8	-6.1	7.18	0.046	0.20	0.65
94835	5814.	4.43	0.05	4.8	-54.0	-5.5	6.81	0.041	0.25	0.35
97037	5797.	4.27	-0.14	7.8	-13.8	-33.8	7.96	0.281	0.07	0.82
99126	6101.	4.14	-0.15	-4.6	2.2	-33.2	8.50	0.276	0.01	0.64
99233	5741.	4.35	-0.62	13.3	26.0	6.6	9.42	0.054	0.10	...
99984	6084.	3.64	-0.35	-3.9	16.6	-31.9	9.04	0.279	0.06	0.35
100067	6179.	4.37	-0.31	69.2	16.4	13.9	9.37	0.123	0.22	0.65
100446	5996.	4.25	-0.45	-22.2	-48.0	6.0	6.99	0.045	0.23	0.90
101472	6043.	4.41	-0.15	-7.2	9.6	-4.0	8.75	0.030	0.04	-0.98
101676	6071.	4.10	-0.46	-31.8	-0.1	-46.9	8.51	0.444	0.10	0.81
101716	5879.	3.70	-0.18	1.4	-24.1	-21.8	7.62	0.171	0.12	0.42
102080	6006.	4.22	-0.36	-46.1	-32.7	2.7	7.49	0.020	0.21	0.81
102618	5935.	4.13	-0.31	6.1	2.2	-41.1	8.51	0.359	0.02	0.84
103891	5978.	3.75	-0.25	17.5	-11.5	14.1	8.03	0.109	0.08	0.41
106510	5818.	4.40	-0.46	-0.5	7.5	46.5	8.72	0.427	0.025	0.85
107038	5876.	3.88	-0.39	-12.0	-11.8	-15.5	8.01	0.119	0.073	0.58
108134	5755.	4.22	-0.38	-52.5	-2.6	-29.7	8.50	0.261	0.16	1.07
109154	5944.	3.77	-0.42	-38.5	6.6	16.9	8.74	0.139	0.12	0.51
109303	5903.	4.01	-0.44	20.7	-22.7	33.7	7.70	0.283	0.13	0.84
110989	5978.	3.87	-0.48	-49.3	-23.8	-0.5	7.77	0.003	0.19	0.59
112756	5993.	4.40	-0.35	18.7	17.6	-8.3	9.08	0.067	0.08	0.65
112887	6422.	3.88	-0.32	-17.0	7.3	0.3	8.68	0.002	0.055	0.36
118687	5994.	4.44	-0.45	-17.2	-25.6	36.6	7.61	0.311	0.13	0.65
121560	6081.	4.40	-0.38	18.9	-14.7	5.8	7.92	0.044	0.095	0.65
124819	6079.	4.17	-0.28	-14.0	2.8	-2.0	8.50	0.015	0.043	0.74
126053	5597.	4.44	-0.41	-31.8	-10.1	-32.8	8.14	0.280	0.11	...
127667	6038.	4.22	-0.39	42.0	-37.9	20.4	7.33	0.163	0.22	0.79
130253	5749.	3.79	-0.23	-56.8	-18.5	-38.0	8.01	0.345	0.20	0.58
131039	6164.	3.88	-0.23	-25.9	-30.3	5.2	7.47	0.039	0.16	0.43
131599	6091.	4.33	-0.44	-7.4	6.2	0.3	8.62	0.002	0.03	0.77
133641	6032.	3.91	-0.42	-23.7	-37.2	40.5	7.30	0.354	0.19	0.62
136925	5615.	4.25	-0.38	45.0	-48.6	-0.1	7.05	0.001	0.26	...
139457	5953.	4.06	-0.49	-97.3	-24.6	-9.1	8.20	0.077	0.32	0.86
140324	5822.	4.06	-0.36	-30.8	0.6	34.8	8.50	0.305	0.09	0.86
140750	5597.	3.98	-0.37	-37.0	-29.8	-5.9	7.53	0.045	0.18	...
145937	5813.	4.07	-0.60	-65.3	8.4	10.8	9.00	0.091	0.20	...
146946	5691.	4.30	-0.37	34.1	21.9	-28.6	9.34	0.259	0.13	...
148049	5955.	4.18	-0.36	-11.3	-9.1	-24.2	8.10	0.193	0.06	0.85
149576	6380.	4.12	-0.17	47.9	-42.4	3.6	10.5	0.458	0.19	0.45
152449	6096.	4.18	-0.05	7.3	-15.0	6.1	7.90	0.045	0.08	0.57
152986	6074.	4.25	-0.17	5.9	9.1	19.3	8.73	0.154	0.03	0.68
153240	6135.	4.31	-0.09	8.6	-15.0	3.4	7.90	0.025	0.081	0.44
153627	5827.	4.22	-0.38	-25.2	2.2	-16.1	8.52	0.128	0.08	0.97
153668	6029.	4.20	-0.22	16.9	-4.2	28.9	8.28	0.237	0.06	0.72
155646	6201.	3.80	-0.07	-75.0	11.5	14.2	9.23	0.125	0.23	0.33
156635	6136.	4.28	-0.10	0.3	-22.5	10.7	7.66	0.081	0.11	0.65
157466	5932.	4.41	-0.41	-49.8	20.9	11.4	9.38	0.097	0.17	0.46
157467	6016.	3.72	0.11	9.70	-16.9	5.2	7.84	0.039	0.09	...
159333	5863.	3.79	-0.27	-2.20	-30.7	-7.2	7.42	0.054	0.15	0.48
160078	6015.	4.05	-0.14	-50.6	-6.3	-16.7	8.35	0.137	0.16	0.59
163363	6038.	3.79	0.00	-72.8	7.7	-13.8	9.05	0.120	0.22	0.38
167588	5829.	3.93	-0.37	-51.2	-12.2	-9.9	8.15	0.079	0.17	0.69
169359	5809.	4.12	-0.31	-16.5	9.5	-31.6	8.78	0.271	0.06	0.93
171620	6019.	4.18	-0.46	56.7	10.2	-31.3	9.02	0.288	0.18	0.88
171886	6290.	4.27	-0.33	27.8	-45.1	-9.3	7.08	0.071	0.22	0.55
174160	6196.	4.34	-0.09	-11.8	8.7	4.4	8.72	0.034	0.04	0.10
176796	5974.	3.79	-0.44	-63.2	10.9	5.1	9.08	0.043	0.20	0.52

Table 1 – *continued*

Star HD	T_{eff} (K)	$\log g$ (cm s^{-2})	[Fe/H]	U_{LSR} (km s^{-1})	V_{LSR} (km s^{-1})	W_{LSR} (km s^{-1})	R_{m} (kpc)	Z_{max} (kpc)	e	$\log \tau_9$ (yrs)
182758	5894.	4.13	-0.53	-26.8	5.3	-27.6	8.65	0.233	0.08	1.08
186379	5806.	3.99	-0.39	-42.2	-21.5	-38.0	7.83	0.336	0.16	0.77
186408	5670.	4.32	0.00	-28.0	-24.9	7.0	7.64	0.053	0.15	0.82
190681	6105.	3.95	-0.08	-38.5	-21.2	3.7	7.79	0.028	0.16	0.46
191649	5911.	4.23	-0.26	11.5	-1.3	3.2	8.36	0.024	0.04	0.81
191672	5963.	4.10	-0.46	17.1	-18.0	2.6	7.82	0.019	0.10	0.89
192145	5964.	3.89	-0.35	-4.6	-19.4	19.9	7.76	0.155	0.09	0.57
193664	5782.	4.44	-0.19	30.6	-0.3	-14.5	8.45	0.115	0.09	0.85
194497	6327.	3.91	-0.29	34.4	-24.2	14.2	7.69	0.111	0.16	0.43
195200	6031.	4.21	-0.20	-8.6	-19.6	-3.0	7.75	0.022	0.10	0.72
198089	5770.	4.35	-0.30	13.3	-17.2	18.1	7.84	0.141	0.09	0.850
198109	6095.	4.21	-0.44	-5.0	22.7	-29.6	9.29	0.262	0.08	0.83
198390	6337.	4.31	-0.32	0.8	17.4	7.2	9.05	0.057	0.06	0.53
199085	6391.	4.31	-0.11	8.6	-16.4	15.2	7.86	0.117	0.09	0.35
200580	5853.	4.05	-0.54	-106.0	-69.6	16.4	7.06	0.139	0.44	0.98
201444	5926.	3.83	-0.63	27.9	2.2	16.5	8.53	0.132	0.08	0.64
201490	6006.	4.06	-0.23	22.5	3.0	-20.3	8.54	0.164	0.07	0.67
201639	6071.	4.18	-0.54	-27.0	43.1	32.4	10.3	0.324	0.19	0.92
201835	6172.	4.11	-0.39	27.7	46.3	-6.3	10.4	0.057	0.20	0.67
202884	6141.	4.36	-0.24	5.4	-1.4	-16.9	8.35	0.130	0.02	0.65
204306	5892.	4.09	-0.66	-14.9	28.1	-11.9	9.52	0.100	0.11	...
204559	6028.	4.23	-0.36	24.3	-13.5	17.2	7.98	0.135	0.10	0.79
204712	5888.	4.12	-0.48	-46.5	-38.7	17.5	7.33	0.139	0.23	0.97
206860	5820.	4.48	-0.12	4.6	-16.1	-3.8	7.86	0.028	0.08	0.35
209320	5994.	4.14	-0.18	7.6	-39.4	28.4	7.20	0.230	0.18	0.72
209858	5911.	4.26	-0.27	-32.5	-16.0	-34.4	7.95	0.295	0.13	0.80
210457	6152.	4.02	-0.27	-3.4	-11.1	1.4	8.02	0.010	0.06	0.54
210640	6218.	3.96	-0.36	7.7	0.9	-19.3	8.44	0.151	0.03	0.57
210718	6025.	3.81	-0.34	14.9	-2.5	22.0	8.33	0.175	0.05	0.45
210923	6019.	3.96	-0.21	5.0	5.2	23.6	8.59	0.189	0.02	0.55
210985	6058.	4.07	-0.57	-26.4	-20.6	8.6	7.76	0.065	0.13	0.87
212858	5856.	4.25	-0.39	56.9	34.6	-12.7	10.1	0.116	0.22	0.85
214111	5994.	3.56	-0.14	52.8	-5.3	2.4	8.39	0.019	0.17	0.23
214435	5908.	4.30	-0.31	-20.6	-27.8	-11.8	7.53	0.090	0.15	0.87
214557	5879.	4.08	-0.05	-58.7	-29.4	-9.2	7.67	0.073	0.23	0.71
214576	6300.	3.95	-0.55	-27.7	27.5	-3.8	9.53	0.031	0.13	0.35
215442	5872.	3.80	-0.22	43.8	-15.0	10.0	8.01	0.078	0.15	0.16
216106	5890.	3.74	-0.33	-47.2	-35.3	-24.9	7.43	0.205	0.22	0.46
216385	6240.	3.77	-0.16	48.1	-1.6	-26.8	8.51	0.231	0.15	0.31
216631	5985.	4.44	-0.39	-50.9	-36.2	-11.4	7.42	0.089	0.23	0.65
217877	5872.	4.28	-0.18	35.2	-11.7	1.3	8.08	0.010	0.12	0.83
218059	6253.	4.27	-0.27	2.0	-33.0	-20.1	7.36	0.157	0.15	0.49
218172	5958.	3.84	-0.21	-4.1	13.2	7.3	8.88	0.057	0.045	0.47
218470	6476.	4.07	-0.06	19.6	-4.0	17.4	8.28	0.137	0.067	0.34
218637	5981.	3.99	-0.30	30.6	-52.6	11.4	6.89	0.087	0.26	0.66
219306	5962.	4.06	-0.31	-6.0	9.2	-24.0	8.74	0.195	0.03	0.76
219476	5879.	3.75	-0.54	54.2	-3.4	-5.9	8.47	0.047	0.17	0.60
219497	5871.	3.92	-0.51	-10.9	31.3	-4.6	9.65	0.038	0.12	0.71
219983	6102.	3.93	-0.20	36.0	-42.3	-16.6	7.18	0.130	0.22	0.52
220842	5761.	4.17	-0.31	-27.0	-7.5	54.5	8.25	0.532	0.09	...
220908	5991.	3.94	-0.16	16.5	-18.9	6.4	7.79	0.048	0.11	0.54
221356	6005.	4.42	-0.24	-0.9	-28.3	2.0	7.49	0.015	0.13	0.65
222155	5561.	3.94	-0.29	6.1	-55.9	-23.4	6.77	0.185	0.26	0.91
223436	6158.	4.05	-0.04	-64.6	2.8	-11.0	8.78	0.092	0.20	0.49
223583	5881.	4.08	-0.48	45.8	-34.2	0.00	7.45	0.170	0.21	0.94
223854	5987.	3.84	-0.58	15.9	24.5	-2.0	9.36	0.016	0.10	0.62
224233	5609.	4.17	-0.24	46.1	-15.4	62.5	8.10	0.662	0.16	...
225239	5557.	3.85	-0.53	114.8	-46.1	-3.8	7.79	0.032	0.40	1.01

Table 2. Adopted line list and atomic data. Δ_6 is the enhancement factor with which classical van der Waals damping constant multiplied, and all other columns are self explanatory.

Ion	Wavelength (Å)	LEP (eV)	$\log gf$	$\delta\Gamma_6^{5/2}$	$W_{\lambda_{\odot}}$ (mÅ)	Ref.
C I	5052.150	7.68	-1.30	9.9	37.8	WFD
	5380.320	7.68	-1.61	9.9	21.9	WFD
	6587.620	8.54	-1.00	9.9	14.0	WFD
	7113.170	8.65	-0.77	9.9	22.7	WFD
	7115.170	8.64	-0.93	9.9	26.7	WFD
	7116.960	8.65	-0.91	9.9	18.5	WFD
N I	7468.270	10.34	-0.19	9.9	4.1	WFD
	8629.160	10.68	0.07	9.9	3.4	WFD
[O I]	6300.310	0.000	-9.75	9.9	4.1	LAM
O I	7771.950	9.150	0.37	9.9	79.9	WFD
	7774.180	9.146	0.22	9.9	65.7	WFD
	7775.400	9.146	0.00	9.9	49.6	WFD
Na I	6154.230	2.10	-1.57	6.4	39.8	LW
	6160.750	2.10	-1.27	6.4	58.4	LW
Mg I	4730.040	4.340	-2.39	9.9	76.8	LL
	6318.710	5.108	-1.97	9.9	39.8	LL
	7657.610	5.110	-1.28	9.9	103.1	LL
Al I	6698.670	3.14	-1.63	9.9	21.9	LL
	7835.320	4.02	-0.58	9.9	47.6	LL
	7836.130	4.02	-0.40	9.9	61.7	LL
	8772.880	4.02	-0.25	9.9	74.0	LL
	8773.910	4.02	-0.07	9.9	94.1	LL
Si I	5793.080	4.930	-2.06	1.9	44.9	LUCK
	6125.030	5.610	-1.51	1.9	33.8	LUCK
	6142.490	5.620	-1.54	1.9	36.8	LUCK
	6145.020	5.610	-1.48	1.9	40.3	LUCK
	6244.480	5.610	-1.36	1.9	48.4	LUCK
	6721.840	5.863	-1.06	1.9	49.1	LUCK
	7800.000	6.180	-0.71	1.9	59.8	LUCK
Si II	6371.360	8.120	-0.05	1.9	31.7	LL
S I	6046.02	7.866	-0.51	9.9	17.1	KUR
	6052.67	7.866	-0.63	9.9	10.0	KUR
	6757.17	7.866	-0.31	9.9	17.0	KUR
K I	7698.980	0.000	-0.17	9.9	166.2	LW
Ca I	5867.570	2.93	-1.57	4.3	25.2	AP
	6166.440	2.52	-1.14	4.3	72.3	SR
	6169.040	2.52	-0.80	4.3	104.1	SR
	6455.610	2.52	-1.29	4.3	58.7	SR
	6572.800	0.00	-4.28	4.3	33.2	AP
Sc II	5318.360	1.357	-2.00	9.9	13.2	LD
	6245.620	1.510	-1.02	9.9	36.2	YA
	6604.600	1.357	-1.30	9.9	37.1	LD

Table 2 – *continued*

Ion	Wavelength (Å)	LEP (eV)	log gf		$W_{\lambda_{\odot}}$ (mÅ)	Ref.
Ti I	5024.850	0.818	-0.56	9.9	73.2	OXF
	5113.450	1.443	-0.73	9.9	27.6	OXF
	5219.710	0.021	-2.24	9.9	29.1	OXF
	5866.460	1.066	-0.76	9.9	48.7	OXF
	6091.180	2.267	-0.37	9.9	15.3	OXF
	6126.220	1.066	-1.37	9.9	23.2	AP
	6258.110	1.443	-0.31	9.9	52.3	OXF
V I	5727.060	1.082	-0.01	9.9	39.6	WHL
	6039.740	1.064	-0.65	9.9	13.2	WHL
	6090.220	1.081	-0.06	9.9	34.0	WHL
	6111.650	1.043	-0.71	9.9	11.7	WHL
	6216.360	0.275	-0.83	9.9	38.0	AP
	6251.830	0.287	-1.34	9.9	16.1	WHL
Cr I	5300.750	0.983	-2.13	9.9	62.2	OXF
	5783.870	3.322	-0.29	9.9	45.8	OXF
	5787.930	3.322	-0.08	9.9	48.3	OXF
	6330.100	0.941	-2.90	9.9	27.1	AP
Cr II	5305.870	3.827	-1.97	9.9	26.7	AP
Mn I	5394.670	0.000	-3.50	9.9	81.1	KUR
	5420.360	2.143	-1.46	9.9	87.1	KUR
	6021.800	3.070	0.03	9.9	104.2	KUR
Fe I	5141.750	2.424	-2.18	2.3	89.4	AP
	5247.060	0.087	-4.94	2.3	67.6	OXF
	5358.120	3.300	-3.16	2.3	10.2	AP
	5412.788	4.440	-1.71	2.3	20.1	HAN
	5661.348	4.280	-1.75	2.3	24.2	HAN
	5778.458	2.590	-3.45	2.3	22.6	OXH
	5784.661	3.400	-2.53	2.3	27.8	HAN
	5809.220	3.884	-1.61	2.3	50.8	MOR
	5849.690	3.695	-2.93	2.3	7.6	OXF
	5852.230	4.549	-1.17	2.3	41.1	AP
	5855.090	4.608	-1.48	2.3	22.2	HAN
	5856.100	4.294	-1.56	2.3	33.7	AP
	5858.790	4.220	-2.18	2.3	13.0	AP
	5859.600	4.550	-0.61	2.3	73.0	AP
	5862.370	4.550	-0.25	2.3	97.3	AP
	5956.700	0.859	-4.60	2.3	52.9	OXF
	6027.060	4.070	-1.17	2.3	66.2	AP
	6151.620	2.176	-3.28	2.3	51.1	OXH
	6159.380	4.610	-1.83	2.3	12.7	AP
	6165.360	4.143	-1.46	2.3	46.6	AP
	6173.340	2.223	-2.88	2.3	69.4	OXF
	6200.320	2.609	-2.44	2.3	79.4	OXF
	6213.440	2.223	-2.56	2.3	88.0	AP
	6240.652	2.220	-3.23	2.3	49.9	HAN
	6265.141	2.176	-2.55	2.3	90.7	OXF
	6271.283	3.330	-2.70	2.3	24.6	HAN
	6297.801	2.223	-2.73	2.3	75.1	OXH
	6322.694	2.588	-2.43	2.3	74.2	OXF
	6358.690	0.859	-4.00	2.3	85.0	AP
6436.410	4.186	-2.36	2.3	10.1	AP	
6481.878	2.279	-2.97	2.3	65.4	OXF	
6498.950	0.958	-4.69	2.3	48.3	OXF	
6518.374	2.830	-2.45	2.3	58.9	HAN	
6574.233	0.990	-5.00	2.3	28.9	OXF	

Table 2 – *continued*

Ion	Wavelength (Å)	LEP (eV)	log gf		$W_{\lambda_{\odot}}$ (mÅ)	Ref.
	6581.214	1.480	-4.68	2.3	19.6	HAN
	6591.330	4.593	-1.95	2.3	10.7	AP
	6608.040	2.279	-3.91	2.3	18.8	AP
	6625.027	1.010	-5.34	2.3	16.6	OXF
	6699.142	4.590	-2.10	2.3	8.4	HAN
	6713.750	4.795	-1.39	2.3	21.7	AP
	6725.360	4.103	-2.17	2.3	17.9	AP
	6733.150	4.638	-1.40	2.3	27.5	HAN
	6739.524	1.560	-4.79	2.3	11.9	HAN
	6750.160	2.424	-2.62	2.3	76.1	OXH
	6752.711	4.640	-1.20	2.3	37.5	HAN
	6837.009	4.590	-1.69	2.3	18.3	HAN
	6857.250	4.076	-2.04	2.3	23.4	AP
	6971.936	3.020	-3.34	2.3	13.4	HAN
	7112.173	2.990	-2.99	2.3	32.8	HAN
	7751.120	4.990	-0.73	2.3	47.0	AP
	7802.510	5.080	-1.31	2.3	15.8	AP
	7807.920	4.990	-0.51	2.3	60.9	AP
	8365.644	3.250	-2.04	2.3	70.2	HAN
	8757.200	2.845	-2.12	2.3	97.8	OXF
Fe II	5234.620	3.221	-2.22	9.9	85.0	AP
	5425.260	3.200	-3.16	9.9	42.5	AP
	6149.250	3.889	-2.63	9.9	37.4	AP
	6247.560	3.892	-2.27	9.9	54.4	AP
	6369.460	2.891	-4.02	9.9	19.8	AP
	6432.680	2.891	-3.52	9.9	41.7	HAN
	6456.390	3.903	-2.06	9.9	65.2	AP
	7479.700	3.892	-3.53	9.9	9.2	AP
	7515.840	3.903	-3.42	9.9	12.6	HAN
Co I	4792.860	3.250	-0.15	9.9	33.1	AP
	5342.710	4.020	0.54	9.9	32.7	AP
	5352.050	3.576	0.06	9.9	26.5	CAR
Ni I	5082.350	3.658	-0.59	9.9	69.1	AP
	5088.540	3.850	-1.04	9.9	33.6	AP
	5088.960	3.678	-1.24	9.9	31.3	AP
	5094.420	3.833	-1.07	9.9	32.6	AP
	5115.400	3.834	-0.28	9.9	79.2	AP
	5847.010	1.676	-3.41	9.9	23.2	AP
	6111.080	4.088	-0.81	9.9	35.8	AP
	6130.140	4.266	-0.94	9.9	22.4	AP
	6175.370	4.089	-0.55	9.9	50.5	AP
	6176.820	4.088	-0.26	9.9	67.3	WL
	6177.250	1.826	-3.51	9.9	15.2	AP
	6204.610	4.088	-1.11	9.9	22.8	WL
	6378.260	4.154	-0.83	9.9	33.1	WL
	6643.640	1.676	-2.03	9.9	101.4	AP
	6772.320	3.658	-0.97	9.9	50.9	AP
	7748.890	3.700	-0.38	9.9	91.1	AP
	7797.590	3.900	-0.35	9.9	80.7	AP
	7826.770	3.700	-1.84	9.9	13.0	AP
	9861.740	5.064	-0.50	9.9	74.0	AP
Cu I	5105.550	1.52	-1.52	9.9	90.8	KUR
	5218.210	3.820	0.47	9.9	55.6	KUR
	5220.090	3.820	-0.45	9.9	16.1	KUR
Zn I	4810.540	4.080	-0.17	9.9	76.6	BG
	6362.350	5.790	0.14	9.9	20.6	BG

Table 2 – *continued*

Ion	Wavelength (Å)	LEP (eV)	log gf		$W_{\lambda_{\odot}}$ (mÅ)	Ref.
Sr I	4607.340	0.000	0.28	9.9	46.9	MB
Y II	4900.120	1.03	-0.09	9.9	57.4	HANN
	5087.430	1.084	-0.16	9.9	48.6	HANN
	5200.420	0.992	-0.57	9.9	39.0	HANN
	5402.780	1.839	-0.44	9.9	12.6	HANN
Zr II	5112.280	1.66	-0.59	9.9	9.7	BTR
Ba II	5853.690	0.604	-0.91	9.9	66.7	DSV
	6141.730	0.704	-0.03	9.9	132.8	DSV
	6496.910	0.604	-0.41	9.9	112.2	DSV
Ce II	4523.080	0.51	0.04	16.	14.4	AP
	4628.160	0.52	0.23	16.	20.3	AP
	4773.960	0.92	0.25	16.	10.5	AP
Nd II	5092.800	0.38	-0.65	9.9	7.6	AP
	5319.820	0.55	-0.28	9.9	11.7	AP
Eu II	6645.130	1.380	0.20	9.9	5.6	KUR

References for the gf values:- AP: astrophysical values derived from inverting solar and stellar spectra; BG: Biémont & Godfroid (1980); BTR: ; CAR: Cardon et al. (1982); DSV: Davidson et al. (1992); HAN: Group at Hannover (Bard et al. 1991; Bard & Kock 1994); HANN: Hannaford et al. (1982); KUR: Kurucz (1998); LAM: Lambert (1978) LD: Lawler & Dakin (1989); LL: Lambert & Luck (1978); LUCK: R.E. Luck (1997, private communication); LW: Lambert & Warner (1968); MB: Migdalek & Baylis (1987); MOR: Milford, O'Mara, & Rose (1994) ; OXH: mean values of HANN and OXF; OXF: Group at Oxford (Blackwell et al. 1995 references therein); SR: Smith & Raggett (1981); WFD: Wiese, Fuhr & Deters (1996); WHL: Whaling et al. (1985); WL: Wickliffe & Lawler (1997); YA: Youssef & Amer (1989)

Table 5. Abundance ratios $[X/Fe]$ for elements from C to Ti for the programme stars

HD	C	N	O	[O]	Na	Mg	Al	Si	S	K	Ca	Sc	Ti
70	0.21	0.29	-0.04	0.02	-0.02	0.08	0.08	0.10	0.12	0.08	0.08	0.01
101	0.19	0.24	0.09	0.01	0.01	0.04	0.05	0.12	0.11	0.02	0.06	-0.01
153	0.28	0.42	0.40	0.01	0.11	0.06	0.15	0.11	0.21	0.21	0.00	0.00	-0.03
330	0.33	0.32	0.35	0.12	0.05	0.07	0.09	0.07	0.12	0.18	0.02	0.00	-0.03
912	0.15	0.43	0.08	0.09	0.08	0.08	0.16	0.34	0.06	-0.03	0.04
2663	0.20	0.30	0.05	0.07	0.04	0.04	0.12	0.22	0.04	0.01	0.00
3079	0.20	0.43	0.27	-0.07	0.01	-0.03	0.04	0.03	0.15	0.12	-0.01	0.02	-0.05
3440	0.33	0.25	0.33	0.03	0.10	0.11	0.06	0.15	0.21	0.03	0.06	0.03
3454	0.22	0.36	0.10	0.11	0.07	0.07	0.11	0.28	0.05	0.05	0.04
3532	0.14	0.37	0.05	0.11	0.04	0.07	0.06	0.32	0.08	0.04	0.03
3894	0.05	0.18	0.03	0.09	0.18	0.03	-0.05	0.26	0.06	0.01	0.09
5065	0.19	0.28	0.30	-0.02	0.06	0.14	0.06	0.08	0.17	0.03	0.08	0.02
5494	0.22	0.35	0.16	-0.07	0.05	0.11	0.16	0.20	0.02	-0.12
5750	0.07	0.20	0.08	0.01	0.06	0.08	-0.10	0.07	-0.19	0.06
6250	0.09	0.15	0.21	0.00	0.05	0.03	0.02	0.03	0.01	-0.04	0.00
6312	0.24	0.28	0.02	0.00	0.07	0.04	0.04	0.05	0.03	0.07	-0.02
6834	0.39	0.08	0.16	0.16	0.08	0.01	0.02
6840	0.10	0.33	0.05	0.15	0.11	0.16	0.09	0.04	0.32	0.06	-0.07	0.07
7228	0.16	0.25	0.02	0.01	0.13	0.05	0.08	0.25	0.03	-0.10	0.07
8671	0.04	0.04	0.26	-0.01	0.05	0.03	0.06	0.01	0.03	0.46	0.01	-0.01	0.03
9091	0.13	0.31	0.05	-0.02	0.10	0.12	0.03	0.11	0.20	0.04	0.04	0.03
9670	0.09	0.26	0.21	0.07	0.05	0.11	0.02	0.04	0.05	0.23	0.03	0.03	0.04
11007	0.08	0.22	0.06	0.03	0.05	0.11	0.02	0.08	0.21	0.01	0.00	0.01
11045	0.30	0.46	0.08	0.19	0.25	0.14	0.24	0.19	0.09	0.12	0.15
11592	-0.01	0.25	0.24	0.02	0.03	0.00	0.02	0.02	0.32	0.01	-0.05	0.05
14877	0.15	0.30	0.06	0.09	0.08	0.06	-0.02	0.25	0.02	-0.14	0.02
15029	-0.10	0.24	0.21	0.07	0.05	0.08	0.03	-0.01	0.38	0.04	-0.12	0.07
15398	-0.19	0.06	0.24	-0.02	0.02	0.11	0.03	0.01	0.06	-0.12	0.03
16067	0.14	0.35	-0.15	0.04	0.06	0.15	0.08	0.14	0.24	0.06	-0.03	-0.01
20427	0.21	0.40	0.12	0.12	0.10	0.13	0.05	0.06	-0.06	0.06
20717	0.06	0.22	0.06	0.06	0.02	0.06	-0.03	0.02	-0.01	0.03
21922	0.27	0.41	0.07	0.14	0.16	0.07	0.16	0.29	-0.02	0.05	0.04
22255	0.13	0.27	0.06	0.10	0.09	0.06	0.07	0.22	0.02	0.05	0.02
22521	0.19	0.28	0.15	0.06	0.09	0.11	0.04	0.18	0.43	0.09	0.11	0.06
22718	0.18	0.34	-0.03	0.06	0.09	0.15	0.06	0.21	0.37	0.03	0.05	0.00
23438	0.21	0.34	0.06	0.03	0.07	0.11	0.07	0.17
24421	0.05	0.31	0.10	0.02	0.04	0.09	0.03	0.03	0.26	0.01	0.02	0.02
26421	0.25	0.36	0.01	0.12	0.16	0.07	0.10	0.47	0.06	0.01	0.04
27816	0.10	0.29	0.12	0.14	0.12	0.07	999	0.38	0.10	-0.04	0.10
36066	0.05	0.08	0.17	-0.01	0.11	0.05	0.02	0.06	0.14	-0.01	0.04	-0.01
36667	0.34	0.39	0.09	0.14	0.13	0.10	0.20	0.25	0.05	0.11	0.03
36909	0.22	0.30	0.00	-0.06	0.02	0.04	0.23	0.13	-0.01	-0.05	-0.07
41640	0.11	0.26	0.09	0.10	0.09	0.06	0.10	0.23	0.03	0.01	0.04
42618	0.13	0.18	0.10	-0.04	-0.07	0.00	0.01	0.12	-0.06	-0.02	0.11	-0.04
45067	0.08	0.15	0.19	0.00	0.07	0.08	0.03	0.10	0.20	-0.01	0.00
52711	0.16	0.21	0.25	-0.01	0.06	0.07	0.04	0.18	0.07	-0.02	0.09	-0.02
54182	0.24	0.25	0.42	0.05	0.07	0.09	0.08	0.26	0.25	0.01	0.07	-0.02
59360	0.17	0.34	-0.09	0.06	0.09	0.05	0.18	0.07	0.00	0.06	-0.02
63332	-0.01	0.04	0.17	-0.11	0.07	0.07	0.02	-0.01	0.14	0.01	-0.13	-0.04
63333	0.15	0.27	0.32	0.21	0.08	0.05	0.03	0.05	0.13	0.32	0.08	0.00	0.02
69897	0.04	0.17	0.20	0.04	0.10	0.00	0.05	0.00	0.31	0.00	0.00	0.03
71148	0.10	0.22	0.15	0.03	-0.02	0.04	0.03	0.01	0.14	-0.03	-0.03	-0.02
73400	0.04	0.21	0.03	0.00	0.10	0.13	0.04	0.00	0.28	0.08	0.06	0.11
76272	0.18	0.33	0.06	0.09	0.09	0.07	0.12	0.26	0.04	0.08	0.06
76349	0.13	0.28	0.07	0.08	0.06	0.05	0.10	0.26	0.00	0.03	0.02
77134	0.11	0.21	0.11	-0.04	0.06	0.00	0.03	0.12	0.08	0.00	-0.06	0.00
77408	0.00	0.14	0.01	0.11	0.11	0.02	-0.02	0.28	0.02	-0.02	-0.02
80218	0.21	0.44	0.38	0.23	0.01	0.11	0.06	0.09	0.08	0.33	0.04	0.04	0.04
85902	0.25	0.36	0.07	0.06	0.10	0.03	0.25	0.11	0.03	0.04	-0.01
86560	0.24	0.33	-0.06	0.03	0.09	0.08	0.04	0.17	0.03	0.07	0.01
86884	0.10	0.27	0.03	0.05	0.08	0.11	0.04	0.04	0.30	0.02	0.04
87838	-0.04	0.22	0.04	0.14	0.07	0.08	0.02	0.24	0.02	0.05	0.05
88446	0.34	0.41	0.06	0.15	0.12	0.09	0.14	0.32	0.07	0.12	0.10
89010	0.23	0.44	0.29	0.07	0.04	0.13	0.08	0.18	0.03	-0.05	0.02	-0.04

Table 5 – *continued*

HD	C	N	O	[O]	Na	Mg	Al	Si	S	K	Ca	Sc	Ti
90878	0.02	0.39	0.10	0.06	0.02	0.05	0.01	0.47	0.03	-0.12	0.07
91638	0.01	0.22	0.02	0.09	0.01	0.01	-0.02	0.31	-0.04	0.03	0.03
94012	0.19	0.33	0.17	0.08	0.05	0.08	0.04	0.16	0.26	0.07	0.10	0.04
94835	0.17	0.32	0.19	0.00	0.01	0.06	0.07	0.16	0.02	-0.05	0.12	-0.05
97037	0.07	0.18	0.17	-0.02	0.06	0.08	0.02	0.10	0.11	-0.01	0.06	0.00
99126	0.12	0.30	0.22	-0.01	0.11	0.12	0.05	0.05	-0.04	-0.09	0.01
99233	0.21	0.38	-0.01	0.10	0.15	0.08	0.12	0.16	0.05	0.07	0.09
99984	0.10	0.32	-0.13	0.06	0.05	0.13	0.05	0.10	0.50	0.06	-0.05	0.08
100067	0.05	0.17	0.20	0.05	0.07	0.06	0.04	-0.04	0.26	0.00	0.05	0.04
100446	0.18	0.29	0.19	0.09	0.11	0.13	0.02	0.08	0.29	0.07	0.03	0.04
101472	0.16	0.26	-0.12	-0.02	-0.04	0.00	0.10	0.16	-0.04	-0.05	-0.02
101676	0.22	0.34	0.08	0.09	0.17	0.15	0.09	0.08	0.37	0.04	0.08	0.06
101716	0.19	0.38	0.12	0.05	0.13	0.10	0.07	0.19	0.40	0.04	-0.01	0.01
102080	0.14	0.22	0.29	0.05	0.05	0.10	0.04	0.09	0.28	0.03	0.02	0.02
102618	0.18	0.34	0.12	0.04	0.05	0.08	0.05	0.12	0.33	0.03	0.03	0.02
103891	0.04	0.19	0.05	0.07	0.06	0.08	0.04	0.06	0.41	0.05	-0.01	0.05
106510	0.14	0.30	0.03	0.10	0.10	0.07	0.19	0.12	0.03	0.12	0.06
107038	0.11	0.18	0.09	0.08	0.09	0.08	0.06	0.05	0.33	0.05	0.01	0.05
108134	0.23	0.32	0.03	0.03	0.13	0.06	0.21	0.11	0.05	0.05	-0.01
109154	0.23	0.43	0.09	0.11	0.07	-0.04	0.10	0.13	0.39	0.08	0.03	0.08
109303	0.32	0.55	0.09	0.11	0.07	0.11	0.08	0.14	0.34	0.04	0.11	0.01
110989	0.22	0.59	0.18	0.16	0.33	0.31	0.23	0.20	0.50	0.18	0.08	0.26
112756	0.12	0.58	0.22	0.00	0.10	0.04	0.04	-0.01	0.15	0.01	0.05	0.06
112887	-0.02	0.34	0.10	0.11	0.01	0.06	-0.02	0.11	0.03	0.15
118687	0.25	0.34	0.08	0.08	0.12	0.07	0.16	0.25	0.01	0.12	0.02
121560	0.07	0.25	0.15	0.04	0.04	0.04	0.00	0.04	0.22	0.04	0.06	0.00
124819	0.13	0.36	0.03	-0.03	0.05	0.06	0.11	0.17	0.04	-0.01
126053	0.18	0.25	0.00	0.04	0.14	0.07	0.12	0.06	0.04	0.15	0.07
127667	0.10	0.26	0.15	0.07	0.08	0.00	0.05	0.01	0.27	0.00	-0.02	-0.01
130253	0.18	0.29	-0.01	0.08	0.08	0.17	0.07	0.18	0.19	0.08	0.00	0.01
131039	0.12	0.41	0.04	0.13	0.09	0.07	0.05	-0.05	-0.05
131599	0.24	0.37	0.07	0.06	0.09	0.04	0.20	0.25	0.04	0.05	0.01
133641	0.20	0.36	0.14	0.06	0.13	0.08	0.10	0.12	-0.08	0.07
136925	0.33	0.49	0.11	0.21	0.30	0.20	0.28	0.20	0.13	0.22	0.19
139457	0.28	0.38	0.08	0.08	0.11	0.08	0.16	0.42	0.07	0.06	0.08
140324	0.23	0.35	0.04	0.12	0.11	0.08	0.16	0.24	0.01	0.10	0.04
140750	0.39	0.51	0.33	0.06	-0.05	0.16	0.11	0.35	0.17	0.04	0.13	-0.02
145937	0.23	0.49	0.08	0.11	0.16	0.08	0.17	0.36	0.11	0.06	0.07
146946	0.30	0.30	0.05	0.09	0.05	0.15	0.04	0.24	0.25	-0.07	0.13
148049	0.19	0.28	0.00	0.07	0.09	0.09	0.05	0.16	0.35	0.05	0.02	0.04
149576	0.12	0.33	0.05	0.04	0.03	0.05	0.06	-0.09	-0.08
152449	0.06	0.21	0.00	0.01	0.02	0.02	0.12	0.18	-0.01	-0.02	-0.08
152986	0.18	0.23	0.08	0.03	0.02	0.05	0.10	-0.01	0.00	-0.02
153240	0.11	0.24	0.02	0.04	0.18	0.06	-0.09
153627	0.26	0.34	0.07	0.11	0.12	0.08	0.19	0.02	0.09	0.02
153668	0.16	0.12	0.26	0.06	-0.03	0.05	0.05	0.15	0.26	0.01	0.04	0.00
155646	-0.03	0.34	0.00	0.07	0.04	0.04	0.02	0.37	0.02	0.02	0.03
156635	0.33	0.51	0.26	0.10	0.00	0.03	0.07	0.12	0.21	0.04	0.03	0.00
157466	0.18	0.24	-0.01	0.02	0.07	0.02	0.05	0.08	0.00	0.00	-0.04
157467	0.04	0.03	0.19	0.06	0.08	0.22	0.10	0.13	0.25	-0.05	-0.19	-0.04
159333	0.26	0.39	0.11	0.03	0.11	0.09	0.21	0.26	0.04	0.00	0.00
160078	0.24	0.29	0.50	-0.13	0.02	0.07	0.11	0.20	0.42	0.04	-0.11	-0.05
163363	0.05	0.17	0.09	0.15	0.08	0.01	0.04	0.02	-0.22	-0.02
167588	0.19	0.29	0.05	0.08	0.13	0.04	0.11	0.28	0.00	0.08	0.06
169359	0.24	0.30	0.00	0.09	0.08	0.08	0.14	0.19	-0.01	0.10	0.01
171620	0.26	0.30	0.26	0.12	0.06	0.12	0.07	0.08	0.06	-0.01	0.00
171886	0.07	0.33	0.00	0.02	0.05	0.00	0.06	0.02	-0.01
174160	0.11	0.17	0.21	-0.12	0.06	0.06	0.04	0.03	0.03	0.26	0.03	0.04	-0.02
176796	0.22	0.44	0.14	0.10	0.14	0.12	0.19	0.39	0.07	0.05	0.06
182758	0.15	0.39	0.03	0.12	0.17	0.04	0.13	0.30	0.00	0.05	0.07
186379	0.12	0.28	0.19	0.01	0.08	0.14	0.06	0.13	0.22	0.01	0.01	0.05
186408	0.18	0.21	0.03	0.00	0.01	0.08	0.06	0.21	-0.02	-0.01	0.15	-0.04
190681	0.12	0.25	0.09	-0.02	0.03	0.06	0.12	0.05	-0.04	-0.05
191649	0.22	0.32	0.02	0.01	-0.05	0.08	0.20	0.25	0.03	-0.02	-0.01

Table 5 – *continued*

HD	C	N	O	[O]	Na	Mg	Al	Si	S	K	Ca	Sc	Ti
191672	0.15	0.30	0.18	0.07	0.09	0.11	0.08	0.09	0.34	0.08	0.04	0.06
192145	0.14	0.31	0.13	0.09	0.09	0.07	0.16	0.33	0.03	0.02	0.00
193664	0.13	0.17	0.10	-0.05	0.00	0.01	0.02	0.18	0.06	-0.02	0.02	-0.03
194497	-0.04	-0.02	0.22	0.03	-0.01	-0.01	0.03	0.00	0.46	0.04	0.05	0.07
195200	0.16	0.03	0.25	0.01	-0.01	0.06	0.01	0.11	0.17	-0.02	-0.03	-0.04
198089	0.19	0.30	0.02	0.07	0.10	0.06	0.19	0.10	0.00	0.11	0.02
198109	0.19	0.29	0.06	0.07	0.06	0.03	0.04	0.33	0.03	0.02	0.06
198390	0.09	0.34	0.03	0.05	0.01	0.02	0.05	0.37	0.08	-0.01	0.00
199085	0.04	0.14	-0.01	-0.04	-0.01	0.01	-0.08	0.36	0.04	0.01	-0.03
200580	0.07	0.17	0.18	0.06	0.17	0.01	999	0.26	0.09	-0.13	0.15
201444	0.30	0.53	0.14	0.12	0.16	0.13	0.16	0.45	0.06	0.08	0.07
201490	0.06	0.28	0.19	-0.02	0.03	0.04	0.07	0.03	0.02	0.26	0.03	-0.11	0.01
201639	0.25	0.22	0.09	0.09	0.07	0.09	0.14	0.28	0.07	0.06	0.04
201835	0.12	0.35	0.07	0.13	0.13	0.11	0.03	0.14	0.10	0.10
202884	0.09	0.21	-0.01	0.04	0.04	0.02	0.05	0.20	0.01	0.01	0.02
204306	0.30	0.53	0.10	0.14	0.17	0.14	0.27	0.29	0.10	0.12	0.07
204559	0.15	0.41	0.32	0.17	0.06	0.06	0.08	0.04	0.07	0.30	0.03	0.02	0.04
204712	0.26	0.44	0.08	0.11	0.09	0.10	0.18	0.32	0.07	0.14	0.07
206860	0.11	0.20	0.22	0.00	-0.11	-0.01	0.02	0.18	0.12	-0.01	-0.03	-0.02
209320	0.20	0.34	0.05	0.08	0.10	0.08	0.21	0.05	-0.04	-0.06
209858	0.20	0.27	0.05	0.00	0.04	0.04	0.17	0.15	0.01	0.04	0.01
210457	0.11	0.31	0.01	0.09	0.03	0.03	0.05	0.12	0.34	0.00	-0.04	0.00
210640	0.08	0.37	0.05	0.03	0.03	0.08	0.07	0.33	0.08	-0.13	0.04
210718	0.04	0.18	0.08	0.08	0.13	0.07	0.05	0.33	0.06	-0.09	0.03
210923	0.14	0.33	-0.01	0.06	0.05	0.07	0.04	0.12	0.29	0.02	0.03	-0.01
210985	0.08	0.36	0.20	0.08	0.17	0.11	0.11	0.32	0.14	-0.04	0.08
212858	0.18	0.29	0.02	0.04	0.09	0.00	0.05	0.17	-0.01	-0.01	-0.02
214111	0.17	0.34	0.16	0.01	0.09	0.14	0.38	0.05	-0.19
214435	0.15	0.24	0.02	0.04	0.04	0.03	0.11	0.12	-0.01	-0.01	-0.03
214557	0.18	0.37	0.26	0.04	0.07	0.12	0.07	0.20	0.10	-0.05	0.10	-0.04
214576	0.13	0.37	0.08	0.09	0.01	0.11	0.06	0.11	0.01	0.07
215442	0.30	0.50	0.08	0.08	-0.03	0.11	0.26	0.04	-0.10	-0.04
216106	0.28	0.43	0.10	0.12	0.10	0.09	0.22	0.38	0.07	0.01	0.02
216385	-0.04	-0.02	0.18	0.02	0.07	0.03	0.01	-0.06	0.40	-0.01	-0.07	0.02
216631	0.13	0.25	0.02	-0.03	0.07	-0.02	0.06	0.16	0.00	0.02	0.02
217877	0.13	0.30	0.22	-0.02	0.06	0.05	0.09	0.04	0.16	0.17	0.04	0.08	-0.02
218059	0.03	0.25	-0.03	0.06	0.00	0.03	0.05	0.26	0.03	-0.06	-0.01
218172	0.12	0.08	0.28	0.00	0.03	0.00	0.07	0.06	0.13	0.40	0.04	0.04	0.05
218470	-0.01	0.29	0.08	0.03	-0.01	0.01	0.33	0.00	-0.15	-0.03
218637	0.03	0.17	0.10	0.16	0.12	0.08	0.01	0.36	0.09	-0.01	0.05
219306	0.15	0.30	0.05	0.10	0.07	0.06	0.13	0.28	0.01	0.04	0.03
219476	0.15	0.37	0.12	0.12	0.08	0.08	0.10	0.43	0.05	0.04	0.10
219497	0.32	0.44	0.17	0.09	0.13	0.09	0.31	0.08	0.08	0.03
219983	0.02	0.14	0.22	-0.02	0.02	0.02	0.08	0.03	0.02	0.37	0.06	-0.02	0.04
220842	0.39	0.40	0.12	0.02	0.08	0.06	0.07	0.25	0.15	0.01	0.06	-0.03
220908	0.07	0.31	-0.09	0.07	0.04	0.10	0.06	0.15	0.32	0.06	-0.02	0.02
221356	-0.03	0.09	-0.06	0.01	0.05	-0.01	-0.02	0.13	0.06	-0.05	0.05
222155	0.49	0.38	0.04	0.11	0.18	0.11	0.27	0.10	0.01	0.13	0.00
223436	0.12	0.20	0.25	0.05	0.05	0.06	0.07	-0.04	0.26	0.04	-0.02	0.01
223583	0.23	0.34	0.16	0.07	0.11	0.08	0.07	0.14	0.35	0.04	0.00	0.06
223854	0.12	0.34	0.07	0.10	0.11	0.11	0.02	0.13	0.07	0.14
224233	0.29	0.35	0.31	0.31	0.00	0.09	0.21	0.12	0.25	0.11	0.02	0.14	0.05
225239	0.34	0.43	0.09	0.11	0.18	0.09	0.30	0.22	0.05	0.09	0.05

Table 6. Abundance ratios [X/Fe] for elements from V to Eu for the programme stars

HD	V	Cr	Mn	Co	Ni	Cu	Zn	Sr	Yr	Zr	Ba	Ce	Nd	Eu
70	-0.05	0.01	-0.08	0.02	-0.02	-0.03	0.11	-0.12	-0.05	-0.10	0.03	0.08
101	-0.06	-0.02	-0.13	0.01	-0.02	-0.11	0.10	-0.01	0.08	0.00	0.01	0.05	0.07
153	-0.04	0.01	-0.07	0.00	0.01	-0.03	0.05	-0.02	0.00	-0.03	-0.19	-0.16	-0.10	0.01
330	-0.07	-0.03	-0.15	-0.03	-0.03	-0.07	0.08	-0.02	-0.01	0.01	-0.13	-0.07	-0.01	0.00
912	-0.05	-0.02	-0.17	-0.08	-0.03	-0.14	0.00	0.10	0.07	0.04	0.02	0.00	-0.06	0.01
2663	-0.05	-0.05	-0.18	-0.04	-0.03	-0.13	0.07	0.02	0.01	-0.01	-0.01	0.10
3079	-0.03	-0.06	-0.13	-0.04	-0.05	-0.12	0.06	-0.02	-0.01	0.02	-0.09	-0.05	0.03	-0.06
3440	-0.03	-0.03	-0.06	-0.03	-0.03	-0.04	0.08	-0.11	-0.05	-0.16	-0.08	0.03	-0.02
3454	0.04	-0.04	-0.13	-0.05	-0.03	-0.13	0.08	0.04	-0.06	-0.02	-0.05	-0.05	0.21
3532	0.06	-0.02	-0.18	0.00	-0.05	-0.15	0.13	0.08	0.01	0.01	0.06	0.09	0.04
3894	-0.01	0.01	-0.20	-0.06	-0.05	-0.15	-0.02	0.03	-0.04	-0.08	-0.04	0.06
5065	-0.05	-0.02	-0.16	0.00	-0.01	-0.07	0.06	-0.02	-0.01	-0.02	-0.10	0.04	0.03	0.16
5494	0.06	-0.08	-0.02	0.00	-0.03	-0.08
5750	0.03	-0.27	-0.05	-0.05	-0.18	-0.06	-0.02
6250	-0.05	-0.03	-0.13	-0.07	-0.05	-0.15	0.01	0.06	0.03	-0.06	0.03	-0.03	0.07
6312	-0.07	-0.03	-0.12	0.04	-0.02	-0.06	0.00	-0.07	-0.02	0.03	-0.07	0.00	0.05	0.09
6834	-0.21	-0.02	-0.15	-0.04	-0.12	0.01
6840	-0.01	0.02	-0.14	0.02	0.01	-0.06	0.03	0.04	-0.11	-0.10	-0.13	-0.11	-0.04
7228	0.00	0.01	-0.12	0.01	-0.01	-0.32	0.05	-0.03	-0.04	0.11	0.02	-0.05
8671	0.01	-0.02	-0.16	-0.06	-0.04	-0.12	0.04	0.08	0.13	0.22	-0.04	0.06	0.03
9091	-0.04	-0.05	-0.17	-0.04	-0.04	-0.07	0.06	-0.08	-0.08	-0.07	-0.11	-0.06	0.06	0.00
9670	-0.02	-0.01	-0.12	-0.02	-0.02	-0.07	0.05	0.03	0.01	-0.07	0.06	-0.03	0.02	0.13
11007	-0.06	-0.03	-0.16	-0.02	0.00	-0.05	0.08	-0.04	-0.05	-0.07	-0.02	-0.06	-0.02	0.16
11045	0.00	-0.03	-0.22	0.05	-0.01	0.01	0.20	-0.07	-0.07	-0.31	-0.06	0.14
11592	0.02	-0.05	-0.21	0.03	-0.06	-0.23	-0.02	0.02	-0.05	0.00	0.09	0.03
14877	-0.04	-0.04	-0.16	-0.01	-0.02	-0.11	0.01	0.00	-0.14	-0.09	-0.19	-0.13	-0.03
15029	0.02	-0.02	-0.18	0.02	-0.04	-0.12	0.07	0.03	-0.12	-0.03	-0.04	-0.03
15398	0.00	-0.02	-0.12	0.00	-0.02	-0.15	-0.02	0.04	0.08	0.12	0.04	-0.03
16067	-0.07	0.01	-0.13	-0.03	0.00	-0.11	-0.05	0.06	0.06	0.05	-0.04	-0.09	-0.06	0.02
20427	0.02	-0.01	-0.24	0.11	-0.03	-0.06	0.08	0.01	-0.06	0.07	-0.08	0.01	-0.09
20717	0.01	-0.03	-0.20	0.05	-0.04	-0.18	-0.04	0.05	-0.04	-0.08	0.18	0.03
21922	-0.03	-0.07	-0.18	-0.02	-0.02	-0.03	0.19	0.25	0.23	0.18	0.33	0.34	0.17
22255	-0.05	0.03	-0.19	0.00	0.00	0.09	0.06	0.15	0.08
22521	0.02	0.04	-0.15	0.07	0.05	-0.04	0.09	-0.06	-0.03	-0.02	-0.03	0.03	0.01	0.17
22718	-0.04	-0.02	0.01	-0.01	-0.01	0.03	-0.06	-0.05	-0.05	-0.13	-0.14	-0.03	-0.01
23438	0.00	-0.07	-0.09	-0.10	-0.07	-0.14	-0.07	-0.04	0.14
24421	-0.02	-0.05	0.04	-0.02	-0.09	-0.04	-0.06	-0.07	-0.07	-0.06	-0.10	0.04	0.09
26421	-0.04	-0.01	-0.18	-0.03	-0.04	-0.09	0.03	-0.10	-0.16	-0.18	-0.19	-0.10	0.03	0.08
27816	0.01	-0.03	0.01	-0.01	-0.06	0.00	0.01	-0.15	-0.07	-0.09	0.07
36066	-0.06	0.00	-0.10	-0.02	-0.05	-0.03	0.03	-0.01	0.00	0.00	-0.05	-0.03	0.03
36667	-0.04	-0.01	-0.16	0.01	-0.02	-0.05	0.14	0.33	0.38	0.33	0.47	0.26	0.40	0.14
36909	-0.10	-0.06	-0.14	-0.11	-0.06	-0.16	0.01	0.00	0.09	0.01	0.11	0.08	-0.06
41640	0.00	-0.01	-0.21	-0.06	-0.03	-0.10	0.03	-0.04	-0.05	-0.09	0.02	0.08	-0.04
42618	-0.05	-0.04	-0.07	-0.03	-0.02	-0.03	0.09	-0.10	0.10	0.05	0.10	0.12
45067	-0.07	-0.01	-0.08	-0.04	-0.02	-0.07	0.03	0.02	-0.06	-0.02	-0.05	-0.06	-0.02	-0.03
52711	-0.06	-0.03	-0.06	-0.01	-0.01	-0.06	0.08	-0.01	0.05	0.07	0.02	0.07	0.12	0.08
54182	-0.10	-0.02	-0.14	-0.05	-0.01	-0.10	0.09	0.01	0.06	0.11	0.04	-0.05	0.08
59360	-0.10	-0.04	-0.15	-0.04	-0.04	-0.10	0.05	-0.13	-0.06	-0.01	-0.07	-0.02	0.07	0.07
63332	0.14	0.00	-0.15	-0.12	-0.05	-0.27	-0.08	0.08	0.08	-0.01
63333	-0.02	-0.02	-0.19	-0.01	-0.02	-0.11	0.05	0.01	-0.02	-0.07	0.04	-0.04	-0.01	0.05
69897	-0.03	0.00	-0.14	-0.05	-0.04	-0.14	0.01	0.08	0.03	0.16	0.03	0.06	0.05
71148	-0.09	-0.01	-0.02	-0.03	-0.06	-0.04	-0.03	-0.03	0.00	-0.14	-0.05	0.01
73400	0.06	-0.04	-0.15	-0.07	-0.03	-0.12	-0.03	0.06	-0.04	0.09	0.04	0.16
76272	0.02	-0.02	-0.15	0.00	-0.01	-0.11	0.12	0.00	-0.04	-0.05	-0.07	-0.01
76349	-0.06	-0.02	-0.14	-0.05	-0.02	-0.08	0.09	-0.05	-0.08	-0.09	-0.04	-0.10
77134	-0.05	-0.04	-0.18	-0.06	-0.06	-0.15	-0.04	0.06	0.09	0.13	0.13
77408	-0.03	0.00	-0.19	-0.04	-0.04	-0.15	-0.05	-0.55	0.05	0.01
80218	-0.06	-0.04	-0.20	-0.02	-0.03	-0.06	0.08	0.33	0.26	0.16	0.00	-0.07	0.04	0.05
85902	-0.04	-0.02	-0.06	-0.04	-0.03	-0.05	0.21	-0.03	0.00	-0.06	-0.04	0.11	0.08
86560	-0.01	-0.01	-0.18	-0.03	-0.02	-0.05	0.11	-0.12	-0.09	-0.11	-0.13	0.06
86884	-0.02	-0.01	-0.13	-0.02	-0.02	-0.07	0.06	0.06	-0.01	0.08	0.01	-0.02	0.00	0.12
87838	-0.04	0.00	-0.19	0.02	-0.02	-0.08	0.07	-0.05	-0.08	0.01	-0.05	-0.08	-0.01	0.21
88446	0.00	-0.04	-0.22	0.01	-0.01	-0.06	0.10	0.57	0.58	0.65	0.66	0.58	0.69	0.24

Table 6 – continued

HD	V	Cr	Mn	Co	Ni	Cu	Zn	Sr	Yr	Zr	Ba	Ce	Nd	Eu
89010	-0.07	-0.03	-0.08	0.03	0.02	0.04	0.13	-0.10	0.02	0.07	-0.07	0.04	0.01	0.15
90878	0.14	0.03	-0.13	0.04	-0.06	-0.18	-0.01	-0.52	0.22	0.10
91638	-0.04	-0.05	-0.12	-0.05	-0.03	-0.12	0.05	0.03	-0.01	-0.12	0.00	-0.03	0.13
94012	-0.03	-0.03	-0.13	0.01	-0.02	-0.09	0.09	-0.06	0.01	-0.02	0.03	0.11	-0.07
94835	-0.08	-0.03	-0.05	0.00	0.02	0.00	0.10	0.00	0.15	0.05	0.04	0.08	0.02
97037	-0.04	-0.02	-0.09	-0.02	-0.02	-0.03	0.09	-0.14	-0.02	-0.09	-0.02	0.03	0.09
99126	-0.13	0.00	-0.13	-0.04	0.00	-0.13	0.01	0.00	-0.08	0.00	0.01	0.12
99233	-0.01	-0.03	-0.18	0.00	-0.02	-0.09	-0.03	-0.10	-0.13	0.01	-0.12	-0.06	-0.05
99984	0.06	0.04	-0.14	-0.08	-0.02	-0.11	-0.01	0.11	0.04	-0.02	0.12	-0.08	0.10
100067	-0.02	-0.03	-0.21	-0.04	-0.03	-0.15	0.08	0.04	0.00	0.07	0.05	-0.01	0.18
100446	-0.02	-0.06	-0.15	-0.01	-0.02	-0.06	0.08	0.03	-0.04	0.08	-0.02	0.10
101472	-0.06	0.03	-0.13	-0.10	-0.06	-0.21	-0.02	0.13	0.12	0.08	0.23	0.03	-0.02
101676	0.01	-0.01	-0.17	0.03	0.00	-0.05	0.08	0.01	0.00	0.18	0.03	0.08	0.07	0.09
101716	-0.07	0.00	-0.11	-0.02	-0.02	-0.07	0.05	0.07	0.09	0.12	0.12	-0.03
102080	0.05	-0.02	-0.11	-0.02	0.01	-0.05	0.08	0.07	-0.04	-0.08	-0.05	-0.09	0.02	0.04
102618	-0.10	-0.02	-0.14	-0.03	-0.02	-0.06	0.15	-0.03	-0.05	-0.02	-0.02	-0.08
103891	0.00	0.03	-0.14	-0.05	-0.01	-0.09	0.00	0.09	-0.01	0.08	0.00	-0.03	0.09	0.07
106510	-0.02	-0.01	-0.15	0.01	-0.01	-0.03	0.09	-0.11	0.00	-0.09	0.07	0.16	0.09
107038	0.98	-0.03	-0.15	-0.05	-0.01	-0.07	0.02	-0.05	-0.08	-0.14	-0.04	-0.09	-0.02	0.06
108134	-0.06	-0.04	-0.11	0.00	-0.02	-0.08	0.03	-0.07	-0.10	-0.03	-0.15	-0.09	-0.04	-0.06
109154	0.03	-0.04	-0.20	-0.06	0.00	-0.11	0.02	0.38	0.09	0.29	0.06	-0.03	0.09	0.15
109303	-0.07	-0.05	-0.20	-0.06	-0.03	-0.14	0.07	0.05	0.11	0.19	0.20	-0.07	0.12	0.23
110989	0.04	-0.02	-0.28	0.15	0.04	-0.06	0.24	0.10	-0.11	-0.01	-0.28	-0.18
112756	-0.03	-0.04	-0.17	-0.04	-0.06	-0.15	0.02	0.02	0.07	0.08	0.09	0.23	0.24
112887	0.08	-0.01	-0.15	0.08	-0.04	-0.20	0.02	0.12	0.07	0.30	0.19	0.09	0.14
118687	-0.05	-0.03	-0.14	0.00	-0.01	-0.08	0.03	0.09	0.21	0.11	0.20	0.15
121560	-0.04	-0.06	-0.17	-0.06	-0.04	-0.10	0.06	0.04	0.14	-0.02	0.01	0.05	0.09
124819	-0.05	-0.03	-0.16	-0.04	-0.05	0.08	-0.13	-0.09	-0.10
126053	-0.01	-0.02	-0.09	0.01	-0.01	0.01	0.16	-0.13	-0.04	-0.15	-0.12	-0.02	0.01	0.32
127667	0.00	-0.04	-0.12	-0.02	-0.01	-0.11	0.04	-0.01	-0.08	0.00	-0.03	0.06	0.14
130253	-0.06	-0.02	-0.14	-0.01	0.01	-0.07	-0.05	-0.07	-0.05	-0.03	-0.12	-0.08	0.04	-0.06
131039	0.13	-0.03	-0.19	-0.02	-0.04	-0.22	0.09	0.12	0.00
131599	-0.06	-0.02	-0.19	-0.01	-0.03	-0.05	0.06	0.01	0.03	0.08	0.00	0.04	-0.07
133641	0.20	0.04	-0.11	-0.06	-0.04	-0.18	0.02	0.14	-0.05	-0.26	-0.07	0.00	-0.11	0.06
136925	0.07	-0.01	-0.20	0.11	0.05	0.07	0.27	-0.09	-0.02	-0.20	0.01	0.24
139457	0.09	-0.02	-0.16	-0.05	-0.02	-0.09	0.05	-0.05	-0.03	-0.04	-0.06	0.02	0.04	0.07
140324	0.06	0.00	-0.15	0.00	-0.01	-0.04	0.11	0.29	0.18	0.29
140750	-0.09	-0.02	-0.14	0.01	0.01	-0.04	0.18	-0.08	0.04	0.00	-0.05	0.01	0.03	0.19
145937	0.01	0.00	-0.16	0.02	-0.02	-0.12	0.04	-0.03	-0.13	-0.15	-0.22	-0.19	0.00
146946	0.17	-0.02	-0.07	-0.06	-0.05	-0.11	-0.01	0.01	0.00	0.03
148049	0.03	-0.07	-0.14	0.00	-0.02	-0.07	0.08	-0.06	-0.04	-0.04	-0.11	-0.06
149576	-0.04	-0.16	-0.12	-0.07	-0.20	0.18	0.08
152449	-0.09	-0.03	-0.13	-0.07	-0.03	-0.20	-0.02	0.06	0.02	-0.15	-0.02	-0.07	-0.12
152986	0.00	-0.02	-0.14	-0.04	-0.03	-0.08	0.05	0.08	0.08	0.04	0.05	0.04	0.00	-0.01
153240	0.14	0.08	-0.12	-0.05	-0.04	-0.23	0.08	0.10	-0.04
153627	-0.07	-0.04	-0.16	-0.01	0.00	-0.02	0.15	-0.02	0.03	0.02	-0.04	0.02	0.09
153668	-0.08	-0.02	-0.14	-0.04	-0.03	-0.07	0.05	0.03	0.03	-0.04	0.01	0.01
155646	-0.05	-0.01	-0.15	-0.04	-0.03	-0.18	-0.03	0.10	0.07	0.29	0.11	0.01
156635	-0.01	-0.03	-0.10	-0.01	0.01	0.00	0.06	0.07	-0.02	0.06	-0.02
157466	-0.06	-0.06	-0.20	-0.02	-0.08	-0.18	-0.01	-0.04	-0.04	-0.04	0.01	0.04
157467	-0.07	-0.04	-0.03	0.02	-0.06	0.01	-0.12	-0.17	-0.26
159333	-0.09	-0.01	-0.11	-0.02	0.00	-0.01	0.04	0.00	0.01	0.00	0.03	-0.05	0.01
160078	-0.07	0.02	-0.16	-0.07	-0.02	-0.19	0.01	0.04	0.01	0.08	-0.03	0.05
163363	-0.02	-0.03	-0.07	-0.01	-0.01	-0.02	-0.16	-0.14	-0.21
167588	0.00	0.01	-0.20	-0.01	-0.02	-0.07	0.01	-0.06	-0.08	-0.04	0.06
169359	-0.03	-0.04	-0.13	-0.02	-0.03	-0.06	0.06	-0.07	-0.02	0.0	-0.03	0.04	0.03
171620	-0.01	-0.05	-0.18	-0.05	-0.01	-0.05	0.03	-0.04	-0.09	-0.15	0.01	-0.02	-0.01
171886	0.02	-0.16	0.01	-0.06	-0.16	0.14	0.05
174160	0.01	0.07	-0.15	-0.09	-0.04	-0.17	-0.06	0.10	0.05	0.08	0.06	0.03	0.00
176796	0.09	0.02	-0.18	0.00	0.00	-0.08	0.07	0.10	0.05	0.02	0.04	0.04	0.06
182758	-0.04	-0.07	-0.21	-0.02	-0.03	-0.06	0.18	-0.05	-0.15	-0.15	-0.13	-0.08	-0.05
186379	-0.01	-0.02	-0.18	-0.01	-0.03	-0.06	0.05	-0.12	-0.13	-0.10	-0.20	-0.11	0.01	0.22
186408	-0.09	-0.05	-0.07	-0.01	0.02	0.00	0.06	-0.09	0.08	0.03	0.04	0.06	0.14
190681	-0.04	-0.03	-0.14	-0.03	-0.04	-0.07	0.04	0.03	0.01	-0.01	-0.09	-0.18
191649	-0.07	-0.03	-0.15	-0.06	-0.03	-0.13	0.00	0.01	-0.02	0.06	-0.06	0.03	0.23

Table 6 – *continued*

HD	V	Cr	Mn	Co	Ni	Cu	Zn	Sr	Yr	Zr	Ba	Ce	Nd	Eu
191672	0.03	0.02	-0.16	-0.01	-0.01	-0.06	0.04	-0.06	-0.04	-0.14	-0.17	-0.17
192145	-0.02	-0.01	-0.14	0.01	0.00	-0.04	0.08	0.02	-0.03	-0.14	-0.04	-0.02	-0.19
193664	-0.10	-0.02	-0.11	-0.08	-0.04	-0.11	0.04	0.01	0.10	0.08	0.06	0.16	0.16
194497	0.00	0.01	-0.18	-0.03	-0.05	-0.09	-0.02	0.15	0.07	-0.12	0.17	0.12	0.12
195200	-0.06	-0.03	-0.12	-0.06	-0.05	-0.09	0.02	0.03	0.04	-0.01	0.05	0.01	-0.02
198089	-0.01	-0.06	-0.13	0.00	-0.02	-0.03	0.10	-0.15	-0.03	-0.04	-0.04	-0.03	0.07	0.24
198109	0.02	-0.06	-0.17	-0.02	-0.05	-0.13	0.00	-0.09	-0.06	-0.06	-0.11	-0.03	0.01
198390	0.15	-0.05	-0.20	-0.09	-0.05	-0.20	0.04	0.12	0.10	0.21	0.14
199085	0.15	0.00	-0.10	-0.14	-0.06	-0.12	0.00	0.13	-0.03	0.19	0.09
200580	0.18	0.04	-0.06	0.00	-0.01	-0.09	-0.01	0.03	-0.23	-0.17	-0.12	-0.09
201444	-0.04	-0.05	-0.23	0.02	-0.03	-0.09	0.07	0.04	0.00	0.12	0.12	0.13	0.29
201490	-0.01	-0.04	-0.14	-0.04	-0.01	-0.10	-0.03	-0.01	-0.10	-0.01	-0.10	-0.19	0.04
201639	-0.01	-0.02	-0.15	-0.02	-0.01	-0.08	0.07	0.02	0.01	-0.06	0.05	0.07	0.24
201835	0.12	0.04	-0.17	0.06	0.01	-0.12	-0.01	0.03	0.14	0.11
202884	-0.02	-0.04	-0.20	-0.01	-0.05	-0.19	0.00	0.06	0.08	-0.04	0.18	0.05	0.13	0.24
204306	-0.01	-0.01	-0.20	0.07	0.00	-0.09	0.13	-0.05	-0.03	-0.10	-0.04	-0.15	0.03
204559	-0.04	-0.03	-0.13	-0.06	-0.02	-0.10	0.05	-0.05	-0.02	0.02	0.06	0.03
204712	-0.06	-0.04	-0.19	0.03	-0.01	-0.04	0.14	-0.05	0.02	0.00	-0.01	-0.08	0.08	0.18
206860	-0.11	0.00	-0.14	-0.18	-0.04	-0.18	0.07	0.09	0.18	0.07	0.29	0.18	0.12
209320	0.02	0.03	-0.09	-0.05	0.00	-0.07	-0.02	0.02	0.01	0.05	-0.02	-0.03	-0.06
209858	-0.05	-0.03	-0.13	-0.04	-0.03	-0.03	0.05	-0.08	-0.02	-0.01	-0.03	-0.02	0.06	0.16
210457	-0.06	-0.01	-0.18	-0.04	-0.04	-0.17	0.00	0.09	0.05	0.03	0.14	-0.11	0.01	0.09
210640	0.01	-0.02	-0.07	-0.04	-0.04	-0.17	0.03	0.01	0.05	0.09
210718	-0.03	-0.03	-0.15	-0.06	-0.03	-0.09	0.03	-0.14	-0.24	-0.15	-0.27
210923	-0.01	-0.03	-0.12	-0.06	-0.03	-0.05	0.04	0.05	0.10	0.03	0.11	-0.02	0.10	0.02
210985	-0.01	-0.20	0.01	-0.02	-0.08	0.00	-0.02	-0.09	0.09
212858	-0.09	-0.04	-0.16	-0.08	-0.04	-0.12	0.07	-0.03	-0.05	-0.09	-0.06	0.00	0.04	0.10
214111	0.16	0.10	-0.10	0.02	0.01	-0.10	-0.10	-0.23	0.09
214435	-0.05	-0.02	-0.15	-0.05	-0.03	-0.11	0.07	0.02	0.03	-0.07	0.04	0.09	0.03	-0.06
214557	-0.07	-0.01	-0.13	-0.03	-0.01	-0.05	0.04	0.00	0.08	0.05	-0.06	-0.06	0.25
214576	0.03	0.00	-0.19	-0.06	-0.01	-0.20	0.03	0.09	-0.02	-0.03	0.09	0.08
215442	-0.10	0.01	-0.03	-0.01	-0.11	0.00	0.00	0.00	0.02	-0.02	-0.02	0.03
216106	-0.09	-0.03	-0.17	-0.04	-0.02	-0.11	0.08	0.06	0.09	-0.03	0.22	-0.07	0.02	0.02
216385	0.01	0.00	-0.15	-0.07	-0.04	-0.16	-0.05	0.04	-0.11	-0.08	0.04	-0.14	-0.02	-0.02
216631	-0.03	-0.08	-0.21	-0.11	-0.07	-0.16	0.02	-0.03	0.02	-0.09	-0.01	-0.03
217877	-0.06	-0.03	-0.05	-0.02	-0.01	-0.03	0.08	-0.03	0.01	-0.02	-0.03	-0.04	0.09	0.01
218059	-0.01	0.00	-0.15	-0.06	-0.06	-0.20	0.02	0.06	-0.02	-0.02	0.10	0.06
218172	-0.03	-0.01	-0.10	-0.05	-0.04	-0.11	0.02	0.08	0.09	0.08	0.08	-0.06	0.10	0.11
218470	0.19	-0.16	-0.01	-0.21	-0.11	0.04	0.17	-0.04
218637	0.05	-0.02	-0.09	0.03	0.02	0.02	-0.04	0.05	-0.10	-0.14	-0.01	-0.06
219306	-0.05	-0.05	-0.18	0.00	0.00	-0.04	0.05	0.02	-0.01	-0.04	0.03	-0.11	-0.01	-0.04
219476	-0.03	-0.02	-0.21	0.00	-0.03	-0.08	0.06	-0.02	-0.08	-0.08	0.06	-0.15	-0.02	0.10
219497	-0.08	-0.04	0.04	-0.05	-0.11	0.15	0.06	0.07	0.08	0.04	0.02	0.07
219983	0.00	-0.02	-0.13	-0.05	-0.01	-0.12	-0.05	0.07	-0.02	0.00	0.00	-0.08	0.13	-0.02
220842	-0.10	-0.02	-0.14	-0.03	-0.03	0.01	0.16	0.27	0.35	0.27	0.09	0.05	0.12	0.17
220908	0.00	-0.01	-0.12	-0.04	0.00	-0.11	0.00	0.04	0.02	0.04	0.03	-0.06
221356	-0.02	-0.03	-0.21	-0.04	-0.05	-0.16	-0.06	0.05	0.09	0.08	0.08	0.12
222155	-0.07	-0.02	-0.12	0.02	0.00	-0.02	0.19	0.11	0.22	0.22	0.16	0.08	0.21	0.25
223436	0.01	0.02	-0.08	-0.05	-0.02	-0.05	-0.01	0.08	0.03	0.07	0.00	-0.03	0.03	0.11
223583	0.01	0.00	-0.17	-0.02	-0.01	-0.04	0.09	-0.09	-0.14	-0.15	-0.15	-0.08	0.01	-0.05
223854	0.01	0.00	-0.19	0.06	0.01	-0.09	0.05	0.02	-0.06	-0.15	-0.06	0.00
224233	-0.05	-0.03	-0.14	0.00	0.01	0.01	0.16	-0.13	0.02	0.02	-0.05	0.08	0.40	0.21
225239	-0.02	-0.01	-0.14	0.01	-0.01	-0.01	0.12	-0.09	-0.05	-0.10	-0.01	0.07	0.14

This figure "reddy_fig9.jpeg" is available in "jpeg" format from:

<http://arxiv.org/ps/astro-ph/0211551v2>

This figure "reddy_fig10.jpeg" is available in "jpeg" format from:

<http://arxiv.org/ps/astro-ph/0211551v2>

This figure "reddy_fig11.jpeg" is available in "jpeg" format from:

<http://arxiv.org/ps/astro-ph/0211551v2>

This figure "reddy_fig12.jpeg" is available in "jpeg" format from:

<http://arxiv.org/ps/astro-ph/0211551v2>

This figure "reddy_fig15.jpeg" is available in "jpeg" format from:

<http://arxiv.org/ps/astro-ph/0211551v2>

This figure "reddy_fig16.jpeg" is available in "jpeg" format from:

<http://arxiv.org/ps/astro-ph/0211551v2>